Investigating the Regulation of ACC1 Activity in Pancreatic Beta cells

Rula Tayseer Bany Bakar

DPhil Candidate

Department of Physiology, Anatomy and Genetics,

Linacre College, University of Oxford

Supervisors:

Dr. James Cantley

Prof. Helen Christian

Submitted in fulfilment of the requirements for the degree of Doctor of Philosophy (DPhil) in Physiology, Anatomy & Genetics

“One, remember to look up at the stars and not down at your feet. Two, never give up work. Work gives you meaning and purpose, and life is empty without it. Three, if you are lucky enough to find love, remember it is there and don't throw it away.” Stephen Hawking

Acknowledgement

I would like to gratefully and sincerely thank my supervisor, Dr James Cantley, for giving me the chance to undertake this research in his lab, and for his guidance, patience, understanding, availability, support and for the valuable discussions that inspired me throughout the work, from him I have learned beyond what I learned from textbooks and papers. I learned how to be creative, and how to be a scientist. Thank you so much for making my DPhil journey very exciting and incredibly valuable.

I thank all members of the Cantley's group for their encouragement and support. In particular, I would like to thank Nchimunya Nelisa Tebeka for her friendship, support and the good times we shared.

I would like to extend my sincere appreciation to Prof. Helen Christian for her help and support.

I would also like to thank Prof. Shabaz Mohammed and Dr. Sabrina Liberatori from the advanced proteomics facility for their advice, training in phosphoproteomics techniques and data analysis, for their contribution to this project and for helping analysing the data and in writing the phosphoproteomics method section.

I am also grateful to Dr. Joey Riepsaame from the Dunn's School of pathology for his help in designing gRNA and for his advice on CRISPR technique.

My warm thanks to my mum for her selfless love, care and sacrifice she has done to shape my life. Her endless faith inspired me to become the person who I am today. I learnt from her how to be a strong independent woman and how to be a hard worker. An enormous thank you to my dad for his special support and encouragement. Also, thank you to my father in law, Zaal, for his tireless help and support and for teaching me how to dream and the sky is the limit.

And finally, but perhaps most of all, thanks to my husband Malek, who has supported me and encouraged me to pursue my dreams. His continued and unfailing love, support, encouragement and understanding have been so important. Thank you for your friendship, assistance, and invaluable feedback. Thank you for being always there for me during the happy and hard times. Abraham Lincoln once said " I'm a success today because I had a friend who believed in me and I didn't have the heart to let him down", and I would say that I'm here today because of you.

Thank you also to my son Alsharif for being such a good boy and for making this journey easier and more exciting. Thank you for your effort in attending the nursey for the last three years; every day from 8:00 am till 6:00 pm without complaining. Thank you for your patience and for your commitment. Words would never say how grateful I am to both of them.

For all that, this thesis is dedicated to both of them.

وَآخِرُ دَعْوَاهُمْ أَنِ الْحَمْدُ لِلَّهِ رَبِّ الْعَالَمِينَ

Investigating the Regulation of ACC1 Activity in Pancreatic Beta cells

Rula Bany Bakar

Department of Physiology, Anatomy and Genetics, Linacre College, University of Oxford.
A thesis presented for the degree of Doctor of Philosophy, 2020.

Abstract

Aims:

Acetyl-coA Carboxylase 1 (ACC1) is an enzyme that couples glucose metabolism with de novo lipid synthesis in lipogenic tissues, by converting acetyl-CoA to malonyl-CoA. In beta cells, ACC1 plays a critical role in beta cell growth and insulin secretion[1]. However, very little is known about how ACC1 activity is regulated in beta cells. The aims of the current project were to 1) assess the role of the AMP-activated protein kinase phospho-site serine 79 (ACC1S79) in beta cell function and whole body glucose homeostasis; and 2) screen for novel phospho-sites that may regulate ACC1 activity in beta cells.

Methods:

(i) To investigate the functional role of the ACC1S79 phospho-site in beta cell function, we studied a mouse model with ACC1S79 mutated to alanine (ACC1S79A), which were obtained by crossing ACC1 double knock-in mice [2] with wild type mice to isolate the ACC1S79A point mutation. We assessed glucose homeostasis *in vivo* and insulin secretion from primary islets.

(ii) We purified the ACC1 protein from transformed INS1 beta cells following culture with different glucose concentrations, and performed quantitative unbiased phosphoproteomics to characterise ACC1 phospho-sites. Mass spectrometry (LC-MS/MS) was performed using a Q-Exactive MS, mascot searches run against the Uniprot data base, and data analysed using MaxQuant and Perseus. We generated phospho-specific antibodies against key phospho-sites

identified that exhibited a dynamic response to glucose stimulation, and used western blotting to investigate these sites further.

Results:

(i) Female ACC1S79A mice exhibited normal glucose homeostasis, whilst males showed lower fasting blood glucose, and a modest reduction in blood glucose during glucose and insulin tolerance tests compared to wild type littermate controls. No significant differences in fasted or glucose-stimulated serum insulin levels were found between the genotypes *in vivo*. Likewise, there was no significant change in insulin secretion from isolated ACC1S79A islets at baseline (2 mmol/l glucose) or in response to glucose-stimulation (7.5 and 20 mmol/l glucose).

(ii) Using quantitative phosphoproteomics, we identified twenty phospho-sites on the ACC1 protein in beta cells. ACC1S1215 was highly-phosphorylated at 2 mmol/l glucose, and showed a marked and highly significant reduction in phosphorylation in response to 15 mmol/l glucose, in contrast to the more modest changes in phosphorylation of ACC1S79. In contrast, phosphorylation of ACC1S25 and ACC1S49 was lower at basal glucose and increased upon glucose stimulation. Validation by western blotting confirmed that ACC1S1215 phosphorylation was highly-regulated by glucose, with ACC1S79 phosphorylation more subtle.

Conclusions:

Our data demonstrate that phosphorylation of ACC1S79 does not play a major role in insulin secretion *in vivo* or *ex vivo*. However, other phospho-sites identified by our phosphoproteomic screen may play a role in regulating ACC1 activity in beta cell and other ACC1-expressing tissues.

Table of Contents

CHAPTER 1 INTRODUCTION 23

Chapter 1.1 Glucose Homeostasis 23

Chapter 1.2 Diabetes Mellites 26

Chapter 1.3 Glucose Stimulated Insulin Secretion in Beta Cells 29

Chapter 1.4 Evidence Supporting the Role of Lipid Signalling Pathway in Insulin Secretion 32

Chapter 1.5 The Role of ACC1 in Insulin Secretion and Beta Cells Function. 33

Chapter 1.6 ACC Reaction, Structure, Isoforms, And Tissues Distribution 34

Chapter 1.6.1 ACC Reaction and Structures 34

Chapter 1.6.2 ACC Isoforms, Tissues Distribution and Cellular Localisation 37

Chapter 1.7 ACC Function and Role in Metabolic Diseases 38

Chapter 1.8 ACC1 Regulation 40

Chapter 1.8.1 Transcriptional Regulation 40

Chapter 1.8.2 Allosteric Regulation 42

Chapter 1.8.3 Post-Translational Modifications 42

Chapter 1.9 ACC1 Regulation in Pancreatic Beta Cells 47

Chapter 1.10 Hypothesis And Aims 48

CHAPTER 2 MATERIALS AND METHODS 49

Chapter 2.1 Animal Studies 49

Chapter 2.1.1 Animal Husbandry 49

Chapter 2.1.2 Animal Source 49

Chapter 2.1.3 Mice Genotyping 50

Chapter 2.2 In Vivo Metabolic Studies 51

Chapter 2.2.1 Fasting Blood Glucose and Body Weight Measurement 51

Chapter 2.2.2 Glucose Tolerance Test (GTT) 51

Chapter 2.2.3 Insulin Tolerance Test (ITT) 51

Chapter 2.2.4 Serum Insulin Assay *52*

CHAPTER 2.3 ISLETS ISOLATION AND CULTURE 54

Chapter 2.3.1 Islets Isolation *54*

Chapter 2.3.2 In Vitro Glucose Stimulated Insulin Secretion *55*

Chapter 2.3.3 Insulin Assay *56*

Chapter 2.3.4 Islets Lysis for Protein Extraction *56*

CHAPTER 2.4 RADIOACTIVE STUDIES 58

Chapter 2.4.1 Glucose Oxidation *58*

Chapter 2.4.1 De Novo Lipogenesis (DNL) *58*

CHAPTER 2.5 CELL CULTURE 60

Chapter 2.5.1 Thawing Cells *60*

Chapter 2.5.2 Passaging Cells *60*

Chapter 2.5.3 Counting Cells *62*

Chapter 2.5.4 Freezing Cells *63*

Chapter 2.5.5 Lipofectamine Transfection of Plasmids *63*

Chapter 2.5.6 siRNA Transfection *64*

CHAPTER 2.6 PROTEINS METHODS 65

Chapter 2.6.1 Cell Lysis and Proteins Extraction *65*

Chapter 2.6.2 Liver Proteins Extraction *65*

Chapter 2.6.3 BCA Assay *66*

Chapter 2.6.4 ACC1 and PC Pull Down *67*

Chapter 2.6.5 Gel Electrophoresis *69*

Chapter 2.6.6 Immunoblotting *70*

Chapter 2.6.7 Bands Densitometry *71*

CHAPTER 2.8 CRISPR-CAS9 71

CHAPTER 2.9 ANTIBODY GENERATION 72

CHAPTER 2.10 STATISTICAL ANALYSIS 72

CHAPTER 2.11 DIAGRAMS 73

CHAPTER 3 THE ROLE OF ACC1S79 IN BETA CELLS FUNCTION 74

Chapter 3.1 Introduction *74*

Chapter 3.2 Methods *76*

Chapter 3.2.1 Breeding Plan for ACCDKI Mice to Generate ACC1SKI Mouse Model *76*

Chapter 3.2.2 Phenotyping Pipeline for ACC1SKI mice *78*

Chapter 3.2.3 Chemicals preparation *78*

CHAPTER 3.3 RESULTS 79

Chapter 3.3.1 The Role of ACC1S79 in Glucose Homeostasis in Vivo *79*

Chapter 3.3.2 ACC1S79 as A Glucose Regulated Phospho-Site in Wild Type Islets: *85*

Chapter 3.3.3 Testing AMPK Activators Effect on Insulin Secretion and ACC1S79 Phosphorylation in Islets *87*

Chapter 3.3.4 The Role of ACC1S79 in Insulin Secretion Ex-Vivo *92*

Chapter 3.3.5 The Role of ACC1S79 in Glucose Oxidation and DNL *93*

CHAPTER 3.4 DISCUSSION 95

Chapter 3.4.1 Role Of ACC1S79 In Glucose Homeostasis In Vivo *95*

Chapter 3.4.2 The Role of ACC1S79 in Islets Function Ex Vivo *96*

Chapter 3.4.3 Conclusion *98*

CHAPTER 4 DEVELOPING A PHOSPHO-PROTEOMIC WORKFLOW TO STUDY ACC1 PHOSPHORYLATION 99

CHAPTER 4.1 INTRODUCTION 99

CHAPTER 4.2 METHODS 102

Chapter 4.2.1 In gel digestion *102*

Chapter 4.2.2 LC−MS/MS Analysis *102*

Chapter 4.2.3 Database Searching, MS Data Analysis and Computational analysis *103*

CHAPTER 4.3 RESULTS 104

Chapter 4.3.1 Optimising Bead Concentration for ACC1 Pull Down *104*

Chapter 4.3.2 Optimising ACC1 Pull Down to Decrease Contaminating Proteins *107*

Chapter 4.3.3 ACC1 Pull Down Reproducibility *110*

Chapter 4.3.4 Re-Optimising Bead Concentration to Increase Protein Coverage *112*

Chapter 4.3.5 Increasing LC-MS/MS Coverage of ACC1 Protein *113*

Chapter 4.3.6 Optimising Chymotrypsin Digestion *116*

Chapter 4.3.7 Chymotrypsin Digestion Reproducibility *118*

Chapter 4.3.8 Phospho-Profiling of PC *119*

CHAPTER 4.4 DISCUSSION: 121

CHAPTER 5 LABEL-FREE QUANTITATIVE PHOSPHOPROTEOMICS 122

CHAPTER 5.1 INTRODUCTION 122

CHAPTER 5.2 RESULTS 123

Chapter 5.2.1 Quantification of ACC1 and PC Phospho-Sites upon 30 Minutes of Glucose Treatment *123*

Chapter 5.2.2 Optimising ACC1 Phosphorylation Model *129*

Chapter 5.2.3 Validating the New ACC1 Phosphorylation Model *133*

Chapter 5.2.4 Quantification of ACC1 Phospho-Sites upon 120 Minutes of Glucose Treatment *136*

Chapter 5.2.5 Looking into other Types of PTMS *145*

CHAPTER 5.3 DISCUSSION 146

CHAPTER 6 PHOSPHOPROTEOMICS DATA VALIDATION 151

CHAPTER 6.1 INTRODUCTION 151

CHAPTER 6.2 METHODS 154

Chapter 6.2.1 Dot blot *154*

Chapter 6.2.3 Genomic DNA extraction *154*

CHAPTER 6.3 RESULTS 156

Chapter 6.3.1 Generation of ACC1S1215 and ACC1S49 Phosphospecific Antibodies *156*

Chapter 6.3.2 Validating the Glucose Response in ACC1S1215 and ACC1S49 in INS1 Cells. *159*

Chapter 6.3.3 Exploring the Dynamics of ACC1S1215 and ACC1S49 Phosphosites in Alpha Cell and the Liver. *162*

Chapter 6.3.4 Applying Bioinformatic Tools for Kinase Prediction and Test them Using ACC1S1215 and ACC1S49 Phosphospecific Antibodies *164*

Chapter 6.3.5 CRISPR-Cas9-Mediated Knockout of ACC1 in INS1 Cell *168*

Chapter 6.3.6 ACC1 Overexpression in INS1 Cell Line *174*

CHAPTER 6.4 DISCUSSION 178

CHAPTER 7 GENERAL DISCUSSION AND SUMMARY 184

CHAPTER 7.1 ACHIEVEMENT OF OBJECTIVES AND AIMS 184

CHAPTER 7.2 THE ROLE OF ACC1S79 IN BETA CELL FUNCTION 185

CHAPTER 7.3 PHOSPHOPROTEOMICS ANALYSIS OF ACC1 186

CHAPTER 7.4 FUTURE PERSPECTIVES 187

REFERENCES: 189

Table of Figures

Figure 1-1 Glucose homeostasis. Insulin is secreted from beta cells in response to high glucose levels. It stimulates glucose uptake in skeletal muscles and adipose tissues, and stimulates glycogen storage and lipogenesis, respectively. In the liver, insulin inhibits gluconeogenesis and stimulates glycogenesis. Glucagon secreted in response to low blood glucose levels. It promotes glycogenolysis and stimulates gluconeogenesis in the liver to increase endogenous blood glucose. The net effect is to maintain a narrow range of blood glucose level. 25
Figure 1-2 Glucose-stimulated insulin secretion. Pyruvate, the end product of glycolytic pathway, is converted into acetyl-CoA by PDH, leading eventually to ATP production via oxidative phosphorylation. Elevation of the ATP/ADP ratio leads to ATP-dependent K^+ channel closure, cell membrane depolarisation, opening voltage-gated calcium channels, fusion of the insulin-containing vesicles with the cell membrane and secretion of insulin into the extracellular fluid by exocytosis. Alternatively, Pyruvate is carboxylated by PC to form Oxaloacetate, excess citrate in the Krebs cycle will be transported to the cytosol and converted to acetyl-CoA, which is then carboxylated by ACC1 to produce malonyl-CoA. 31
Figure 1-3 ACC1 structure and reaction. Eukaryotic ACC consist of four domains; biotin carboxylase (BC), biotin carboxyl carrier protein (BCCP), carboxyl transferase (CT) domains, and a non-catalytic central domain region (CD), which together bridge the BC and CT domain. The overall reaction of ACC involves a two-step reaction; the first one is the ATP-dependent carboxylation of biotin with bicarbonate, the carboxyl group is transferred from biotin to acetyl-CoA to form malonyl-CoA in the second reaction. Source: http://aralip.plantbiology.msu.edu/hehos/2 35
Figure 1-4 ACC1 sequence and different domains, Rattus norvegicus (Rat). 36
Figure 1-5 Overall structure of rat ACC1. The structure of ACC1 starting from L847 amino acid (PDB 6g2d.1). The location of ACC1S1215 and ACC1S1200 are shown. The structure figure was produced with PyMOL software (www.pymol.org) 46
Figure 2-1 ACC1 pull down protocol principle and workflow. (A) ACC1 pull down principle (B) ACC1 pull down protocol workflow, adopted from (abramagnetic beads) 68
Figure 3-1 Breeding strategy for generation of ACC1SKI model. Mice that were homozygous for both mutation (ACC1S79A, ACC2S212A) were crossed with wild type mice to generate heterozygous mice for both mutations. Then, we crossed heterozygous F2 mice; from which we crossed mice that were heterozygous for ACC1S79A and wild type for ACC2S212A to generate mice with ACCS79A homozygous mutation and their littermate control. After 9 months of breeding cycles, we generated 5 cohorts of mice in total to reach minimum n= 12 per genotype per sex. 77
Figure 3-2 Phenotyping pipeline for ACC1SKI mice. 78
Figure 3-3 Body weight, fed blood glucose and fasting blood glucose in ACC1SKI mouse model. (A,B) Body weight at 12 weeks of age in the males(n=16 ACC1Wt mice and 12 ACC1SKI) and females (n=13 ACC1Wt mice and 14 ACC1SKI) **(C,D)** Fed blood glucose in males (n=12 ACC1Wt mice and 12 ACC1SKI) and females (n=4 ACC1Wt mice and 6 ACC1SKI) at 12 weeks of age **(E,F)** Fasting blood glucose (16-hours fast) in males (n=16 ACC1Wt mice and 12 ACC1SKI) and females (n=13 ACC1Wt mice and 14 ACC1SKI) at 12 weeks of age **(G,H)** Fasting blood glucose (6-hours fast) in males (n=16 ACC1Wt mice and 12 ACC1SKI) and females (n=13 ACC1Wt mice and 14 ACC1SKI). Data are presented as mean ± SEM. *$p<0.05$ (unpaired two-tailed t test). 80

Figure 3-4 Glucose tolerance test in ACC1SKI mice.(A) GTT at 12 weeks of age in the males after 16 hours of fasting (n=16 ACC1Wt mice and 12 ACC1SKI) **(B)** GTT at 12 weeks of age in the males after 6 hours of fasting (n=16 ACC1Wt mice and 12 ACC1SKI) **(C)** GTT at 12 weeks of age in the females after 16 hours of fasting (n=13 ACC1Wt mice and 14 ACC1SKI**) (D)** GTT at 12 weeks of age in the females after 6 hours of fasting (n=4 ACC1Wt mice and 6 ACC1SKI). Data are presented as mean ± SEM. (two-way ANOVA with Bonferroni multiple comparisons test for time plots, unpaired two-tailed t tests for bar charts)..... 82
Figure 3-5 Circulating insulin and insulin tolerance test in ACC1SKI mice. (A,B) Circulating insulin measured at fasting state (16-hours fast) and after 30 minutes of glucose injection in males (n=13 ACC1Wt mice and 10 ACC1SKI**)** and females (n=10 ACC1Wt mice and 8 ACC1SKI**)** at 12 weeks of age (**C,D)** ITT for males (n=12 ACC1Wt mice and 9 ACC1SKI) and females (n=13 ACC1Wt mice and 14 ACC1SKI). Data are presented as mean ± SEM(two-way ANOVA with Bonferroni multiple comparisons test for time plots, unpaired two-tailed t tests for bar charts).. 84
Figure 3-6 ACC179 phosphorylation in response to glucose in wild type islets compared to the liver. Isolated wild type islets were treated with low (2 mmol/l) and high (20 mmol/l) glucose conditions for 1 hour. Wild type mice (C57BL6 background) were fasted overnight, then liver was collected after injecting with glucose (2g/kg) or PBS. 30 μg of proteins was loaded in the gel for each condition. Commercial p-ACC1S79 antibody (Cell Signalling 11818), molecular weight: 269 kDa, was used at 1:1000 dilution, B-Actin (Cell Signalling 8457), molecular weight: 42 kDa, was used as a loading control at 1:100 dilution, and a rabbit HRP conjugated secondary antibody (Cell Signalling 8457) was used at 1:5000 dilution. 86
Figure 3-7 The potential regulatory role of AMPK on ACC1 activity and insulin secretion. 88
Figure 3-8 Testing metformin effect on ACC1S79 phosphorylation and insulin secretion. (A) Western blot analysis of islets treated with indicated metformin doses acutely (for two hours) and chronically (for 24 hours). 30 μg of proteins was loaded in the gel for each condition. p-ACC1S79 antibody (Cell Signalling 11818), molecular weight: 269 kDa, was used at 1:1000 dilution. p-AMPK antibody (Cell Signalling 2535), molecular weight: 64 kDa kDa, was used at 1:100 dilution, and a rabbit HRP conjugated secondary antibody (Cell Signalling 8457) was used at 1:5000 dilution. Note: the band in the middle (lane 6) is a leak from the adjacent lane. 89
Figure 3-9 Testing AICAR and PFZ compound effects on ACC1S79 phosphorylation and insulin secretion. (A) Western blot analysis of islets treated with different AMPK activators: AICAR (500 μM), Metformin (500 μM), and PFZ compounds (50 μM) for 1 hour, and quantification of band densities using image J (which shows protein levels in each sample relative to the mean control signal. 30 μg of proteins was loaded in the gel for each condition. p-ACC1S79 antibody (Cell Signalling 11818), molecular weight: 269 kDa, was used at 1:1000 dilution. p-AMPK antibody (Cell Signalling 2535), molecular weight: 64 kDa kDa, was used at 1:100 dilution, and a rabbit HRP conjugated secondary antibody (Cell Signalling 8457) was used at 1:5000 dilution. Tubulin was used as a loading control, molecular weight 55 kDa. 91
Figure 3-10 GSIS in ACC1SKI islets. Data are presented as mean ± SEM. *p<0.05, **p<0.01 and ***p<0.001. Analysis done using two-way ANOVA with Bonferroni multiple comparisons tests. n > 10 batches of islets collected from 10 independent mice. 92
Figure 3-11 De novo lipogenesis and glucose oxidation in ACC1SKI islets. (A) Flux of d-[U-14C] glucose tracer into total lipid pools (B) flux into aqueous pool (C)glucose oxidation. *p<0.05, **p<0.01 and ***p<0.001. Analysis done using two-way ANOVA with Bonferroni multiple comparisons tests. n > 4 batches of islets collected from 4 independent mice. 94

Figure 4-1 ACC1 pull down protocol principle and workflow. (A) ACC1 pull down principle (B) ACC1 pull down protocol workflow, adopted from (abramagnetic beads) (C) Separation of the elute by gel electrophoresis, followed by in gel digestion and LC-MS/MS analysis..... 101
Figure 4-2 ACC1 pull down using different beads volume. (A) 1 mg of INS1 cells protein lysates were incubated overnight at 4ºC with escalating concentrations of magnetic beads, the elutes then were analysed by gel electrophoresis and stained with Coomassie blue stain (B) Western blot analysis of the elute was used to confirm if ACC1 is present in the elute, 30 μg of proteins was loaded in the gel for each condition. ACC1S79 antibody, molecular weight: 269 kDa, was used at 1:1000 dilution and a rabbit HRP conjugated secondary antibody was used at 1:5000 dilution. (C) Proteins are first converted into peptides by proteolytic digestion, the resulting peptide mixture is then separated by LC and ionized by electrospray before entering the mass spectrometer (top spectrum). A full MS spectrum is acquired for the peptides that are eluted from the LC column into the gradient (middle spectrum). The tandem-MS (MS/MS) spectrum of the peptide ion of interest (bottom spectrum). D) Mascot software search for band 3. 106
Figure 4-3 Optimising ACC1 pull down to decrease the level of contaminants. (A) Coomassie blue staining of the gel (B) Western blot for ACC1 protein, 30 μg of proteins was loaded in the gel for each condition. ACC1S79 antibody, molecular weight: 269 kDa, was used at 1:1000 dilution and a rabbit HRP conjugated secondary antibody was used at 1:5000 dilution (C) Mascot software for SDS washing buffer condition (D) ACC1 phospho-sites detected in this experiment. 109
Figure 4-4 ACC1 pull down reproducibility. (A&B) Coomassie blue staining of the gel and western blot for ACC1 protein for 2 consecutive experiments (3 replicates in each experiment). 30 μg of proteins was loaded in the gel for each condition. ACC1S79 antibody, molecular weight: 269 kDa, was used at 1:1000 dilution and a rabbit HRP conjugated secondary antibody was used at 1:5000 dilution (C) Mascot software search for sample 2 from the first experiment (D) Mascot software search for sample 2 from the second experiment. 111
Figure 4-5 Re-optimising beads concentration. (A) Coomassie blue staining for elutes using different beads concentrations (B) Coomassie blue staining for flow through (Ft) and washes (W). 112
Figure 4-6 ACC1 pull down scale up and double digestion. (A) Coomassie blue staining of the gel, one band and a half were used for each trypsin and chymotrypsin digestion (B) Mass spectrometry chromatographs for trypsin and chymotrypsin digestion of ACC1 (C) Mascot software search for trypsin digestion (D) Mascot software search for chymotrypsin trypsin digestion (E) ACC1 phospho-sites detected in the band digested with trypsin. 115
Figure 4-7 Optimising Chymotrypsin digestion. (A) Mascot search for trypsin digestion of ACC1 protein (B) Mascot search for chymotrypsin digestion of ACC1 protein at 25°C (C) Mascot search for chymotrypsin digestion of ACC1 protein at 37°C. 117
Figure 4-8 Chymotrypsin digestion reproducibility. (A) Sequence coverage for 3 biological replicates (B) Phoshosites detected in these replicates. 118
Figure 4-9 PC pull down and phospho-profiling. (A) Coomassie blue staining of the gel (B) Mascot search for PC band. 120
Figure 5-1 Quantitative phosphoproteomics workflow. (A) Function of INS1 cells was evaluated with 30 min GSIS (B) Schematic demonstration of the experimental workflow applied to analyse ACC1 phospho-sites (C) Coomassie blue staining of the gel for ACC1 pull down from INS1 cells(D) Western blot for ACC1S79 and total ACC. 30 μg of proteins was loaded in the gel for each condition. p-ACC1S79 antibody, molecular weight: 269 kDa, was used at 1:1000 dilution,

total ACC1 antibody was used as a loading control and a rabbit HRP conjugated secondary antibody was used at 1:5000 dilution (E) Western blot using pan-malonylation antibody. 124
Figure 5-2 Quantification of ACC1 phospho-sites upon 30 minutes of glucose stimulation in INS1 cells. (A) Volcano plot of quantified phospho-sites in ACC1 band digested with trypsin (B) Volcano plot of quantified phospho-sites in ACC1 band digested with chymotrypsin. The dash lines represent a *p-value* of 0.05 126
Figure 5-3 Quantification of PC phospho-sites upon 30 minutes of low glucose (2 mmol/l) or high glucose (15 mmol/l) treatment in INS1 cells. (A) Volcano plot of quantified phospho-sites in PC band digested with trypsin (B) Volcano plot of quantified phospho-sites in PC band digested with chymotrypsin. The dash lines represent a *p-value* of 0.05 128
Figure 5-4 Optimising the pre-incubation step in INS1 cells. (A) Experimental design for the basal (2 mmol/l glucose) and high model (11mmol/l glucose) in INS1 cells (B) Western blot for ACC1S79 phosphorylation to test the difference in phosphorylation between two models for the pre-incubation step: basal model (2 mmol/l glucose) and high model (11mmol/l glucose), 30 μg of proteins was loaded in the gel for each condition. p-ACC1S79 antibody, molecular weight: 269 kDa, was used at 1:1000 dilution, total ACC1 antibody was used as a loading control and a rabbit HRP conjugated secondary antibody was used at 1:5000 dilution (C) Quantification of ACC1S79 phosphorylation in both models using image J software. 130
Figure 5-5 ACC1S79 phosphorylation and dephosphorylation timeline in INS1 cells. (A) ACC1 phosphorylation experimental design (B) Western blot for ACC1S79 phosphorylation at different time points (C) ACC1 dephosphorylation experimental design (D) Western blot for ACC1S79 dephosphorylation at different time points. (E) Quantification of ACC1S79 phosphorylation and dephosphorylation using image J plotted against time points. 132
Figure 5-6 Evaluating the modified ACC1 phosphorylation model in INS1 cells. (A)Western blot for ACC1S79 phosphorylation and pan-p-(Ser/Thr) upon 60 minutes of low glucose (2mmol/l) or high glucose (15mmol/l) treatment (B) Western blot for ACC1S79 phosphorylation and pan-p-(Ser/Thr) upon 120 minutes of low glucose (2mmol/l) or high glucose (15mmol/l) treatment (C) ACC1 pulldown followed by western blot for pan-p-(Ser/Thr). 30 μg of proteins was loaded in the gel for each condition. p-ACC1S79 antibody, molecular weight: 269 kDa, was used at 1:1000 dilution, total ACC1 antibody was used as a loading control and a rabbit HRP conjugated secondary antibody was used at 1:5000 dilution. Quantification of ACC1S79 phosphorylation in both models using image J software. 135
Figure 5-7 Label-free quantification upon 120 minutes of low glucose (2mmol/l) or high glucose (15mmol/l) treatment in INS1 cells: experiment's time line..... 136
Figure 5-8 Pearson correlation coefficients. Scatter plots showing Pearson correlation coefficients between the different biological replicates for samples digested with chymotrypsin (A) and trypsin (B). 137
Figure 5-9 Quantification of ACC1 phospho-sites upon 120 minutes of low glucose (2mmol/l) or high glucose (15mmol/l) treatment in samples digested with chymotrypsin. A) Volcano plot for ACC1 phosphopeptides detected in the band digested with chymotrypsin (B) Volcano plot of the corresponding phospho-sites. The dash lines represent a *p*-value of 0.05 141
Figure 5-10 Quantification of ACC1 phospho-sites upon 120 minutes of low glucose (2mmol/l) or high glucose (15mmol/l) treatment in samples digested with trypsin. (A) Volcano plot for ACC1 phosphopeptides detected in the band digested with chymotrypsin (B) Volcano plot of the corresponding phospho-sites. The dash lines represent a *p*-value of 0.05 142

Figure 5-11 Representative spectra of ACC1glucose responsive phospho-sites. (A) ACC1S25 (B) ACC1S49 (C) ACC1S79 (D) ACC1S1215. 144
Figure 5-12 ACC activity measured across four different conditions in Hardie et al. study[94]. 147
Figure 5-13 Sequence alignment between ACC1 and ACC2 S79 and S1215. (A) rat (B) mouse (C) human. Sequence alignment was performed using https://www.uniprot.org 149
Figure 6-1 Generation of ACC1S49 and ACC1S1215 phospho-specific antibodies. SDS-PAGE protein gels showing elution of Igg chains. For each antibody two rabbits were immunised with site specific phospho-peptide, two rounds of purifications have been carried out using by immunoaffinity chromatography and nine fractions have been collected. Each fraction is assigned with an identification code consisting of 2 numbers; the first one is the purification round number and the second one is the fraction number (for example 1.3: purification round number 1, fraction number 3). Source: (DC Biosciences, Dundee) 157
Figure 6-2 Testing different fractions for ACC1S49 and ACC1S1215. Western blot analysis of cells treated with the corresponding condition for two hours. L: low glucose (2 mmol/l), H: high glucose (15 mmol/l), A: AICAR (500 μM). Fraction 1.8 for ACC1S49 (A) and fraction 1.8 & 1.9 for ACC1S1215 (B) clearly show the glucose response in these sites.4-12% gradient gel was used, primary antibodies were diluted 1:1000, rabbit HRP conjugated secondary antibody (Cell Signalling 8457) was used at 1:5000. 158
Figure 6-3 Validating ACC1S1215 and ACC1S49 antibodies and testing the glucose effect.(A) dot blot assay for ACC1S1215 (B) dot blot assay for ACC1S49 (C) western blot for cell treated with low (L) (2 mmol/l), high (H) (15 mmol/l) and 500 μM AICAR (A) for two hours.(D) western blot performed after ACC1 pulldown for cell treated with low (L) (2 mmol/l) and high glucose (H) (15 mmol/l). 4-12% gradient gel was used, primary antibodies were diluted 1:1000, rabbit HRP conjugated secondary antibody (Cell Signalling 8457) was used at 1:5000. 161
Figure 6-4 ACC1 phosphorylation profile in the liver and alpha cells. (A) Time line for ACC1S79, ACC1S1215 and ACC1S49 phosphorylation in the liver in response to glucose. 10-week old male mice were fasted for 16 hours then injected with normal saline (NS) or glucose (Glc). The livers were then harvested 15, 30, 60, and 120 minutes post injection. Tubulin was used as a loading control for each membrane. (B) ACC1 phosphorylation profile in alpha cell line. Alpha cell line was treated with 500 μM AICAR (A), low (L) (2 mmol/l) and high (H) (15 mmol/l) glucose condition for two hours. 4-12% gradient gel was used, primary antibodies were diluted 1:1000, rabbit HRP conjugated secondary antibody (Cell Signalling 8457) was used at 1:5000. 163
Figure 6-5 ACC1S29 in INS1 cell line. (A)Western blot using phospho-CK2 substrates antibody for purified ACC1 from INS1 cells treated with low (L) (2 mmol/l) and high glucose (H) (15 mmol/l) for two hours, total CK2 antibody was used as a loading control. 4-12% gradient gel was used, primary antibodies were diluted 1:1000, rabbit HRP conjugated secondary antibody (Cell Signalling 8457) was used at 1:5000. (B) The role of CK2 in GSIS: cells were transfected with siCK2 or siControl; GSIS was measured following 48 hours of transfection. Data are presented as mean ± SEM. *p<0.05, **p<0.01 and ***p<0.001 (two-way ANOVA with Bonferroni multiple comparisons test). 167
Figure 6-6 CRISPR/Cas9-mediated knock out of ACC1 in INS1 cells. (A) Schematic diagram of ACC1 gene. (B) Targeting ACC1C domain using 4 different gRNA. (C) ACC1 mutant gene is 423 bp shorter than ACC1 wild type gene. Diagrams are created using Snap gene viewer..... 169

Figure 6-7 CRISPR/Cas9-mediated knock out of ACC1 in INS1 cells. (A) Workflow for generation of ACC1KO INS1 cell line. (B) PCR analysis of INS1 cells transfected with four different combinations of gRNA (1.5% gel stained with Midori green stain and visualised with UV light. (C) Re-genotyping cells transfected with gRNA (2+4) to confirm the result and to sequence the bands. 171
Figure 6-8 Single cells sorting to generate genome-targeted monoclonal cell colonies. (A) Single cells sorting using flow cytometry (B) Colonies seven days after sorting (C) Colonies fourteen days after transfection (D) PCR analysis of seventeen colonies for genotyping (E) Western blotting to assess ACC1 expression on the protein level. (B & C: phase contrast imaging using Evos 4300 microscope (AMF 4300). Scale bar: 200 μm. 173
Figure 6-9 ACC1 overexpression using lipofectamine 2000 and lipofectamine 3000. (A) Cells expressing GFP plasmid transfected with lipofectamine 3000 visualised by fluorescence microscopy 24 hours after transfection (B) Cells expressing GFP plasmid transfected with lipofectamine 2000 visualised by fluorescence microscopy 24 hours after transfection (C) Western blot to assess transfection efficiency on the protein level for cells transfected with lipofectamine 3000. 4-12% gradient gel was used, primary antibodies were diluted 1:1000, rabbit HRP conjugated secondary antibody (Cell Signalling 8457) was used at 1:5000. (A & B visualised by Evos 4300 microscope (AMF 4300)). Scale bar: 400 μm. 175
Figure 6-10 Optimising ACC1 overexpression protocol. (A) Cells expressing GFP plasmid transfected with lipofectamine 3000 using DNA: lipid ratio of 1:3 visualised by fluorescence microscopy 24 hours after transfection (B) Cells expressing GFP plasmid transfected with lipofectamine 2000 using DNA: lipid ratio of 1:3 visualised by fluorescence microscopy 24 hours after transfection (C) Western blot to assess transfection efficiency on the protein level for cells transfected with lipofectamine 2000. 4-12% gradient gel was used, primary antibodies were diluted 1:1000, rabbit HRP conjugated secondary antibody (Cell Signalling 8457) was used at 1:5000. (A & B visualised using Evos 4300 microscope (AMF 4300). Scale bar: 400 μm. 177
Figure 6-11CRISPR/Cas9–gRNA RNP labelling and cell transfection. Adopted from Nasri et.al 2019 183

Table of Tables

Table 5-1 ACC1 phospho-sites detected upon 30 minutes of low glucose (2 mmol/l) or high glucose (15 mmol/l) treatment. 125

Table 5-2 PC phospho-sites detected upon 30 minutes of low glucose (2 mmol/l) or high glucose (15 mmol/l) treatment. 127

Table 5-3 ACC1 Phospho-sites detected upon 120 minutes of low glucose (2mmol/l) or high glucose (15mmol/l) treatment. List of ACC1 phosphosites identified via quantitative phosphoproteomics: The location of each site, localisation probabilities and identification scores (characterised using MaxQuant search software)..... 139

Table 5-4 ACC1 Hydroxylation sites detected upon 120 minutes of low glucose (2mmol/l) or high glucose (15mmol/l) treatment. List of ACC1 Hydroxylation sites identified via quantitative proteomics: The location of each site, localisation probabilities and identification scores (characterised using MaxQuant search software)..... 145

Table 6-1 Bioinformatics tools for kinase prediction 165

Abbreviation List

ACC1	Acetyl CoA Carboxylase 1
ACC2	Acetyl CoA Carboxylase 2
T2D	Type 2 Diabetes
INSR	Insulin Receptors
ATP	Adenosine Triphosphate
GLUT4	Glucose Transporter 4
NEFA	Non-Esterified Fatty Acid
WHO	World Health Organisation
T1D	Type 1 Diabetes Mellitus
NICE	National Institute for Health and Care Excellence guidelines
GSIS	Glucose-Stimulated-Insulin-Secretion
GCK	Glucokinase
PDH	Pyruvate Dehydrogenase Enzyme
GLUT 2	Glucose Transporter 2
PC	Pyruvate Carboxylase
ACLY	ATP-Citrate Lyase
LC-CoA	Long Chain Fatty Acyl-Coa
CPT1	Carnitine Palmitoyl Transferase1
PAA	Phenylacetic Acid
TOFA	5-(Tetradecyloxy)-2-Furoic Acid
BC	Biotin Carboxylase
BCCP	Biotin Carboxyl Carrier Protein

CT	Carboxyl Transferase
CD	Central Domain Region
FAS	Fatty Acid Synthase
DNL	De Novo Lipogenesis
SREBP1c	Sterol Regulatory Element Binding Protein 1c
ChREBP	Carbohydrate Response Element-Binding Protein
PTMs	Post-Translational Modifications
AMPK	AMP-Activated Protein Kinase
LKB1	Liver Kinase B1
CAMKK2	Ca^{2+}/Calmodulin-Dependent Kinase Kinase-B
TAK1	TGFβ-Activated Kinase1
DKI	Double Knock In
NAFLD	Non-Alcoholic Fatty Liver Disease
HFD	High-Fat Diet
PKA	Protein Kinase A
AICAR	5-Aminoimidazole-4-Carboxamide Ribonucleotide
ASPA	Animals Scientific Procedures Act
PCR	Polymerase Chain Reaction
i.p	Intraperitoneally
GTT	Glucose Tolerance Test
ITT	Insulin Tolerance Test
MSD kit	Meso Scale Discovery Kit
BSA	Bovine Serum Albumin

FBS	Fetal Bovine Serum
BCA	Bicinchoninic Acid Assay
ECL	Enhanced Chemiluminescence
PFZ	6-Chloro-5-[4-(1hydroxycyclobutyl)Phenyl]-1H-Indole-3Carboxylic Acid
LC-MS/MS	Label-Free Liquid Chromatography-Tandem Mass Spectrometry
MS	Mass Spectrometry
ACN	Acetonitrile
AB	Ammonium Bicarbonate
TCEP	(Tris(2-Carboxyethyl)Phosphine)
CAA	Chloroacetamide
FA	Formic Acid
HCD	Higher-Energy Collisional Dissociation
DMSO	Dimethyl sulfoxide
AGC	Automatic Gain Control
FDR	False Discovery Rate
LTQ	Linear Trap Quadrupole
S	Serine
T	Threonine
Y	Tyrosine
K	Lysine
M	Methionine
SDS	Sodium Dodecyl Sulphate

PAGE	Polyacrylamide Gel Electrophoresis
SDM	Site Directed Mutagenesis
aTC9	Alpha Cell
CaM-2	Ca2+/Calmodulin-Dependent Protein Kinase
GSK3	Glycogen Synthase Kinase 3
CK2	Casein Kinase 2

Chapter 1 Introduction

Chapter 1.1 Glucose Homeostasis

Blood glucose concentrations are tightly controlled to prevent hypoglycaemia or hyperglycaemia, and associated complications[3]. This is achieved by a complex interaction between different hormones and neuropeptides (secreted from pancreas, brain and intestine), and other tissues (e.g. liver, adipose and muscle tissues). Disruption of this network may lead to metabolic disorders such as type 2 diabetes mellitus (T2D)[4].

The pancreas is a key player in this network, releasing insulin, a potent glucose-lowering hormone, from beta cells and the counter-regulatory hormone glucagon from alpha cells[5].

Insulin is an anabolic hormone secreted in response to elevated blood glucose level[6]. It exerts its actions on peripheral tissues by binding to insulin receptors (INSR). INSR consists of two extracellular α and two intracellular β subunits conferring tyrosine kinase activity. Insulin binds to the α subunit, resulting in conformational change enabling adenosine triphosphate (ATP) to bind to β subunit; triggering phosphorylation of the β subunit that initiates a cascade of cellular phosphorylation reactions that mediate further cellular actions of insulin[7].

In skeletal muscle, the source of energy is highly dependent on the availability of energy substrates and the energy requirements. Skeletal muscles are able to utilise both glucose and fatty acids as a source of ATP production depending on the metabolic state of an individual. During a fed state, when plasma insulin levels are elevated in response to high glucose level, insulin stimulates glucose uptake via translocation of glucose transporter 4 (GLUT4) to the plasma membrane, and storage of excess glucose as glycogen[8]. Glucose cannot be released from skeletal muscles into the blood stream, rather it is utilised as a primary source of energy during periods of muscle activity.

Similarly, in adipose tissue, insulin stimulates glucose uptake via the GLUT4 transporter. In the liver, insulin inhibits gluconeogenesis (glucose production) and stimulates glycogenesis (glycogen synthesis)[9,10]. Insulin also strongly affects lipid metabolism: it increases lipid synthesis in liver and adipocytes while inhibiting lipolysis and the release of circulating non-esterified fatty acid (NEFA)[11].

In contrast, glucagon is a catabolic hormone secreted in response to low blood glucose level. It promotes glycogenolysis (glycogen breakdown) and stimulates gluconeogenesis in the liver to increase endogenous blood glucose[12].

Under physiological conditions, the net effect of the opposing and balanced actions of insulin and glucagon is to maintain a strict and narrow range of blood glucose level of 4-6 mmol/l [4,13] (figure 1-1).

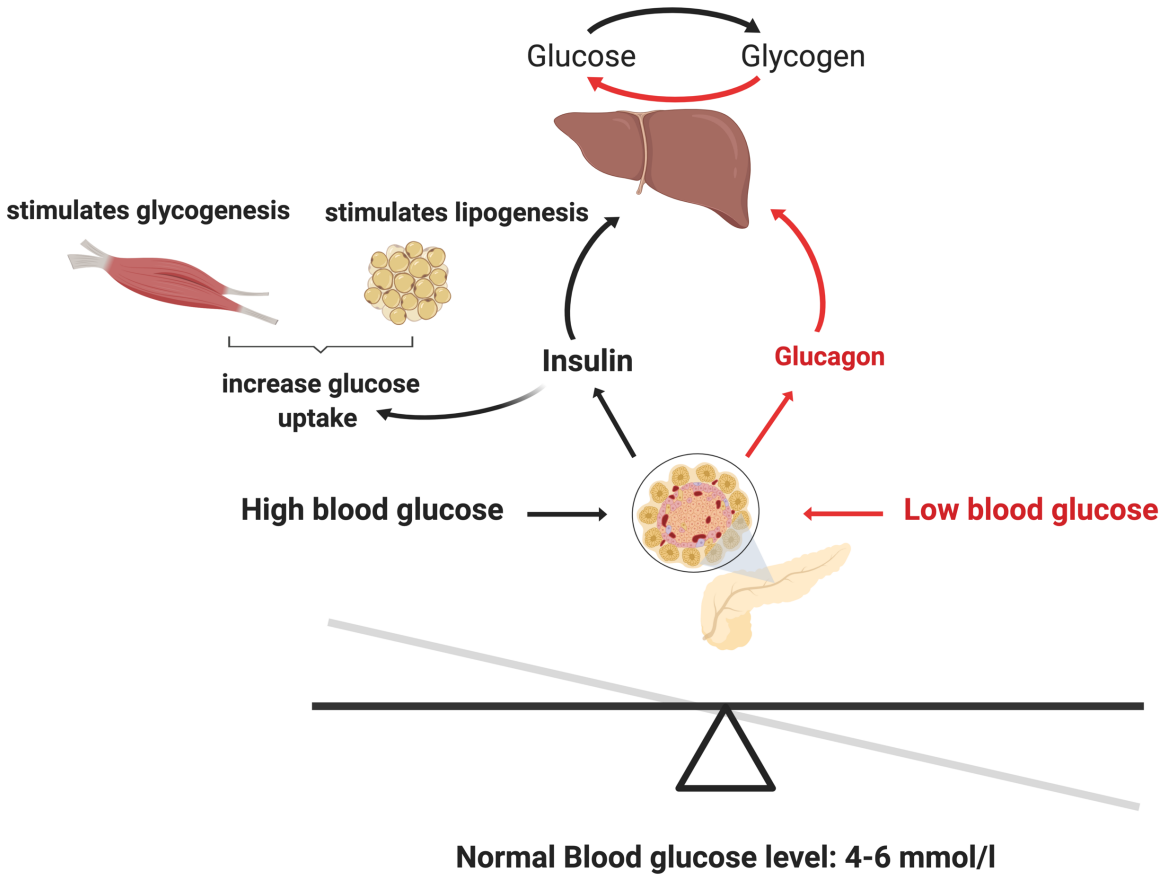


Figure 1-1 Glucose homeostasis. Insulin is secreted from beta cells in response to high glucose levels. It stimulates glucose uptake in skeletal muscles and adipose tissues, and stimulates glycogen storage and lipogenesis, respectively. In the liver, insulin inhibits gluconeogenesis and stimulates glycogenesis. Glucagon secreted in response to low blood glucose levels. It promotes glycogenolysis and stimulates gluconeogenesis in the liver to increase endogenous blood glucose. The net effect is to maintain a narrow range of blood glucose level.

Chapter 1.2 Diabetes Mellites

Diabetes mellitus is a metabolic disease characterised by chronic elevation of blood glucose levels (hyperglycaemia), caused by a defect in insulin secretion and/or insulin action[14]. Even though hyperglycaemia is the main feature of diabetes, metabolic disturbances are more extensive and include abnormal carbohydrate, fat and protein metabolism[15], leading to long term and devastating complications including neuropathy, nephropathy, retinopathy, cardiovascular disease, stroke, and peripheral artery disease[16].

According to the World Health Organisation (WHO), diabetes prevalence has been steadily increasing over the past few decades with massive health-care and economic costs. Worldwide, an estimated 422 million adults over the age of 18 years were diagnosed with diabetes in 2014 compared to 108 million in 1980.

Diabetes and its complications cause substantial problems to health systems and national economies[17]. For example, in the United Kingdom diabetes accounts for about 10% of the NHS budget. Over the next 20 years the overall costs of diabetes are predicted to account for 17% of the entire NHS budget. These figures do not include indirect costs of diabetes complications (e.g. blindness, amputation) in social care and in the reduced work productivity which has an estimated cost of £ 9 billion. (DiabetesUK figures, www.diabetes.org.uk).

Based on pathogenic processes involved in the development of diabetes, it can be categorised into two main groups: Type 1 diabetes mellitus (T1D) and Type 2 diabetes mellitus (T2D). Understanding the aetiology of each of them is essential to improve the treatment and management of this disease[15].

T2D is the most common form of diabetes, accounting for more than 90% of the cases and is characterised by a combination of insulin resistance and loss of beta cell function[14].

The aetiology of T2D has been studied extensively, with many studies showing a strong genetic component in T2D that interacts with environmental factors like obesity and sedentary lifestyle[18]. During insulin resistance, a normal or elevated insulin level produces a diminished biological response (reduced sensitivity to insulin mediated glucose clearance)[13]. Insulin resistance arises as a consequence of obesity, a sedentary lifestyle, genetics and ageing[19]. During insulin resistance, beta cells often attempt to compensate by secreting more insulin to maintain normal glucose levels leading to compensatory hyperinsulinemia[20]. Hyperglycaemia results when insulin secretion is unable to compensate for insulin resistance[21,22]. Ultimately, there is a progressive loss of pancreatic beta cell function in T2D; resulting in insulin deficiency[23]. The metabolic dysfunctions of T2D, including the increase in plasma glucose and NEFA concentrations, have been shown to produce widespread tissues damage and worsening of islet β-cell function[24].

There are various treatment options for T2D, according to The National Institute for Health and Care Excellence guidelines (NICE) lifestyle and dietary modifications are considered the cornerstone in treating T2D, especially in obese patients. Metformin, a therapeutic agent that reduces insulin resistance[25], is the first-line drug treatment that is used to normalise metabolic abnormalities. Treatment with combinations of medicines including (e.g. sulfonylureas, GLP1 mimetics, SGLT-2 inhibitors or DPPIV inhibitors) is used when metabolic abnormalities have not improved with metformin alone. Due to the progressive nature of T2D, eventually, most patients eventually require insulin replacement therapy[26].

T1D is less common than T2D (accounting for less than 10% of cases), resulting from autoimmune destruction of insulin-secreting pancreatic beta cells, leading to significant loss of beta cell mass and profound loss of insulin secretion: therefore, T1D is almost always treated with insulin[27].

Chapter 1.3 Glucose Stimulated Insulin Secretion in Beta Cells

Glucose-stimulated-insulin-secretion (GSIS) in beta cells requires the glucose to be metabolised and generate downstream signals that stimulate insulin secretion, ensuring that insulin secretion is proportional to glucose levels to avoid excessive insulin secretion and hypoglycaemia risk[23].

Beta cells express glucose transporter 2 (GLUT 2), that has a uniquely low affinity for glucose (Km~17 mmol/l)[28]. Glucokinase (GCK), a rate-limiting enzyme in the glycolytic pathway with a low Km for glucose (~0.15 mmol/l)[29], phosphorylates glucose to glucose-6-phosphate, thus committing it to further metabolism in the cell[30]. The passive movement of glucose across the plasma membrane and phosphorylation ensure that intracellular environment of beta cells can accurately sense the blood glucose level[31]. Once inside the cells, Glucose-6-phosphate undergoes subsequent reactions in the glycolytic pathway leading ultimately to the generation of Pyruvate[32] (figure 1-3).

Pyruvate is transported into the mitochondria where it is converted into acetyl-CoA by the pyruvate dehydrogenase enzyme (PDH), a key Krebs cycle intermediate which leads eventually to ATP production via oxidative phosphorylation[33]. Elevation of the ATP/ADP ratio leads to K^+_{ATP} channel closure[34], causing cell membrane depolarisation, thus opening voltage-gated calcium channels resulting in calcium influx which stimulates fusion of the insulin-containing vesicles with the cell membrane and secretion of insulin into the extracellular fluid by exocytosis[35]. This pathway, often called the K^+_{ATP} channel-dependent pathway, is considered to be the major triggering event for glucose-stimulated insulin secretion[36](figure 1-3).

Alternatively, pyruvate enters the mitochondrial Krebs cycle through a second mechanism distinct from PDH (figure 1-3). Pyruvate is carboxylated by Pyruvate Carboxylase (PC) to form Oxaloacetate, an anaplerotic reaction that replenishes Krebs cycle intermediates and provides

substrates for anabolic pathways[37]. Upon glucose stimulation, excess citrate in the Krebs cycle will be transported to the cytosol (cataplerosis) and converted to acetyl-CoA by ATP-Citrate lyase (ACLY). Acetyl-CoA is then carboxylated by Acetyl-CoA Carboxylase 1 (ACC1) to produce malonyl-CoA, the first committed step of de novo lipogenesis (DNL) and the building block for fatty acids synthesis[38]. Malonyl-CoA also inhibits long chain fatty acyl-CoA (LC-CoA) oxidation in the mitochondria by inhibiting carnitine palmitoyl transferase1 (CPT1)[39]. Therefore, this pathway, regarded as the lipid signalling pathway, promotes lipid production and accumulation of potential downstream lipid-derived signals that affect insulin secretion[1,40].The exact biochemical and metabolic nature of these signals and the mechanisms by which LC-CoA and malonyl-CoA affect beta cell function are still largely elusive.

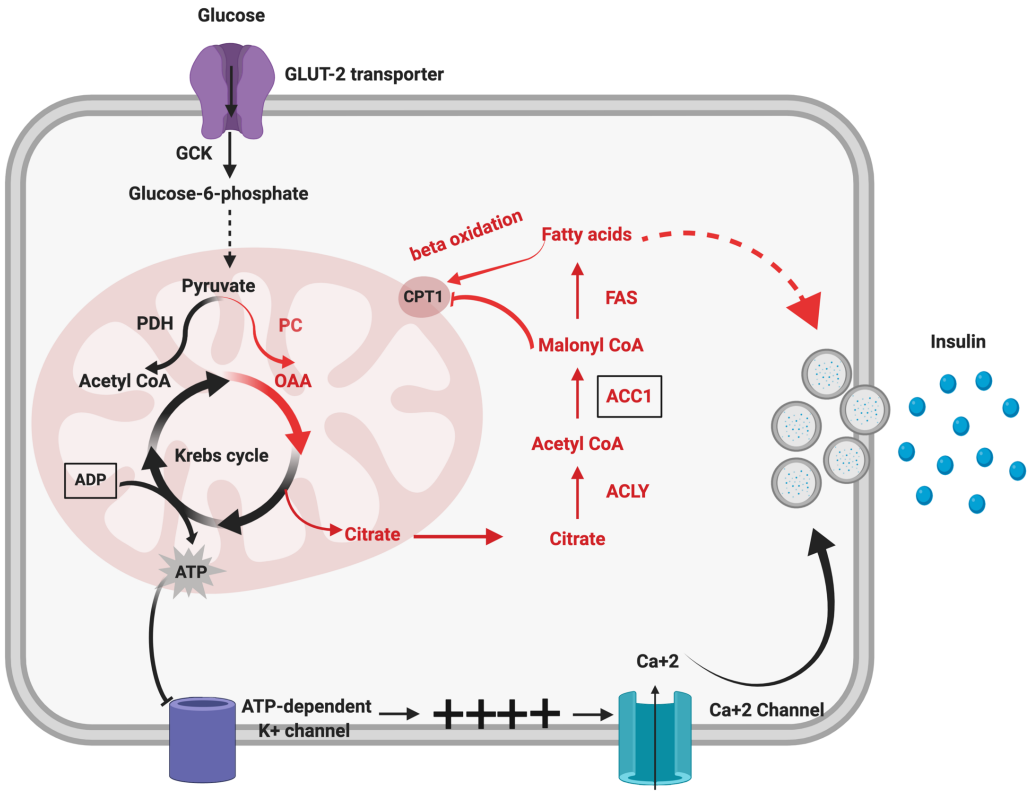


Figure 1-2 Glucose-stimulated insulin secretion. Pyruvate, the end product of glycolytic pathway, is converted into acetyl-CoA by PDH, leading eventually to ATP production via oxidative phosphorylation. Elevation of the ATP/ADP ratio leads to ATP-dependent K^+ channel closure, cell membrane depolarisation, opening voltage-gated calcium channels, fusion of the insulin-containing vesicles with the cell membrane and secretion of insulin into the extracellular fluid by exocytosis. Alternatively, Pyruvate is carboxylated by PC to form Oxaloacetate, excess citrate in the Krebs cycle will be transported to the cytosol and converted to acetyl-CoA, which is then carboxylated by ACC1 to produce malonyl-CoA.

Chapter 1.4 Evidence Supporting the Role of Lipid Signalling Pathway in Insulin Secretion

The role of the lipid signalling pathway in insulin secretion was proposed in 1994 by Prentki et al.[38]. Subsequently, several *in vivo* and *in vitro* studies have established evidence for the role of this pathway in GSIS.

A recent review by Prentki et al. has summarised the evidence supporting the role of this pathway in insulin secretion[41]. **First**, PC levels in islets and beta cells are very high, driving about 40 % of pyruvate into the mitochondria via the anaplerotic pathway; which is high for non-gluconeogenic and non-lipogenic tissues[42]. Moreover, *in vitro* studies showed that inhibition of PC with phenylacetic acid (PAA) or inhibition of PC using RNAi in INS1 cell line results in inhibition of GSIS[43]. **Second**, ACC1 is highly expressed in the INS1 cell line and islets[44], and incubation of beta cells with glucose for a short period of time (30 mins) leads to ACC-1 activation and is associated with increasing insulin secretion[45]. Chronic exposure of INS1 cells to high glucose (three days) results in a 30-fold increase in ACC1 activity[46], whilst pharmacological inhibition of ACC1 using 5-(Tetradecyloxy)-2-furoic acid (TOFA) or inhibition of ACC1 using RNAi inhibits GSIS[44,47]. Furthermore, a recent study has demonstrated that ACC1 is critical for GSIS and beta cell growth using beta cell-specific ACC1 knockout mice[1]. **Third,** inhibition of ACLY by hydroxycitrate or by RNAi caused marked inhibition of GSIS in islets and INS-1 cells[48]. ACLY expression in islets from patients with T2D was 60% less compared to islets from non-diabetic individuals[49]. **Fourth,** inhibition of CPT-1 by 2-bromopalmitate resulted in enhancement of GSIS[50]. **Fifth**, the high ratio of ACC1/FAS in beta cells relative to lipogenic tissues suggests that malonyl-CoA has another function rather than de novo lipogenesis[38].

Chapter 1.5 The Role of ACC1 in Insulin Secretion and Beta Cells Function.

ACC1, the main malonyl-CoA producing enzyme expressed in beta cells, appears to perform a critical role in glucose-stimulated insulin secretion. Although several *in vitro* studies have established evidence linking ACC1 to insulin secretion since the 1990s (explained in the previous section), the role of ACC1 in beta cell function and the physiological role of this pathway has not been examined *in vivo* until recently.

An important contribution to this field has been made through a study by Cantley et al., using beta cell-specific ACC1-knockout mice, the study has shown that beta cell ACC1 plays a critical role in insulin secretion *in vivo* and *ex vivo.* ACC1-knockout mice were glucose intolerant with corresponding reductions in circulating insulin levels compared to littermate control. *Ex vivo* islet studies demonstrated that GSIS was impaired at low (2 mmol/l) and intermediate (7.5 mmol/l) glucose concentration, interestingly, the glucose response at super-physiological (20 mmol/l) glucose concentration was unaffected. This study has also reported for the first time a novel role for ACC1 in regulating beta cell mass prior to adulthood[1].

Chapter 1.6 ACC Reaction, Structure, Isoforms, And Tissues Distribution

Chapter 1.6.1 ACC Reaction and Structures

ACC was discovered by Salih Wakil and his co-workers in 1958[51]. It is a biotin containing enzyme that catalyses the rate-limiting step in de novo lipogenesis; the carboxylation of acetyl-CoA to malonyl-CoA[52]. The overall reaction of ACC involves a two-step reaction; the first one is the ATP-dependent carboxylation of biotin with bicarbonate, the carboxyl group is transferred from biotin to acetyl-CoA to form malonyl-CoA in the second reaction[53].

$$HCO_3^- + \text{biotinyl-ACC} \xrightarrow{ATP} ADP + Pi + \text{carboxy-biotinyl-ACC} \qquad \text{Reaction I}$$

$$\text{Carboxy-biotinyl-ACC} + \text{acetyl-CoA} \longrightarrow \text{biotinyl-ACC} + \text{malonyl-CoA} \qquad \text{Reaction II}$$

In prokaryotes, ACC is composed of three distinct proteins: biotin carboxylase, biotin carboxyl carrier protein, and transcarboxylase[54]. In eukaryotes, these proteins are contained within a single multifunctional protein that is encoded by a single gene[54]. Eukaryotic ACC consists of four domains assembled on a single peptide; biotin carboxylase (BC), biotin carboxyl carrier protein (BCCP), carboxyl transferase (CT) domains, and a non-catalytic central domain region (CD), which together bridge the BC and CT domains[55]. The first step in ACC1 reaction is carried out by BC domain, while the second step is carried out by CT domain[56](figure 1-3 & figure 1-4).

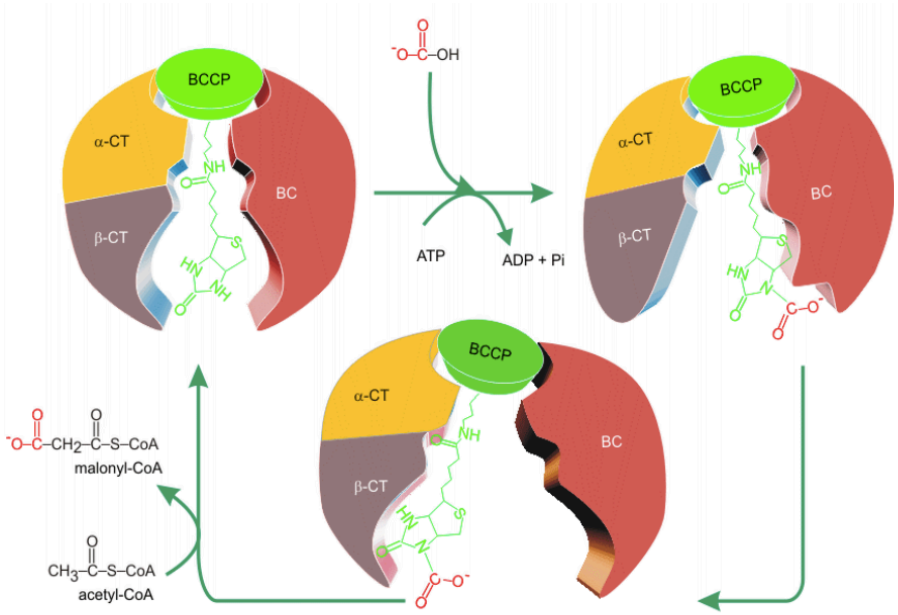


Figure 1-3 ACC1 structure and reaction. Eukaryotic ACC consist of four domains; biotin carboxylase (BC), biotin carboxyl carrier protein (BCCP), carboxyl transferase (CT) domains, and a non-catalytic central domain region (CD), which together bridge the BC and CT domain. The overall reaction of ACC involves a two-step reaction; the first one is the ATP-dependent carboxylation of biotin with bicarbonate, the carboxyl group is transferred from biotin to acetyl-CoA to form malonyl-CoA in the second reaction.
Source: http://aralip.plantbiology.msu.edu/hehos/2

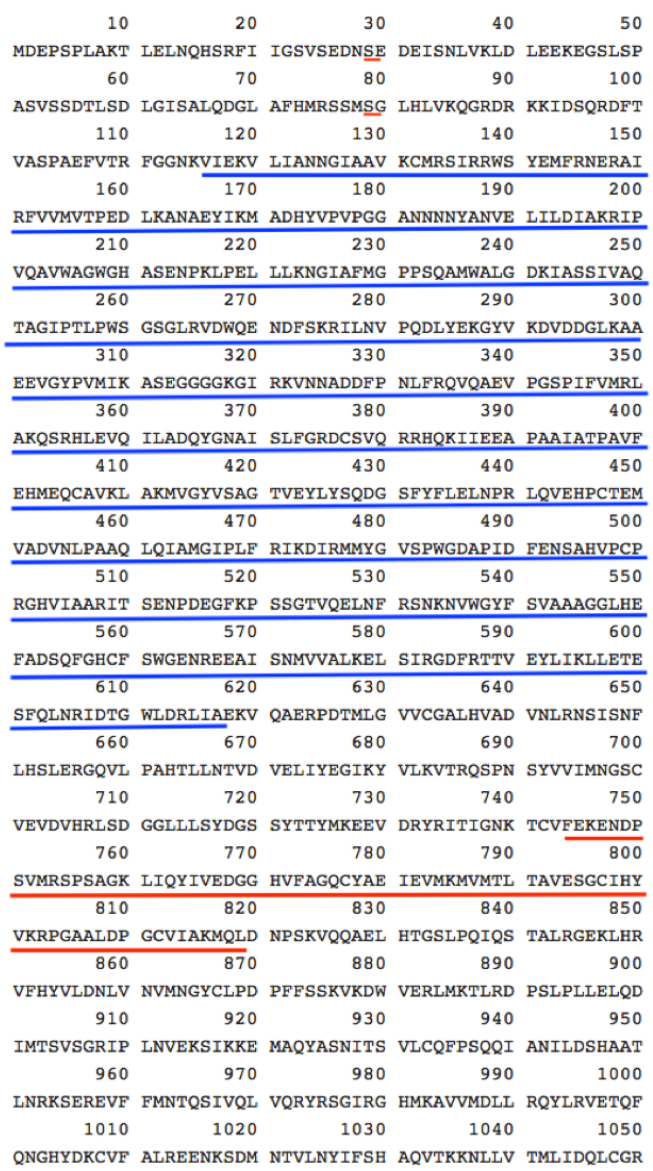


Figure 1-4 ACC1 sequence and different domains, Rattus norvegicus (Rat).
Accession number P11497.

Blue Domain: Biotin carboxylation
Red Domain: Biotinyl-binding
Green Domain: CoA carboxyltransferase N-terminal

Chapter 1.6.2 ACC Isoforms, Tissues Distribution and Cellular Localisation

Mammalian ACC exists as two isozymes; ACC1 and ACC2. They are encoded by separate genes (*Acaca* and *Acacb*) localised at chromosomes 17q12 and 12q23[57], respectively, and display distinct tissues distributions[58].

ACC1 is a cytosolic enzyme, predominantly expressed in lipogenic tissues (liver, adipose tissues, mammary gland), consisting of 2,346 amino acids, and has a predicted molecular weight of 265 kDa[59]. In these tissues, malonyl-CoA is the C2-unit donor for de novo lipogenesis catalysed by fatty acid synthase (FAS)[60].

In contrast, ACC2 is a mitochondrially connected enzyme, highly expressed in oxidative tissues (liver, heart, skeletal muscle), contains 2,458 amino acids, and has a predicted molecular weight of 280 kDa[61]. ACC1 and ACC2 have 75% overall amino acid sequence identity[62], the amino acid sequence of ACC2 has an additional 112 amino acid relative to ACC1, which comprise the unique N-terminal sequence of ACC2 which are believed to be ACC2 mitochondrial targeting motif [63]. In oxidative tissues, ACC2-generated malonyl-CoA regulates fatty acid oxidation through the inhibition of CPT1, which controls the entrance of long-chain fatty acids into the mitochondria for β-oxidation[60,64].

Chapter 1.7 ACC Function and Role in Metabolic Diseases

Fatty acids and their derivatives play an essential role in cell functions and cellular homeostasis[65]. Among the multiple roles of fatty acids, they are critical structural components of cellular membranes and are key energy reserves in the cell[66]. In addition to the structural role of fatty acids they also have regulatory functions as they are involved in cell signalling and affect all phases of cellular activities[67]. For example, fatty acylation of some regulatory proteins affects their function by modulating their trafficking and localisation[68]. Fatty acids can also serve as secondary messengers and mediate the signal transduction of various external and internal agents[69].

The vital regulatory role of ACC in fatty acid synthesis and oxidation pathways and the complex roles that fatty acids play as cellular components made it an attractive target for various metabolic diseases (i.e. obesity, insulin resistance, and T2D). Based on distinctive tissue distributions and cellular localisation of ACC1 and ACC2, it was hypothesised that combined ACC1 and ACC2 inhibition would result in a reduction of DNL in lipogenic tissues while at the same time enhancing fatty acid oxidation in oxidative tissues [70]. Several *in vivo* studies strongly supported this hypothesis and showed that ACC inhibition could be beneficial and have therapeutic potential for the treatment of metabolic diseases[71].

A study by Wakil et al. found that global deletion of ACC1 is embryonically lethal; suggesting a role for malonyl-CoA, generated by ACC1, in the early development of the embryos. This study also observed that the presence of intact copies of the ACC2 gene did not compensate for ACC1 function and did not save the mice embryos from failure to develop[60]. On the other hand, mice with global deletion of ACC2 are viable; however, the effect of this deletion on fatty acid oxidation was controversial. One study showed that these mice have higher fatty acid oxidation rate in muscles and heart, accumulate less fat compared to the wildtype and are protected from diabetes[72],

while another independent study observed no alteration in fatty acid oxidation in these mice[73]. Interestingly, another study showed that ACC2 knock out mice had increased beta oxidation, but it was not beneficial in terms of protection from obesity as the overall metabolic rate remained the same (i.e. ACC2KO mice burnt less glucose but more fat)[74].

The ACC1-liver-specific knock out mouse model was generated independently by two groups[75,76]. Interestingly, both groups showed that hepatic DNL and malonyl-CoA levels were normal in liver-specific ACC1 null mice and that these mice did not exhibit any significant physiological differences from wild type mice; suggesting a compensatory mechanism to adapt to un-physiological conditions caused by ACC1 disruption.

Chapter 1.8 ACC1 Regulation

In order to fulfil the fatty acid requirements of different tissues under different physiological conditions, the catalytic activity of eukaryotic ACCs is tightly regulated by a complex interaction of phosphorylation, binding of allosteric regulators and transcriptional factors.

Long-term regulation of ACC1 is mediated by changes that occur at the transcriptional level in response to a variety of factors including glucose, insulin, and catabolic hormones. Short-term regulation of enzymatic activities occurs by allosteric interactions and by reversible phosphorylation, which are influenced by diet and hormones[77].

Chapter 1.8.1 Transcriptional Regulation

The ACC1 gene has 64 exons, including seven alternatively spliced minor exons (1A, 1B, 1C, 3, 5A', 5A, and 5B)[77]. The ACC1 gene (*Acaca*) is under the control of three promoters, designated PI–PIII[77].

PI transcripts are mainly expressed in adipose tissue, but are also expressed in the liver under lipogenic conditions. PII transcripts function as a significant regulatable promoter of ACC1: it is expressed in all tissues and regulated by various hormones (e.g. thyroxine) and diet (e.g. glucose, cholesterol). PIII is expressed in the lactating mammary gland[77,78]. Insulin has positive effects on all the promoters, while glucagon has negative effect [78].

The functioning of these independent promoters and differential splicing of the primary transcripts lead to heterogeneity in the 5'untranslated region, resulting in various forms of ACC1 mRNA expressed in a tissue-specific manner in response to various hormonal and nutritional stimuli[66]. However, these mRNAs produce the same 265-kDa ACC1 protein since all of these transcripts contain the same coding sequence [66,77]. The physiological significance of the presence of alternatively spliced exons and different forms of mRNA is not known. It has been suggested that

the generation of multiple mRNAs could provide an extra level of ACC regulation at the gene level and also at the translational level[66] by influencing the mRNA stability and translational efficiency or by increasing the stability and specific activity of the ACC1 protein[79,80].

Most of the lipogenic enzymes, including ACC1, are regulated at the transcriptional level by hormones (i.e. insulin, glucagon) and nutritional status, this regulation is mediated by transcriptional factors. Among the key transcription factors that play a central role in controlling ACC1 gene expression in response to hormonal and nutritional factors is Sterol Regulatory Element Binding Protein 1c (SREBP1c)[81], a membrane-bound transcription factor and is considered a master regulator of lipogenesis[78]. In response to insulin, SREBP1c is activated, resulting in significant stimulatory effects on all the promoters of ACC genes with the most prominent effect on PI[78,80]. In beta cells forced activation of SREBP1c is associated with accumulation of triglycerides, that can be sources of lipotoxicity-mediated cellular stress, leading to impaired insulin secretion and glucose intolerance. In SREBP-1 knockout islets, both basal and glucose-stimulated insulin secretion were marginally, but consistently, elevated compared to wild type islets[82].

Other transcriptional factors that regulate ACC1 include carbohydrate response element-binding protein (ChREBP)[53]. In beta cells it has been shown that ChREBP mediates glucotoxicity by upregulating downstream target genes leading to lipid accumulation, increased oxidative stress, stimulated caspase activity and apoptosis[83].

Chapter 1.8.2 Allosteric Regulation

Citrate is the precursor of cytoplasmic acetyl-CoA. It is produced in mitochondria and is used as a substrate by ATP citrate lyase (ACL), which converts citrate to acetyl-CoA, the substrate of ACC1 (figure 1-2)[84]. It is regarded as a feed-forward activator of ACC1 and acts by inducing ACC1 polymerisation which results in stabilising the active conformation of ACC1, thus enhancing ACC1 enzymatic activity[84-86].

Citrate regulation of ACC1 has been questioned as the concentration of citrate required to increase ACC1 activity is much higher than that normally present in cells[84]. However, it has been shown recently that MIG12, a 22 kDa cytosolic protein, facilitates ACC1 polymerisation leading to a left shift of the citrate activation curve, hence, lowering the concentration of citrate required for ACC1 activation to levels within the physiological range[68].

On the other hand, long-chain acyl-CoA esters are potent inhibitors of ACC1[87]; they are considered as classical feedback inhibitors for ACC1, and appear to oppose the activation by citrate[88].

The location of the binding sites of citrate or long-chain acyl-CoA, with respect to the primary structure of the protein, is not known yet[88].

Chapter 1.8.3 Post-Translational Modifications

The third level of ACC1 regulation is by post-translational modifications (PTMs). Phosphorylation, a well-studied and the most common type of PTMs, involves specific protein kinases that phosphorylate and modulate ACC1 activity.

Multiple phosphorylation sites have been identified in mammalian ACC1 and ACC2[88], the most notable of these phospho-sites is ACC1S79 in rat and mouse (ACC1S80 in human), and the equivalent ACC2S218 in the rat (ACC2S212 in mouse and ACC2S222 in human)[89]. AMP-activated protein kinase (AMPK) is the kinase that accounts for the phosphorylation of this site[88].

AMPK is a multi-substrate, heterotrimeric serine/threonine protein kinase that is formed by three subunits: the α catalytic subunit, and two regulatory subunits γ and β[90]. It is considered a metabolic sensor of cellular energy levels and is activated in response to exercise, hormones, and cellular stressors that deplete ATP levels. Activation of AMPK requires phosphorylation of Thr172 by at least one of three upstream kinases, liver kinase B1 (LKB1) and Ca^{2+}/calmodulin-dependent kinase kinase-β (CAMKK2), and TGFβ-activated kinase1 (TAK1)[91]. Once activated, the enzyme switches off ATP-consuming anabolic pathways (e.g. fatty acid synthesis) and switches on ATP-producing catabolic pathways (e.g. fatty acid oxidation)[92].

The role of these phospho-sites in the regulation of mammalian ACC activity in tissues (i.e. liver, adipose tissues and muscles) has been well-characterised. Various *in vitro* studies showed that phosphorylation of ACC1 at S79 inhibits its activity and reduces malonyl-CoA content[93,94].

A study by Kemp et al. has examined the physiological impact of this phosphorylation site *in vivo*. The authors created a mouse model named ACCDKI (double-knock in), in which ACC1S79 and ACC2S212 phosphorylation sites were mutated to alanine, making these enzymes insensitive to inhibition by AMPK at these sites: the absence of phosphorylation at these sites was confirmed by mass spectrometry. Compared to wild type mice, ACCDKI had a higher rate of liver lipogenesis and lower fatty acid oxidation in both liver and skeletal muscle, which contributed to the progression of non-alcoholic fatty liver disease (NAFLD), glucose intolerance and insulin resistance[2]. The authors also observed that ACCDKI mice placed on a high-fat diet (HFD) to induce obesity were refractory to the metformin-mediated effects on insulin sensitivity, glucose homeostasis and liver lipid contents that were observed in wild type mice on a HFD.

These findings suggest that AMPK and its originally defined substrates ACC1S79 and ACC2S212 are critical for the control of lipid metabolism and for metformin-mediated improvements in insulin action.

Other ACC1 phosphorylation sites have been identified; these are ACC1S77, ACC1S1200, and ACC1S1215. However, the role of these phosphosites in ACC1 regulation is less-established compared to ACC1S79. ACC1S77 and ACCS1200 are phosphorylated by Protein Kinase A (PKA), while ACC1S1215 is phosphorylated by AMPK[93,94].

One study by Hardie et al. showed that phosphorylation of ACC1S1215 and ACC1S1200, purified from rat mammary gland, is not associated with a change in the enzyme activity and that the effects of the AMPK on ACC1 activity are mediated entirely by phosphorylation of ACC1S79 in adipose tissues. The study also showed that phosphorylation of ACC1S77 by PKA causes a modest change in ACC1 activity. Moreover, this study showed that cleaving off the highly phosphorylated amino-terminal region (where ACC1S79 and ACC1S77 are located) using proteinases (e.g. trypsin and chymotrypsin) activates ACC1; leading the authors to conclude that ACC1 amino-terminal region is the regulatory domain which inhibits ACC1 catalytic activity when phosphorylated[94].

Interestingly, the authors observed the presence of another proteinase-sensitive region in the centre of ACC1, since proteinases cut the protein into two fragments of almost 120kDa. This region lies between the biotin-binding domain and the carboxyltransferase domain (both domains have a critical role in ACC1 function) and may represent a hinge region between these two domains. Although the location of this hinge region was not precisely defined at the time of this study. The authors predicted it to be in the area of ACCS1200 / S1215.

In contrary to these findings, a subsequent study by Kim et al. found that ACC1S1200, rather than ACC1S77, is the critical phosphorylation site that mediates the effect of PKA on ACC1 activity in Hela cells [93,94]. This study also highlighted the limited available approaches of classical enzymology that has been used at the time of conducting these studies in order to reveal the critical phosphorylation sites for the control of ACC1 activity making it very difficult to draw any firm conclusions[94].

The location of ACC1S1215 and ACC1S1200 with respect to the structure of ACC1 is shown in figure (1-5).

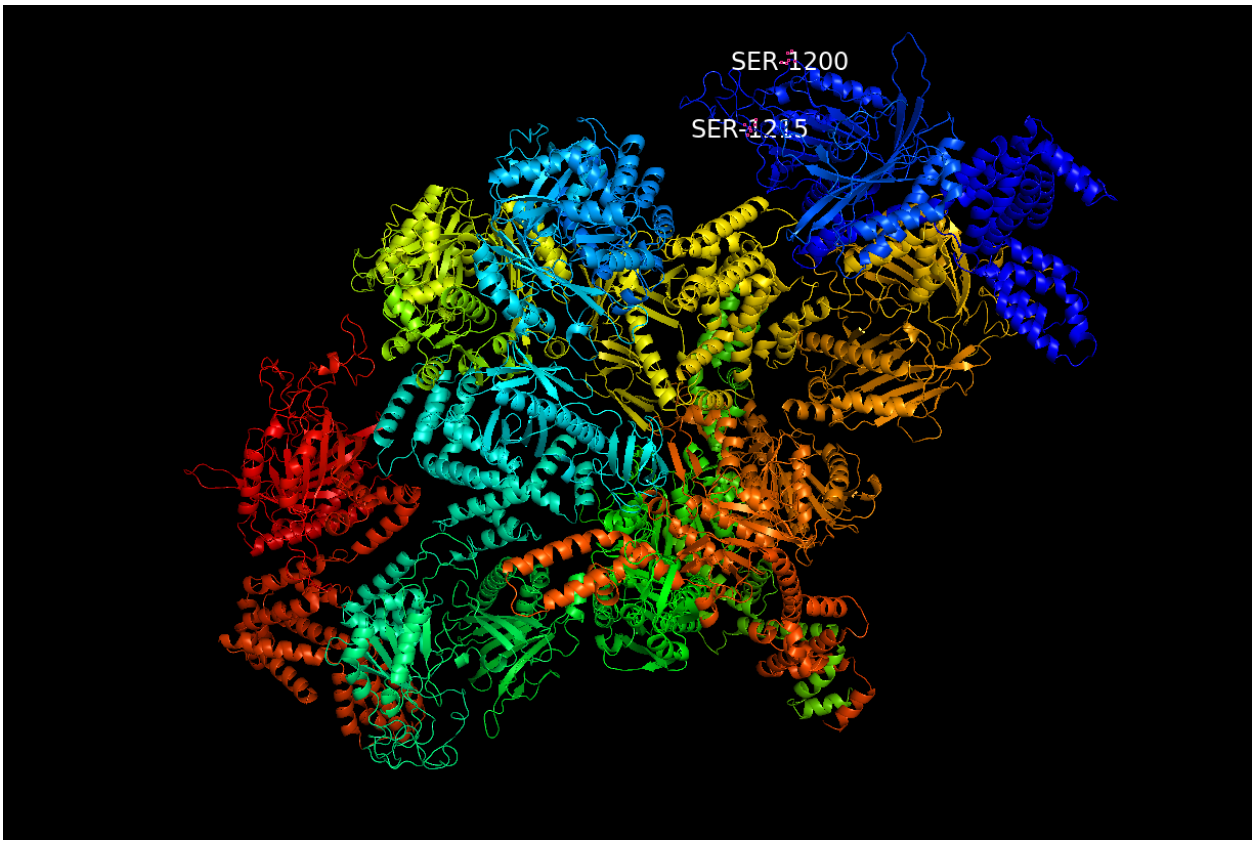


Figure 1-5 Overall structure of rat ACC1. The structure of ACC1 starting from L847 amino acid (PDB 6g2d.1). The location of ACC1S1215 and ACC1S1200 are shown. The structure figure was produced with PyMOL software (www.pymol.org).

Chapter 1.9 ACC1 Regulation in Pancreatic Beta Cells

In spite of plethora evidence for the role of ACC1 in insulin secretion and beta cells function both *in vivo and in vitro* (as explained in chapter 1.5), very little is known about how ACC1 is regulated in pancreatic beta cells.

While data from ACCDKI study indicate that phosphorylation of both ACC1 and ACC2 by AMPK is critical for controlling whole body glucose homeostasis, the importance of ACC1S79, the well-known phosphosite, in insulin secretion and beta cells function was not tested in this study. This is especially relevant as the role of ACC1S79 in beta cell function is not known yet. Moreover, the AMPK activator (e.g. 5-Aminoimidazole-4-carboxamide ribonucleotide (AICAR)) has been show to enhance glucose stimulated insulin secretion in beta cell[95]. However, it is currently unknown whether these pharmacological activators of AMPK mediate their effects through the AMPK–ACC signalling pathway.

It is also not known if other ACC1 phosphorylation sites play a role in ACC1 regulation in beta cells.

Chapter 1.10 Hypothesis And Aims

In order to understand how ACC1 is regulated in beta cells, we hypothesise that:

1- ACC1S79 plays a role in the regulation of insulin secretion by glucose.

2- Additional glucose-regulated phospho-sites control ACC1 activity in beta cells.

This will be tested by achieving the following aims:

1- To characterise the beta cell function in the ACC1SKI mouse model (in which ACC1S79 was mutated to alanine).

2-To develop a protocol to purify ACC1 from INS1 cells.

3- To apply an unbiased quantitative phosphoproteomics approach to identify glucose-regulated phospho-sites across ACC1 protein.

4- To validate these sites and study their functional relevance in beta cells.

Chapter 2 Materials and Methods

Chapter 2.1 Animal Studies

Chapter 2.1.1 Animal Husbandry

Mice were kept and studied in accordance with UK Home Office Legislation and local ethical guidelines. All animal procedures were approved by the British Home Office Animals Scientific Procedures Act (ASPA)1986 (Project License no. P4D4BEF1F, issued to Dr. J. Cantley).

Mice were kept under a controlled environment with 12 hour light-dark cycle (light 7am – 7pm, dark 7pm -7am), temperature 21-23 °C and humidity (~ 55%). The mice had free access to water and were fed ad libitum on a commercial diet (RM1 diet SDS UK Ltd). 12-week-old male mice were used for all studies unless otherwise indicated.

Chapter 2.1.2 Animal Source

ACCDKI mice (Double knock in mutation; ACC1S79A & ACC2S212A) transgenic mice were generated by and obtained from Bruce E Kemp, St. Vincent's Institute of Medical Research in Australia (Kemp, 2013).

All mice were maintained on C57BL6 genetic background. ACCDKI transgenic mice and wild type mice were interbred to generate mice heterozygous for both ACC1S79A and ACC2S212A mutation; these mice were then crossed to generate ACC1SKI (ACC1S79A & ACC2 wild type) and littermate control mice. All genetic combinations of offspring were generated at the expected Mendelian frequency.

Chapter 2.1.3 Mice Genotyping

Mice were tail tipped upon weaning (21 days of age). DNA was extracted by placing the tail tip in 100 µl of digestion buffer (DirectPCR Lysis reagent, Viagen) heating to 95 °C for 10 minutes then adding proteinase K to a final concentration of 3 mg/ml (15 µl of 20 mg/ml stock) and incubating overnight at 55 °C. Each sample was then heated to 95 °C for a further 10 minutes to heat inactivate the proteinase K and samples spun at 13,000 RPM for 5 minutes to sediment tail debris.

To determine the genotype of the mouse 2 µl of supernatant was used per polymerase chain reaction (PCR) in PCR tubes in addition to the following: PCR Master Mix (DreamTaq Green PCR Master Mix, K1082): 10.0 µl, forward Primer (5uM): 1 µl, reverse Primer (5uM): 1 µl and dH_2O: 10 µl.

Then a thermal cycler with lid heated to 105 °C was used with the following cycling conditions: 94°C for 10 minutes, 94°C for 20 seconds, 59°C for 20 seconds, 70°C for 1 minute and 15seconds (these cycles are repeated for 40 times) then 72°C for 3 minutes and finally 10°C.

PCR products were resolved using 1.5 % agarose gel electrophoresis in TAE buffer (Tris 40 mmol/1, acetic acid 20 mmol/l/ l, EDTA1 mmol/l, pH 8.3,) at 80 Volts for 90 mins and visualized by UV excited fluorescence of MidoriGreen Advance DNA stain stained DNA (1 in 25,000 dilution).

ACC1S79 primers sequence:

Forward primer: 5’ TGGCTTCTCCAGCAGAATTT 3’ (20)

Reverse primer: 5’ TGC CCG TAA AAC CAC AAG AT 3’ (20)

ACC2S212 primers sequence:

Forward primer: 5’ TCC AGC ATC AGG CTT TTT CT 3’ (20)

Reverse primer: 5’ GGC TAG CCT GGG ATA CAC AA 3’ (20)

Chapter 2.2 In Vivo Metabolic Studies

Chapter 2.2.1 Fasting Blood Glucose and Body Weight Measurement

Mice were fasted for 15 hours overnight and blood glucose levels were was sampled from the tail using Glucometer. Mouse body mass was also measured following an overnight fast.

Chapter 2.2.2 Glucose Tolerance Test (GTT)

Mice were fasted overnight (for 16 hours) to assess glucose tolerance after a long, catabolic fast associated with basal blood glucose levels, or 6 hours fast (8am - 2pm) preserving post-prandial blood glucose levels. To fast, food hopper was emptied and checked that no food is in base of cage. Mice had free access to drinking water throughout the fasting period. If mice were moved to a new cage, some bedding/cage items were moved across to provide familiar scents.

Fasting blood glucose measured as above. Mice were then injected with 2 g/kg glucose (in a 20 % solution) intraperitoneally (i.p) and blood glucose measured at 15, 30, 60 and 120 minutes after injection (2 ul whole blood was used to measure blood glucose level).

Chapter 2.2.3 Insulin Tolerance Test (ITT)

Mice were short fasted for 6 h (8am-2pm) maximum, so that mice enter test with fed/high physiological blood glucose levels. Blood glucose was measured as above. Due to decreased insulin sensitivity, male mice were injected i.p. with 0.85 international units of recombinant human insulin (Roche Actrapid) per kilogram. Blood glucose was measured at 15, 30, 60 and 120 minutes after injection. (2 ul whole blood was used to measure blood glucose level). Female mice were injected i.p. with 0.5 international units of recombinant human insulin per kilogram. If mice showed any signs of hypoglycaemia an i.p. bolus of glucose was injected, the mouse was

monitored carefully and allowed to recover in a cage placed on a heat pad, isolated from cage mates.

Chapter 2.2.4 Serum Insulin Assay

Insulin was quantified by Meso Scale Discovery Kit (MSD kit, catalogue number k152bzc). According to the manufacture's protocol, this assay detects insulin in a sandwich immunoassay where a plate has been pre-coated with insulin antibody "capture antibody". Insulin in the sample binds to capture antibody. Adding labelled detection antibody, anti-insulin labelled with an electro-chemiluminescent compound (MSD SULFO-TAG™ label), completes the sandwich. MSD SECTOR instrument is used for analysis. Inside the SECTOR instrument, a voltage applied to the plate electrodes causes the labels bound to the electrode surface to emit light.

The instrument measures intensity of emitted light to afford a quantitative measure of insulin present in the sample.

To measure insulin serum levels, detection antibody buffer, read buffer and MSD plate were prepared according to the manufacture's protocol. Then, 150 µl of blocker a solution was dispensed into each well. The plate was sealed with an adhesive plate seal and incubated for 1 hour with vigorous shaking (300–1000 RPM) at room temperature. Then, the plate was washed 3 times with PBS-T. 40 µl of 1x detection antibody solution was dispensed into each well of the MSD plate. For this assay, an 8-point standard curve is recommended with 3-fold serial dilution steps and a zero Calibrator. The concentration of the standards are as following: 50000, 16667, 5556, 1852, 617, 206, 69, 0 (pg/ml). 10 µl of sample or calibrator was immediately added to the appropriate wells of the MSD plate. The calibrators was run in duplicate to generate a standard curve. The plate was sealed with an adhesive plate seal and incubated for 2 hours with vigorous shaking (300–1000 RPM) at room temperature. Finally, the plate was washed 3 times with PBS-

T and 150 µl of 1X read buffer was added to each well of the MSD plate. The plate was then read using MSD reader.

Chapter 2.3 Islets Isolation And Culture

Chapter 2.3.1 Islets Isolation

Mice were killed by cervical dislocation and a laparotomy immediately performed with a cut up to sternum. Gastrointestinal tract was pushed to the right; exposing the liver. The liver lobes were pushed up against diaphragm the common bile duct was exposed. The duodenum/common bile duct junction was clamped. Using a 25G needle and 5ml syringe, 2ml liberase and collagenase solution prepared in HBSS (Gibco; Waltham, Massachusetts, USA) was injected into the common bile duct at the junction with the duodenum (major duodenal papilla), forceps was used to hold duodenum while carefully injecting into duct.

The pancreas was then immediately removed and incubated in 2 ml pancreatic digestion solution at 37 °C for 16 mins. On completion of incubation 20 ml ice cold quenching buffer (HBSS (Gibco) + 10% Fetal bovine serum (FBS) (Gibco) + Pen Strep (Sigma) (0.5ml per 50ml HBSS) + 20 mmol/l Hepes (Sigma)) was added and tube shaken vigorously for 10 seconds to dissociate exocrine tissue from the islets. Digested tissue was poured through 500µM net well (Corning, 24mm) into 50ml falcon tube on ice, another 15ml quench buffer was added to empty incubation tubes to recover tissue stuck to sides and poured through 500µM net well. Then, the tubes were spun down at 1000 RPM for 1 minute at 10°C in a 50 ml conical centrifuge tube, supernatant discarded, and pellets were resuspended in 20 ml quenching buffer to wash islet/exocrine digest. This washing step was repeated two times, and the final pellet was resuspended in 30 ml ficoll-paque plus buffer (GE Healthcare Life Sciences, 17-1440-03). Slowly and carefully 10mL of quench was added on top. Then the tubes were spun at 1375g for 22 minutes at 10°C. Entire ficollpaque and quench were pipetted onto an inverted 70uM cell mesh over a conical flask (islets will be trapped on top). Each

islet prep was washed with 70mL quench by pipetting over/through the mesh and with ~25ml complete islet media.

The mesh was flipped upside down into a 4.5cm petri dish and 4.5ml of complete islet media (RPMI 11 mmol/l (Gibco 31870), 1x pen/strep, 10% FBS (heat inactivated), L-glutamine, 15 mmol/l HEPES (8ml 1M stock into 500ml bottle) was pipetted through the mesh to transfer the islets from the top of the mesh into the dish. The purity of prep and quality of islets were checked under a microscope, then placed in an incubator overnight at 37 °C with 21 % O2, 5 % CO2 and high humidity.

Chapter 2.3.2 In Vitro Glucose Stimulated Insulin Secretion

Isolated mice islets were maintained for 1 hour in Krebs Ringer bicarbonate buffer (KRBH) containing: 136 mmol/l NaCl, 4.7 mmol/l KCl, 10 mmol/l HEPES (pH 7.4), 5 mmol/l $NaHCO_3$, 1.2 mmol/l KH_2PO_4, 1.2 mmol/l $MgSO_4$, 1 mmol/l $CaCl_2$) containing basal (2 mmol/l) glucose concentration with or without AMPK activators as detailed in the results sections.

Then, batches of 5 islets were hand-picked into 96-well plates and stimulated for 1h at 37°C with basal (2 mmol/l), medium (7.5 mmol/l) or high (20 mmol/l) glucose concentrations with or without AMPK activators as detailed in the results sections. The reaction was stopped on ice, 96-well plates were spun at 1000 RPM for 1min (at 10°C). Insulin supernatant was collected into fresh 96-well plates and stored at -80°C until assayed for insulin.

Chapter 2.3.3 Insulin Assay

Insulin in the supernatant was measured using Cisbio Bioassays' Insulin Ultra-Sensitive assay. According to the manufacture's protocol, in this kit insulin is detected in a sandwich assay format using 2 different specific monoclonal antibodies, one labelled with Europium Cryptate (donor) and the second with XL665 (acceptor). When the dyes are nearby, the excitation of the donor with a light source (laser or flash lamp) triggers a Fluorescence Resonance Energy Transfer (FRET) towards the acceptor, which in sequence fluoresces at a specific wavelength (665 nm). The two antibodies bind to the insulin present in the sample, thereby generating FRET.

Signal intensity is proportional to the number of antigen antibody complexes formed and therefore to the Insulin concentration.

To prepare the kit, diluent and detection buffer were allowed to warm up at room temperature before use and then homogenized them with a vortex. Seven standards were prepared with the following concentration: 500, 8, 3.2, 1.28, 0.5, 0.2, 0.08, 0.03, 0 (ng/ml). 10 µL of each Insulin standard was dispensed in the standard wells in duplicate. For islets treated with basal glucose condition (2 mmol/l glucose) the supernatant was diluted 1 in 5 and for islets treated with medium (7.5 mmol/l glucose) and high glucose condition (20 mmol/l glucose) the supernatant was diluted 1 in 10. Each sample was assayed in duplicate. 5 µL of Anti-Insulin-XL665 working solution and 5 µL of Anti Insulin-Eu3+ Cryptate working solution was added to all wells. The plate was sealed and incubated overnight at room temperature. Finally, the plate was read using an HTRF compatible reader.

Chapter 2.3.4 Islets Lysis for Protein Extraction

All steps were done at 4^{o}C or on ice. Batches of 200 islets per condition were collected using a P200 pipette and placed in 1.5ml Eppendorf tube. Then islets were spun at 3500 RPM at 4^{o}C for

1 minute to pellet islets. Then islets were resuspend in 0.5ml ice cold PBS by gently agitating tubes for two times. Then islets were spun for 2 minutes and PBS supernatant was discarded.

Islets were then resuspend by moderate vortexing in 50 µl RIPA lysis buffer (Tris HCL (65 mmol/l), NaCl (150 mmol/l), EDTA (5 mmol/l), Np-40 (1%), Na-deoxycholate (0.5%), SDS (0.1%), Glycerol (10%)). One tablet of proteinase inhibitors (Mini EDTA-free Protease Inhibitor Cocktail, Roche, 4693159001) and one tablet of phosphatase inhibitors (PhosSTOP, Roche, 4906837001) were used per 10 ml of lysis buffer. Islets lysates were frozen down and stored at -80^{o}C.

Chapter 2.4 Radioactive Studies

To perform glucose tracer experiments batches of 50 islets were cultured in KRBH containing 0.1% BSA and 2 mmol/l glucose for 30 minutes at 37°C with or without AMPK activator (PFZ) as explained later in details in the results section.

Chapter 2.4.1 Glucose Oxidation

To measure glucose oxidation islets were washed twice with 2 mmol/l glucose KRBH-free BSA and transferred in 50ul volume to non-tissue culture treated 24-well plate. Islets were then cultured for 2 hours at 37°C in KRBH-free BSA containing 2 or 20 mmol/l D-glucose with 0.5 × 106 or 0.07 × 106 MBq/mol d-[U-^{14}C] glucose, respectively; (Perkin Elmer, Waltham, MA, USA) with or without PFZ. After 2 hours of incubation, media was acidified using perchloric acid and $^{14}CO_2$ was trapped via reaction with 0.1 ml KOH soaked in filter paper. $^{14}CO_2$ trapped in filter paper was assayed by scintillation reader.

Chapter 2.4.1 De Novo Lipogenesis (DNL)

To quantify tracer incorporation into cellular lipids, a chloroform–methanol (2:1 vol./vol.) extraction was performed.

Briefly, islets were washed twice with 2 mmol/l glucose KRBH-free BSA and transferred in 50 ul volume to non-tissue culture treated 24-well plate. Islets were then cultured for 2 hours at 37°C in KRBH-free BSA containing 2 or 20 mmol/l D-glucose with 0.5 × 106 or 0.07 × 106 MBq/mol d-[U-^{14}C] glucose, respectively; (Perkin Elmer, Waltham, MA, USA) with or without PFZ. After 2 hours of incubation the supernatant was discarded and islets were washed twice with ice cold PBS, then spun down at 1000 RPM for 1 minute. PBS wash was aspirated, 250 µl 0.1% SDS in water and 993 µl C:M (2:1) was added. Then a cycle of vortex, rest for 10 minutes, vortex, rest for

10 minutes, then spin for 10 minutes at 13000 rpm was followed. 500 µL of both Aqueous phase (upper phase) and lipid phase (lower phase) was read using scintillation reader.

Chapter 2.5 Cell Culture

Chapter 2.5.1 Thawing Cells

Cryovial was removed from liquid nitrogen. Cryotube containing cells was transported on dry ice from liquid nitrogen store to the tissue culture lab, then thawed quickly in 37°C water bath with constant checking. Thawed cells were then pipetted into 5mL warm culture medium in class 2 hood, centrifuged at 1100 RPM for 5 minutes. Supernatant was aspirated carefully with caution to avoid the loose pellet, cell pellet was resuspend in 2 mL culture medium and seeded into a T25 flask in a total volume of 4-5mL, the cells were placed in the incubator set at 37°C with 5% CO2. Media were changed after 24 hours, then every 48 hours as for passaging protocol.

Chapter 2.5.2 Passaging Cells

INS1 Cells

Complete growth media:

The base medium for this cell line is 500 ml RPMI (Gibco 31870025). To make complete growth medium, the following components were added to the base medium: Heat-inactivated fetal bovine serum (FBS) (Gibco16000044) to a final concentration of 5% (25 ml in 500 ml bottle), PEN/STREP (10U/ml stock) (Gibco 15140122) to a final concentration of 1% (5 ml in 500 ml bottle), L-glutamine (200 mmol/l stock) (Gibco 25030024) to a final concentration of 2 mmol/l (5 ml in 500 ml bottle), pyruvate (100 mmol/l stock) (Sigma S8636) to a final concentration of 2 mmol/l (5 ml in 500 ml bottle), HEPES (1M stock) (Gibco 15630056) to a final concentration of 10 mmol/l (5 ml in 500 ml bottle), and beta-Mercaptoethanol (50 mmol/l stock) (Sigma M3148) to a final concentration of 0.05 mmol/l (500ul in 500 ml bottle).

Passaging procedure:

Cells were passaged when they were 70-80% confluent. The passage ratio was 1-5. The culture media was removed using aspirator, then cells were washed with10 ml sterile PBS (Calcium and magnesium free). Trypsin was then added to the flask, the flask was tilted so that trypsin reaches all cells, then immediately trypsin was completely aspirated. Cells were then incubated for 3 minutes at 37°C in the incubator. The flask was then tapped gently and cells were observed using light microscope to check that trypsinisation is adequate and that cells are all detached from the bottom of off the flask. Pre-warmed media was then added into the flask to neutralise trypsin 5 ml of media for T25 or 10 ml for T75 and T150). The suspension was pipetted up and down few times to disperse clumps of cells while rinsing the sides of the flask. Then cell suspension was transferred into new flask that has pre-warmed media. Cells were split once per week. Media were changed 24 hours post passaging.

Alpha Cells Clone 9

Complete Media:

The base medium for this cell line is Dulbecco's Modified Eagle's Medium 1g glucose/l (5.5 mmol/l) (DMEM low glucose 31885-023, 500 mL). To make complete growth medium, the following components were added to the base medium:

Heat-inactivated fetal bovine serum (FBS) to a final concentration of 10% (50 ml in 500 ml bottle), HEPES to a final concentration of 15 mmol/l (7.5 ml in 500 ml bottle); PEN/STREP to a final concentration of 1% (5 ml in 500 ml bottle), sterile glucose to a final concentration of 15 mmol/l.

Passaging procedure:

Cells were passaged when they are 70-80% confluent. The passage ratio was 1:2 - 1:5. The culture media was removed using aspirator, then cells were washed with10 ml sterile PBS (Calcium and magnesium free). Trypsin was then added to the flask (1ml, 2ml and 3ml for T25, T75, T150 flask, respectively), the flask was tilted so that trypsin reaches all cells. Cells were then incubated for 10 minutes at 37°C in the incubator. The flask was then tapped gently and cells were observed using light microscope to check that trypsinisation is adequate and that cells are all detached from the bottom of off the flask. Pre-warmed media was then added into the flask to neutralise trypsin 5 ml of media for T25 or 10 ml for T75 and T150). Pipette vigorously up and down several times and release the liquid very fast on the wall of the flask to disperse clumps of cells while rising the sides of the flask. Finally cells were then transferred into new flask that has pre-warmed media (with a total amount of 5 ml, 10 ml and 15 ml for T25, T75 and T150 flask, respectively). Cells were split once per week. Media were changed 48 hours post passaging.

Chapter 2.5.3 Counting Cells

Improved Neubauer double cell clear sight haemocytometer (AC1000) was cleaned using 70% ethanol, and a cover slip was placed on the haemocytometer. Cells were diluted 1:10 in complete medium, this dilution was pipetted up and down 5-10 times to break up clumps of cells. Both chambers of the haemocytometer (upper and lower chambers) were filled with 10 µl of cell suspension. Cells were counted in the central gridded squares of the haemocytometer. The average count for cells in both squares were multiplied by 10,000 for cells per ml.

Chapter 2.5.4 Freezing Cells

Cells were trypsinised as described above, resuspended in warm culture medium, then centrifuged at 1100 RPM in for 5 minutes. The supernatant was removed and the pellet was resuspend in 6mL ice-cold complete media per T150. Then, 6 mL of ice-cold complete media containing 20% DMSO drop-wise (Final concentration will be 90% culture media + 10% DMSO) was added per T150. 1mL aliquots was prepared in cryotubes was prepared. Cells were frozen slowly; cryotubes were placed in freezing chamber (i.e. isopropanol bath) and transferred to -80°C overnight. Then vials were moved to liquid nitrogen for long term storage.

Chapter 2.5.5 Lipofectamine Transfection of Plasmids

Prior to transfection, cells were seeded into 6-well plate (300K - 400k cells/well). Once the cells were 70-80% confluent, transfection was started by diluting 40 µl of Lipofectamine 2000 reagent (ThermoFisher 11668019) in 1000 µl of Opti-MEM serum free medium (ThermoFisher 31985062) in one 2-ml Eppendorf tube, while 16 µg of plasmid DNA (ACC1 plasmid along with GFP control plasmid) was diluted 1000 µl of Opti-MEM, separately, in a second tube. Reagents were incubated for 5 minutes at room temperature. Then, the diluted DNA was added to the diluted Lipofectamine 2000 solution at a 1:1 ratio and left to incubate for 20 minutes at room temperature. Meanwhile, the media of cells was changed and 1500 µl of fresh media was added to each well. After incubation, 500 µl of the Lipofectamine-DNA mixture was added (final volume of media was 2000 µl). The cells were left to incubate at 37°C, 5% CO_2 for 24 hours, followed by a media change. Cells were generally harvested after a further 24-48h culture.

For cells transfection with lipofectamine 3000 (ThermoFisher L3000015) the same protocol was followed with some modifications; when diluting DNA in OptiMEM™ Medium, P3000™ reagent (2 µL/µg DNA) was added to the mix.

Chapter 2.5.6 siRNA Transfection

CK2 siRNA (ThermoFisher, 4390815) along with siRNA stealth nonsense control oligo (Thermofisher) were diluted, separately, in Opti-MEM serum free medium (ThermoFisher) in 2-ml Eppendorf tubes (12.5 µL of siRNA in 625 µL of Opti-MEM).

Lipofectamine RNAiMax (ThermoFisher, 13378-150) was also diluted in Opti-MEM media in 2-ml Eppendorf tubes (37.5 µL of lipofectamine in 625 µL of Opti-MEM).

Diluted lipofectamine RNAiMax was mixed diluted siRNA oligo and incubated at room temperature for 20 minutes. Meanwhile INS1 cells were split and diluted in complete growth media so that 100 µL of contains the appropriate number of cells (100,000 cells/well) to give 30-50% confluence 24 hours after plating. 20 µL of siRNA-Lipofectamine complex was added to each well (96-well plate). This was followed by adding 100 µl of the diluted cells to each well. The cells and siRNA-Lipofectamine complex was mixed gently by rocking the plate back and forth. Cells were incubated for 24 - 48 hours at 37°C in a CO2 incubator until they are ready for downstream applications. Medium was changed 24 hours after transfection.

Chapter 2.6 Proteins Methods

Chapter 2.6.1 Cell Lysis and Proteins Extraction

All steps were done at 4°C or on ice to prevent proteins or phosphoproteins degradation . NP40 and RIPA lysis buffer was prepared as follows:

RIPA lysis buffer: Tris HCL (65 mmol/l), NaCl (150 mmol/l), EDTA (5 mmol/l), Np-40 (1%), Na-deoxycholate (0.5%), SDS (0.1%). Glycerol (10%).

Np-40 lysis buffer: Tris HCL (50 mmol/l), NaCl (150 mmol/l), Np 40 (1%), Glycerol (10%).

Protease inhibitors (Roche 04693159001) and phosphatase inhibitors (Roche 04906837001) tablets were added to lysis buffer (1 tablet /10 ml).

Cells were washed twice with ice cold PBS, keeping dishes on ice throughout, the same volume of PBS as for media was used. After second wash, dishes were tiled on ice and all PBS has been removed. An appropriate volume of lysis buffer for the cell density was added (6 well plate: 65-150 µl,10cm dish: 500-1200 µl). Cells were then scraped with a cell scraper, the lysate was transferred to a labelled tube and a sonicator was used to further aid the lysis process. Tubes were centrifuged for 15 minutes at 13K RPM at 4°C in bench top centrifuge. The supernatant was transferred to a fresh tube and the pellet was discarded. Lysates were stored at -80°C for downstream applications.

Chapter 2.6.2 Liver Proteins Extraction

Mouse livers were collected, immediately snapped frozen in liquid nitrogen and stored at -80°C. For lysis, livers were kept on dry ice and crushed into small pieces, then a spoon was used to transfer equal amounts (almost 50 mg) of livers pieces (from different conditions) to fresh tubes,

ice cold RIPA lysis buffer (500 µl), containing proteases and phosphatases inhibitors, was immediately add to the livers. The, the livers were homogenised by a homogeniser at speed 1 for 20-30 seconds. Samples were then kept on ice for 30 seconds then additional bursts of 20-30 seconds homogenisation interspersed with 30-60 seconds rest on ice. Tissue lysates were kept on ice for 1 hour, then spun at 12,000 RPM to remove insoluble debris, supernatants were transferred into fresh tubes and stored at -80°C.

Chapter 2.6.3 BCA Assay

The protein concentrations of INS1 cells, islets, Alpha cells and liver supernatant were determined using Bicinchoninic acid assay (BCA) (Thermo Fisher, Waltham, MA, USA, Catalogue number 23225).

According to the manufacture's protocol, This assay measures the proteins concentration in the sample based on two reactions (1) reduction of Cu^{2+} to Cu^{1+} by protein in an alkaline medium, which is strongly influenced by four amino acid residues (cysteine, cystine, tyrosine, and tryptophan) in the amino acid sequence of the protein(2) bicinchoninic acid (BCA) chelate with Cu^{1+} ion creating a purple-coloured complex that absorbs light at a wavelength of 562 nm.

Protein lysates were read against a known bovine serum albumin (BSA) standard curve. Standards were prepared using serial dilution (0, 0.025, 0.125, 0.25, 0.5, 0.75, 1, 1.5, and 2 µg/ µl), and using PBS as a diluent. In standards wells; 25 µl of standards and 2.5 µl of lysis buffer were loaded in a clear flat-bottomed 96 well plate. In sample wells; 2.5 µl of lysates and 25 µl of PBS were loaded (1 in 11 dilution). Working reagent were prepared by mixing 50 parts reagent A to 1 part reagent B (allowing 0.2ml per well + 2ml multi-channel pipetting buffer). 200 µl working reagent were added to all wells. Plate was sealed and incubated at 37ºC for 30 minutes. The absorbance was measured at 562 nm using Tecan Spark 10M plate reader (Männedorf, Switzerland).

Chapter 2.6.4 ACC1 and PC Pull Down

The fundamental concept of our approach to purify ACC1 and PC in sufficient quantities for proteomic analysis, is to use the naturally biotinylated state of the protein (due to its carboxylase activity) enabling ACC1 and PC to bind streptavidin with a strong non-covalent bond (Fig 2.1 A & B). This approach will purify not only ACC1 and PC but all biotinylated proteins in the cells. Therefore, this protocol will ensure that purified proteins are separated using gel electrophoresis, visualised and fixed using Coomassie blue staining (MS Compatible stain). The corresponding ACC1 band is then excised from the gel, digested using trypsin and analysed by LC-MS/MS.

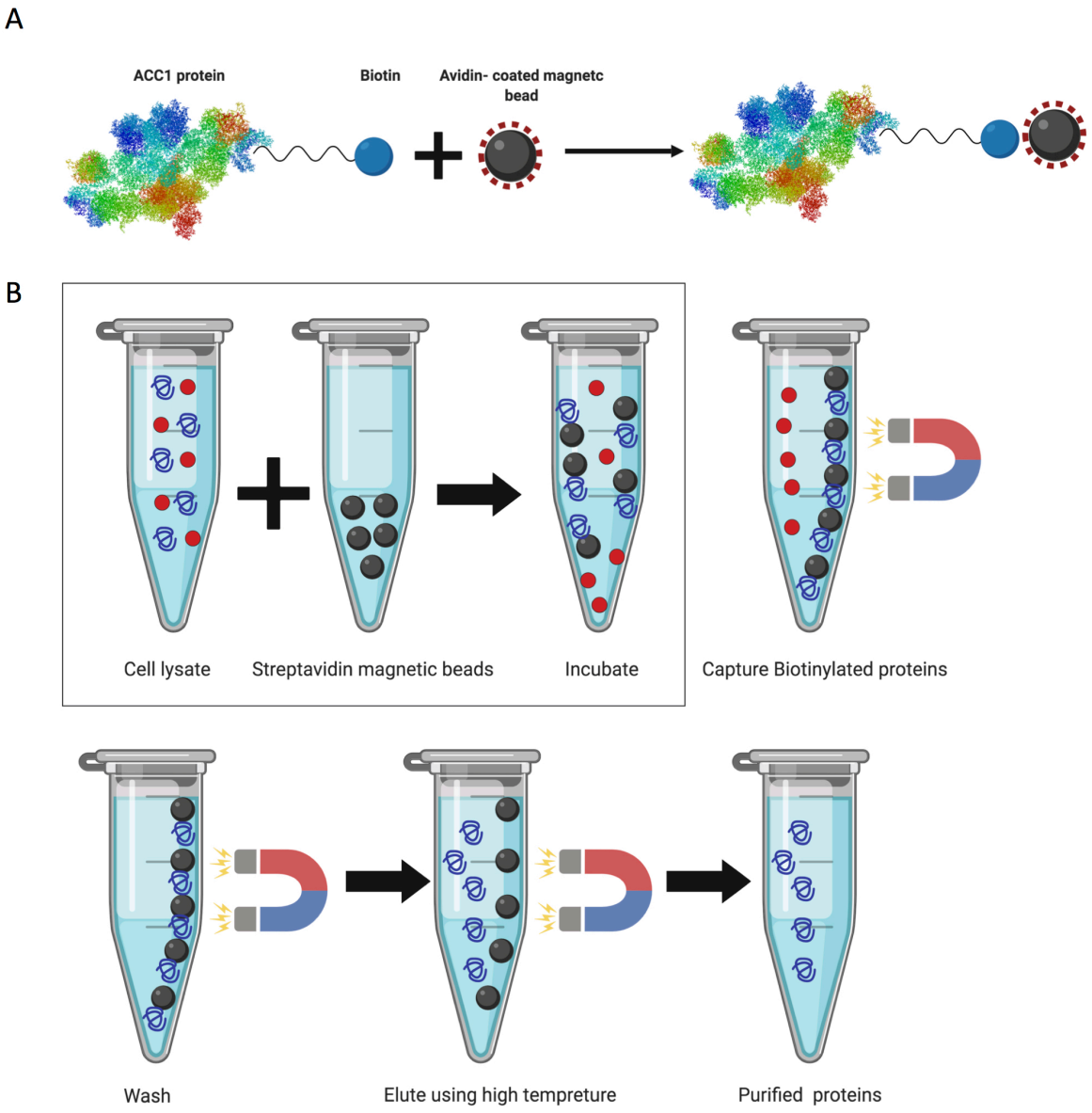


Figure 2-1 ACC1 pull down protocol principle and workflow. (A) ACC1 pull down principle (B) ACC1 pull down protocol workflow, adopted from (abramagnetic beads).

ACC1 Streptavidin magnetic beads (Thermofisher, Waltham, MA, USA Catalogue number 65001) were resuspended first in the vial by vortex for 30 seconds and then transferred to 2 ml Eppendorf tube (400 µl/ condition). The beads were then washed with 1 ml PBS-Tween (1%), and placed near a magnet for three minutes. The supernatants were discarded, the tube were removed from the magnet and re-suspended in a volume of washing buffer equal to the initial volume of beads taken from the vial. The washing step was repeated for two times (total three times washes). Cell lysate for each condition (10 mg of proteins) were distributed into three tubes; with each tubes containing 1 ml of lysates plus 133 µl of magnetic beads. The beads were then incubated overnight at 4^{o}C on a rotator. After overnight incubation the beads were placed near a magnet for three minutes, the supernatant was discarded and the beads were washed then for three times with 2 ml washing buffer; 2% Sodium Dodecyl Sulfate (SDS). In the last wash the beads (for each condition) were combined. 110 µl of 4X loading dye (Catalogue number NP0008) and 40 µl of 10X reducing agent (Catalogue number B0004) were added to each condition. Tubes were then vortexed briefly and heated at 95c for 12 minutes. 60 µl of each condition was loaded into 4-12% linear gradient ready polyacrylamide gel and run for two hours at 130 volts. The gel then was washed three times for 10 minutes with distilled water, then stained for two hours with 25 ml of Coomassie Blue staining (catalogue number LC6060), then washed with distilled water for two hours.

Chapter 2.6.5 Gel Electrophoresis

Proteins samples (30 µg) were mixed with 1X bolt reducing agent and 1X loading dye. Samples were then heated for 10 minutes at 70 ^{o}C. 30 µl of each samples were loaded into 4-12% linear gradient ready polyacrylamide gel with 1x MOPS running buffer (catalogue number NP0001) at 165 volt for 60 minutes using a mini gel tank. 4 µl of MagicMark™ XP (catalogue number LC5602) and Novex Sharp pre-stained protein standard (catalogue number LC5800) were loaded

alongside protein samples to allow molecular weights to be estimated. The separated proteins were transferred from the electrophoresed Bolt Mini Gel onto a PVDF membrane (polyvinylidene difluoride, Invitrogen, pore size: 0.45 µm, catalogue number LC2005) by the Bolt Mini Blot Module (Novex, catalogue number B1000). Before blotting; PVDF membrane was equilibrated in methanol (100 %) for 2-3 minutes and filter papers were equilibrated in transfer buffer (1X, Catalogue number BT0006). The running conditions were 20-volt constant for 60 minutes.

Chapter 2.6.6 Immunoblotting

Membranes were blocked by incubating for 60 minutes in TBST containing 5% BSA powder (w/v) (for phosphorylated proteins) or 5% non-fat milk powder at room temperature with gentle rocking (to block available protein binding sites on the membrane, thereby minimising non-specific antibody binding). Membranes were washed for three times for 10 seconds in TBST to wash off excess milk. Membranes were cut into strips according to the molecular weights of target proteins, to enable different strips to be incubated in different primary antibody solutions. Primary antibodies were typically diluted 1/1000 in antibody dilution buffer which contains BSA as a blocking agent and sodium Azide as a preservative. Membranes were then incubated in 5ml primary antibody dilution in a 50ml falcon tube on a rotator (with protein side facing inward) over night at 4 °C (Detailed information on each primary antibody is within relevant chapters). Membrane were rinsed once, then washed for three time for 10 minutes in TBST. Secondary antibody were diluted 1/5000, added to the membranes and incubated at room temperature on the shaker for one hour. Membrane were rinsed once, then washed for three time for 10 minutes in TBST. Proteins were then detected by enhanced chemiluminescence (ECL) prime (ECL prime, Amersham, GE Healthcare). ECL solutions were mixed in 1:1 ratio (luminol solution: peroxide solution). Typically, 0.75ml:0.75ml were used for a single intact membrane. Membranes were

faced down on ECL solution for 5mins while protected from light. Membranes were then transferred into an X-ray cassette and proteins were visualised using Hyper-film ECL autoradiography film (Amersham, GE Healthcare) .

Chapter 2.6.7 Bands Densitometry

Band density was quantified using Image J software (NIH, Bethesda, MA, USA).

Chapter 2.8 CRISPR-Cas9

Approximately, 500,000 INS1 cells were seeded into 6-well cell culture plates and maintained in RPMI medium supplemented with 5% fetal bovine serum (FBS), at 37°C in a CO2 incubator overnight. For transfection, cells were detached from culture flasks using trypsin and resuspended at a density of 1×10^6 cells/ml. Cells were then transfected with four different combination of Cas-9-gRNA complex (Table below) and transferred into 6-well plates. This strategy was employed to induce Acaca-targeted double strand breaks in INS1 cells at the genomic locus at chromosome 17. Cells were maintained in culture for 48 hours at 37°C post-transfection then transferred into 96 well plates using a cell dilution method to allow isolation of single colonies (genome-targeted monoclonal cell clones). For single cell sorting, cells were detached from plates using trypsin and resuspended in phosphate-buffered saline (PBS) at 1:10000 dilution. Cells were then sorted by fluorescence-activated cell sorting (FACS) into 96-well plates containing pre-warmed medium. Single cells were expanded for 3 weeks to form colonies.

gRNA name	gRNA Sequence
g-119	GCATGCGATCTATCCGGCGG
g-120	AATGCATGCGATCTATCCGG
g-121	CTCTACTGTAGTAAGCGAGT
g-122	GTAAGCGAGTTGGCATCCA

Chapter 2.9 Antibody Generation

ACC1S1215 and ACC1S49 phospho-specific rabbit polyclonal antibodies were custom-made (DC Biosciences, Dundee). For each antibody two rabbits were immunised with site specific phospho-peptide, two rounds of purifications have been carried out and nine fractions have been collected. For ACC1S1215 phospho-specific antibody the peptide sequence: CMTHVA(pS)VSDVLLDN. For ACC1S49 phospho-specific antibody the peptide sequence: CEEKEGSL(pS)PASVSS.

The number of injections: 4, number of bleeds: bleeds after second, third and final immunisations, plus purification fractions. Isotype: igg.

Antibody Preparation: the antibody has been isolated from antisera by immunoaffinity chromatography using antigens coupled to agarose beads.

The antibodies were stored at 4°C short term (1-2 weeks). For long term storage, the antibodies were aliquoted in small aliquots of 200µl and stored at -80°C.

Chapter 2.10 Statistical Analysis

Data are expressed as mean ± standard error of the mean (SEM). Statistical analysis were performed using Prism6 (GraphPad Software, San Diego, CA, USA). Simple pairwise comparisons were made using two-tailed t tests (unpaired unless otherwise stated) to compare the

difference between the means of two groups. Multiple comparisons were made using two-way ANOVA with Bonferroni post-tests. A p-value <0.05 was regarded as statistically significant. The significance levels between groups are indicated by asterisks in each figure above the bars.

Chapter 2.11 Diagrams

All diagrams in this thesis were created with BioRender website unless otherwise stated.

Chapter 3 The Role of ACC1S79 in Beta Cells Function

Chapter 3.1 Introduction

In beta cells, ACC1 plays a role in insulin secretion *in vitro*[44,47,96]. More recently, the Cantley group have revealed a critical role for ACC1 activity in maintaining beta cell growth and insulin secretion *in vivo*[1]. Notwithstanding strong evidence for the role of ACC1 in insulin secretion, very little is known about how ACC1 activity is regulated in beta cells. Incubation of beta cells with glucose for just 30 mins leads to ACC1 activation and is associated with increased insulin secretion[97]. This activation is likely due in part to allosteric activation of ACC1 by citrate, but may also be influenced by post-translational modifications (PTMs) of ACC1. For example, phosphorylation of ACC1S79 by 5'-AMP-activated protein kinase (AMPK) inactivates ACC1 in other tissues (e.g. liver)[98].

While there is extensive evidence that ACC1S79 is a well-established target of AMPK, the functional importance of this site in metabolic regulation of beta cells function and insulin secretion has not been previously explored.

Several studies have shown that AMPK activation is associated with a cessation of insulin secretion in beta cells and islets [99]. However, the underlying mechanisms and how much of this effect is due to phosphorylation of ACC1 at S79 remain largely elusive. Therefore, the aim of this chapter is to assess the role of ACC1S79 in insulin secretion and glucose homeostasis *in vivo*.

Recently, Kemp and co-workers have generated a mouse model with alanine knock-in mutations in both ACC1 (at S79) and ACC2 (at S212). This mouse model named ACC double knock-in (ACCDKI). ACCDKI mice were found to be glucose and insulin intolerant compared to the wild types[2]. In this mouse model, insulin secretion and islet function *ex vivo* have not been examined.

Therefore, we imported this mouse line to Oxford (in collaboration with Prof. Kemp, Melbourne) to generate a mouse model carrying a single mutation only in ACC1 (ACC1S79A).

We were interested in ACC1 only, as ACC2 is barely expressed in beta cells[44]. Moreover, the phenotype of the single ACC1 S79A mutation has not been reported.

We hypothesise that ACC1S79 plays a role in the regulation of insulin secretion by glucose.

The aims of this chapter are:

- To further investigate the role of ACC1S79 in glucose homeostasis *in vivo*.
- To assess the role of ACC1S79 in islets function *ex vivo*; as a glucose and AMPK-regulated phospho-site.

Chapter 3.2 Methods

General methods are described in chapter 2; this section describes the breeding plan for ACCDKI mice to generate ACC1SKI mouse model.

Chapter 3.2.1 Breeding Plan for ACCDKI Mice to Generate ACC1SKI Mouse Model

The breeding plan to generate ACC1SKI mouse model is shown in figure (3-1). We initially crossed mice that were homozygous for both mutation (ACC1S79A, ACC2S212A) with wild type mice (C57Bl/6 background) to generate heterozygous mice for both mutations. Then, we crossed heterozygous F2 mice; which resulted in many outputs, from which we crossed mice that were heterozygous for ACC1S79A and wild type for ACC2S212A to generate mice with ACCS79A homozygous mutation and their littermate control. ACC1SKI mice were born with the expected Mendelian frequency. Eventually, we generated 5 cohorts of mice in total to reach minimum n= 12 per genotype per sex.

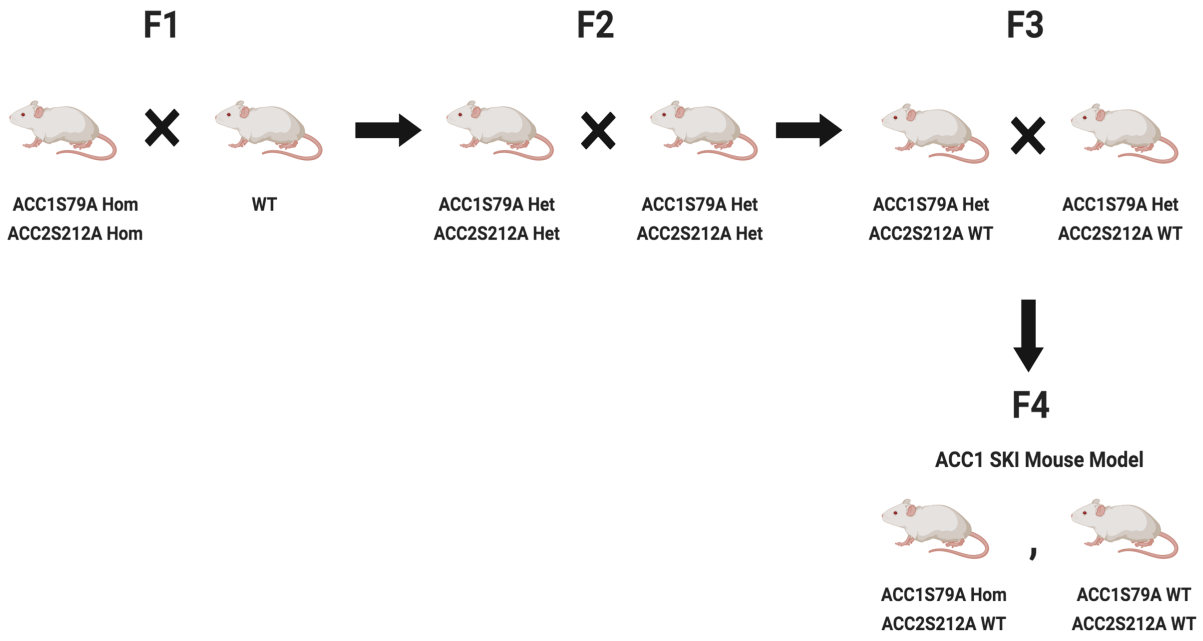


Figure 3-1 Breeding strategy for generation of ACC1SKI model. Mice that were homozygous for both mutation (ACC1S79A, ACC2S212A) were crossed with wild type mice to generate heterozygous mice for both mutations. Then, we crossed heterozygous F2 mice; from which we crossed mice that were heterozygous for ACC1S79A and wild type for ACC2S212A to generate mice with ACCS79A homozygous mutation and their littermate control. After 9 months of breeding cycles, we generated 5 cohorts of mice in total to reach minimum n= 12 per genotype per sex.

Chapter 3.2.2 Phenotyping Pipeline for ACC1SKI mice

5 cohorts of ACC1 SKI were phenotyped at 12-16 weeks of age. The phenotyping pipeline is exhibited in figure 3-2.

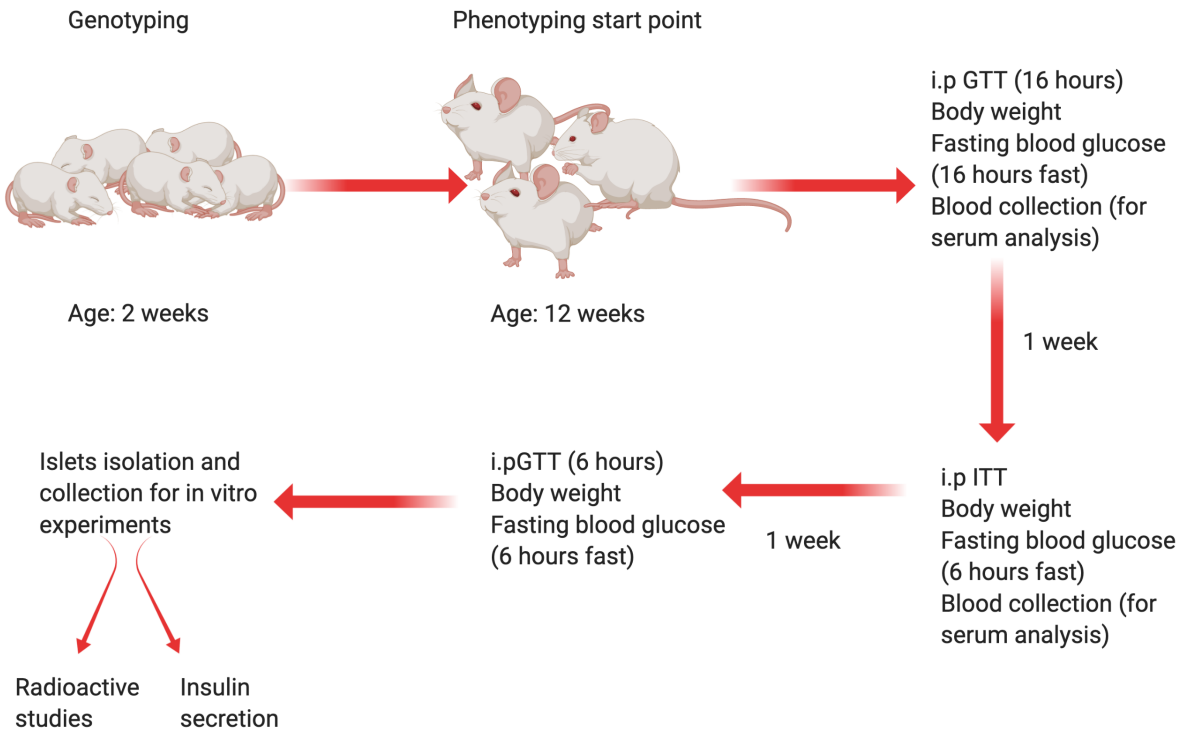


Figure 3-2 Phenotyping pipeline for ACC1SKI mice.

Chapter 3.2.3 Chemicals preparation

Metformin, AICAR and PFZ were purchased from Sigma. Metformin (metformin hydrochloride, CAS number 1115-70-4) stock (500 mmol/l) was prepared in H_2O and stored at -20°C. AICAR (CAS Number 2627-69-2) stock (500 mmol/l) was prepared in H_2O and stored at -20°C. PFZ (CAS Number 1467057-23-3) stock (100 mmol/l) was prepared in DMSO and stored at -20°C.

Chapter 3.3 Results

Chapter 3.3.1 The Role of ACC1S79 in Glucose Homeostasis *in Vivo*.

In order to investigate the functional role of ACC1S79 in glucose homeostasis *in vivo*, we phenotyped the 5 cohorts at 12-16 weeks of age. We observed no difference in the body weight (figure 3-3 A& B) and fed blood glucose (figure 3-3 C&D) between the two genotypes in both sexes. There was also no significant difference in fasting blood glucose levels after 6 hours and 16 hours of fasting in the females (figure 3-3 F&H). However, blood glucose levels after 16 hours of fasting was lower in ACC1SKI male mice compared to the wild type (figure 3-3 E).

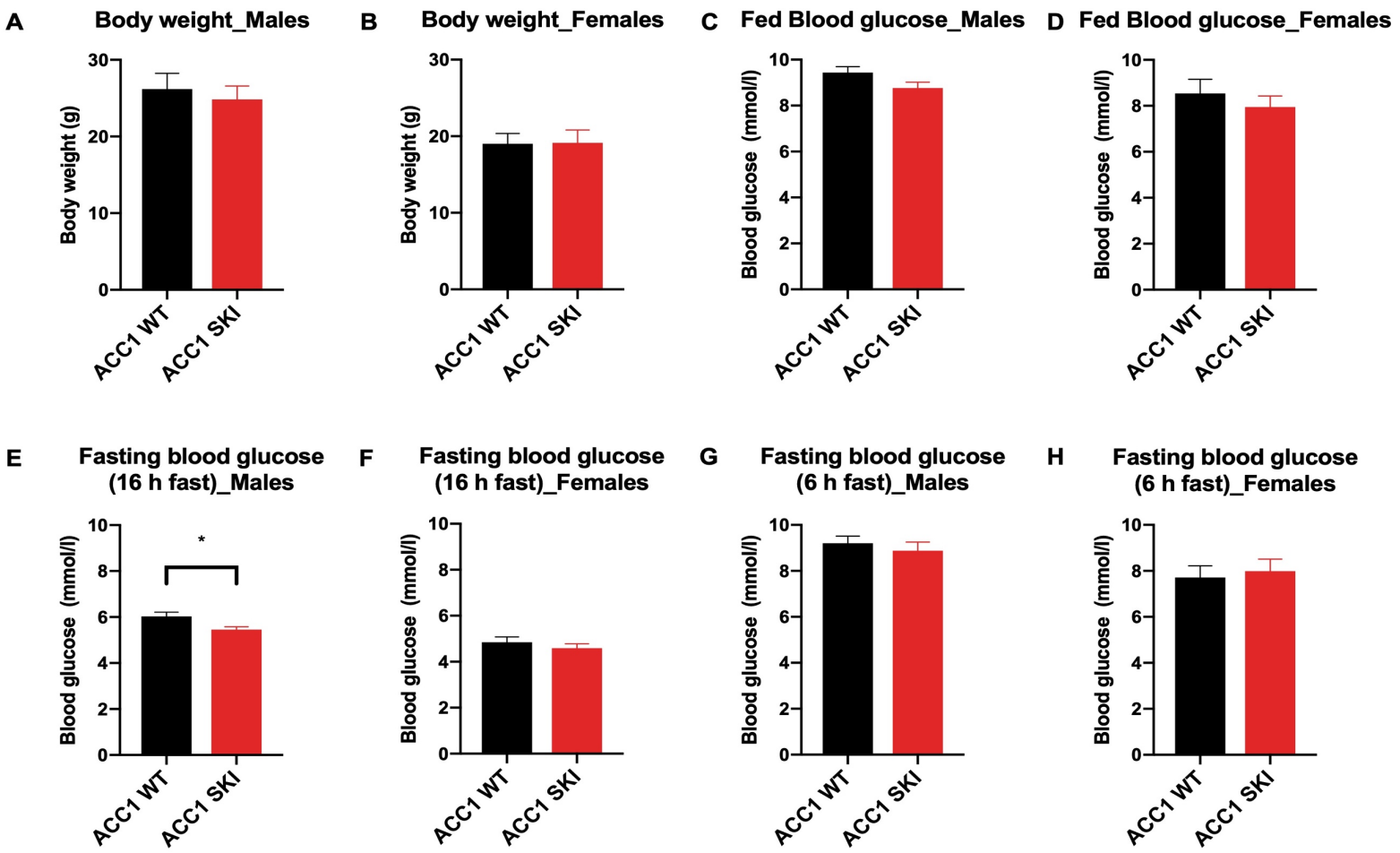


Figure 3-3 Body weight, fed blood glucose and fasting blood glucose in ACC1SKI mouse model. (A,B) Body weight at 12 weeks of age in the males(n=16 ACC1Wt mice and 12 ACC1SKI) and females (n=13 ACC1Wt mice and 14 ACC1SKI) **(C,D)** Fed blood glucose in males (n=12 ACC1Wt mice and 12 ACC1SKI) and females (n=4 ACC1Wt mice and 6 ACC1SKI) at 12 weeks of age **(E,F)** Fasting blood glucose (16-hours fast) in males (n=16 ACC1Wt mice and 12 ACC1SKI) and females (n=13 ACC1Wt mice and 14 ACC1SKI) at 12 weeks of age **(G,H)** Fasting blood glucose (6-hours fast) in males (n=16 ACC1Wt mice and 12 ACC1SKI) and females (n=13 ACC1Wt mice and 14 ACC1SKI). Data are presented as mean ± SEM. *$p<0.05$ (unpaired two-tailed t test).

To assess glucose sensitivity *in vivo*, we performed intraperitoneal glucose tolerance tests (i.pGTTs). We injected 2g/Kg of glucose at baseline; then we measured blood glucose levels at specific time points: 15, 30, 60 and 120 minutes' post glucose injection. We performed this test after 16 hours and 6 hours of fasting to assess glucose tolerance after a long, catabolic fast associated with low blood glucose levels, and a short fast preserving post-prandial blood glucose levels, respectively. As shown in figure (3-4), after 16 hours of fasting ACC1SKI male mice are slightly more glucose tolerant compared to wildtypes, however, it did not reach statistical significance after correction for multiple comparison. GTT after 6 hours of fasting in both males and females was not altered.

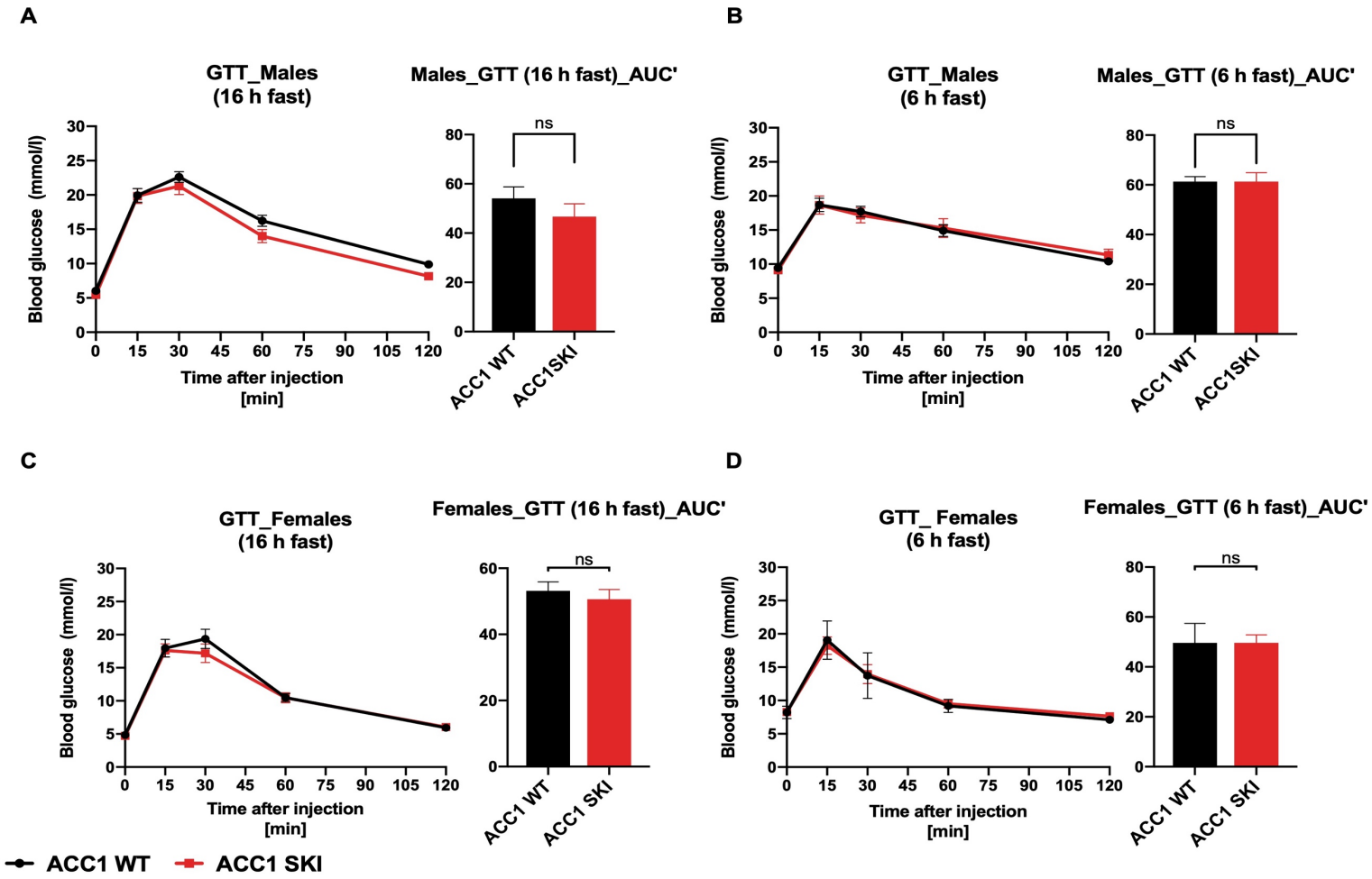


Figure 3-4 Glucose tolerance test in ACC1SKI mice.(A) GTT at 12 weeks of age in the males after 16 hours of fasting (n=16 ACC1Wt mice and 12 ACC1SKI) **(B)** GTT at 12 weeks of age in the males after 6 hours of fasting (n=16 ACC1Wt mice and 12 ACC1SKI) **(C)** GTT at 12 weeks of age in the females after 16 hours of fasting (n=13 ACC1Wt mice and 14 ACC1SKI**) (D)** GTT at 12 weeks of age in the females after 6 hours of fasting (n=4 ACC1Wt mice and 6 ACC1SKI). Data are presented as mean ± SEM. (two-way ANOVA with Bonferroni multiple comparisons test for time plots, unpaired two-tailed t tests for bar charts).

The slight improvement in glucose sensitivity in ACC1SKI compared to the wild types seen in the male cohort could be explained by either increased insulin secretion in ACC1SKI or insulin action (i.e. insulin sensitivity). We measured Insulin levels at baseline and after 30 minutes of glucose stimulation, yet we saw no significant difference in the level of circulating insulin (figure 3-5 A&B). Next, we assessed insulin sensitivity by performing intraperitoneal insulin tolerance tests (i.pITT). We injected males with 0.85U/kg and the females with 0.5U/kg insulin and measured the blood glucose levels at specific time points. The degree to which blood glucose levels fall in response to insulin is suggestive of insulin sensitivity. As shown in figure (3-5 C & D) ACC1SKI male mice were more insulin sensitive compared to the wildtypes, however, it did not reach statistical significance after correction for multiple comparison.

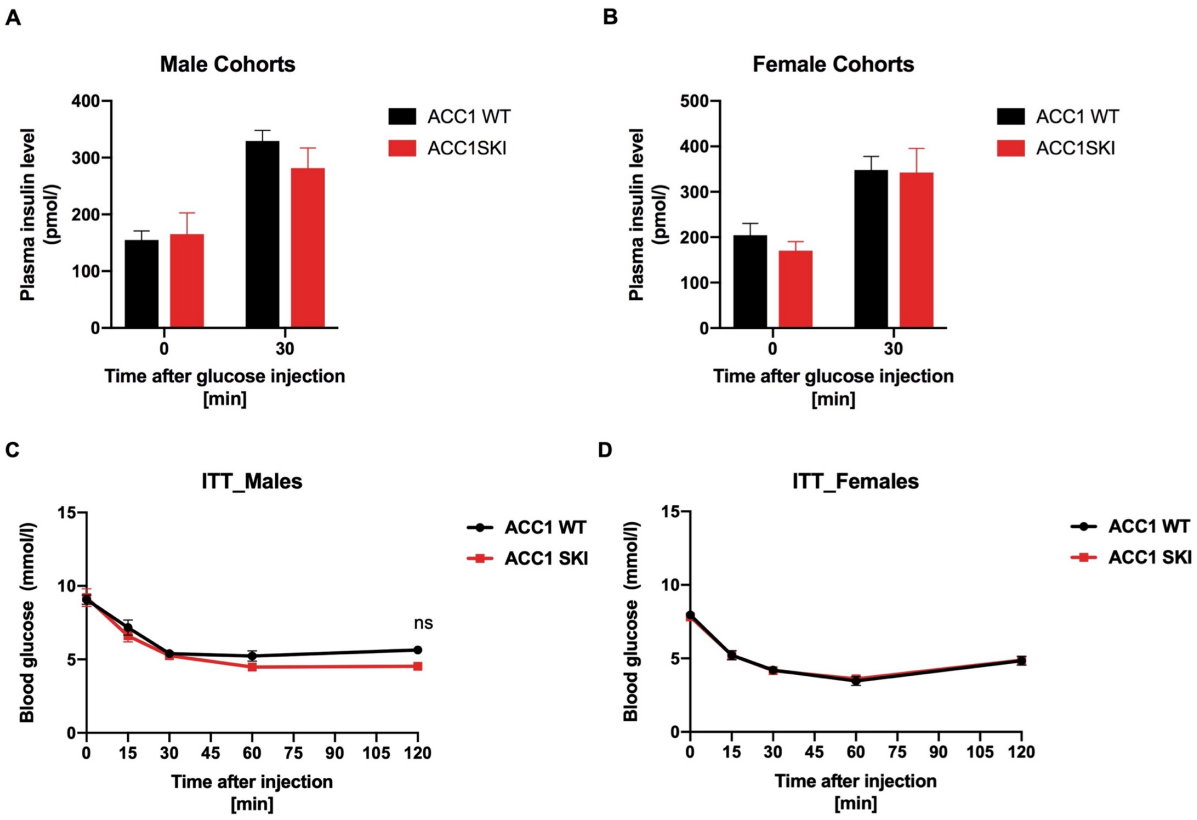


Figure 3-5 Circulating insulin and insulin tolerance test in ACC1SKI mice. (A,B) Circulating insulin measured at fasting state (16-hours fast) and after 30 minutes of glucose injection in males (n=13 ACC1Wt mice and 10 ACC1SKI**)** and females (n=10 ACC1Wt mice and 8 ACC1SKI**)** at 12 weeks of age **(C,D)** ITT for males (n=12 ACC1Wt mice and 9 ACC1SKI) and females (n=13 ACC1Wt mice and 14 ACC1SKI). Data are presented as mean ± SEM(two-way ANOVA with Bonferroni multiple comparisons test for time plots, unpaired two-tailed t tests for bar charts).

Chapter 3.3.2 ACC1S79 as A Glucose Regulated Phospho-Site in Wild Type Islets:

The next aim in this project was to examine the role of ACC1S79 in islet function *ex vivo* as a glucose regulated phospho-site and as an AMPK regulated phospho-site. Before testing ACC1SKI islets function we aimed to characterise this site in wildtype islets first. Even though, ACC1S79 is commonly profiled in islet studies, our data shows that the glucose response is minimal in beta cells following treatment of wild type islets for one hour in low (2 mmol/l) and high (20 mmol/l) glucose conditions (Figure 3-6). In contrast, ACC1S79 shows dramatic response in the liver after 15 minutes of glucose injection.

In this experiment wild type mice (C57BL6 background) were injected with glucose (2g/kg) or PBS, liver was then collected and snap frozen to asses ACC1 phosphorylation *in vivo* in the liver. On the other hand, considering the time required to isolate islets; ACC1 phosphorylation in response to glucose in islets was assessed *in vitro* (i.e. isolated islets). However, it should be emphasised that the *in vivo* assessment of ACC1S79 phosphorylation in the liver cannot be compared to the *in vitro* assessment of ACC1S79 phosphorylation in islets.

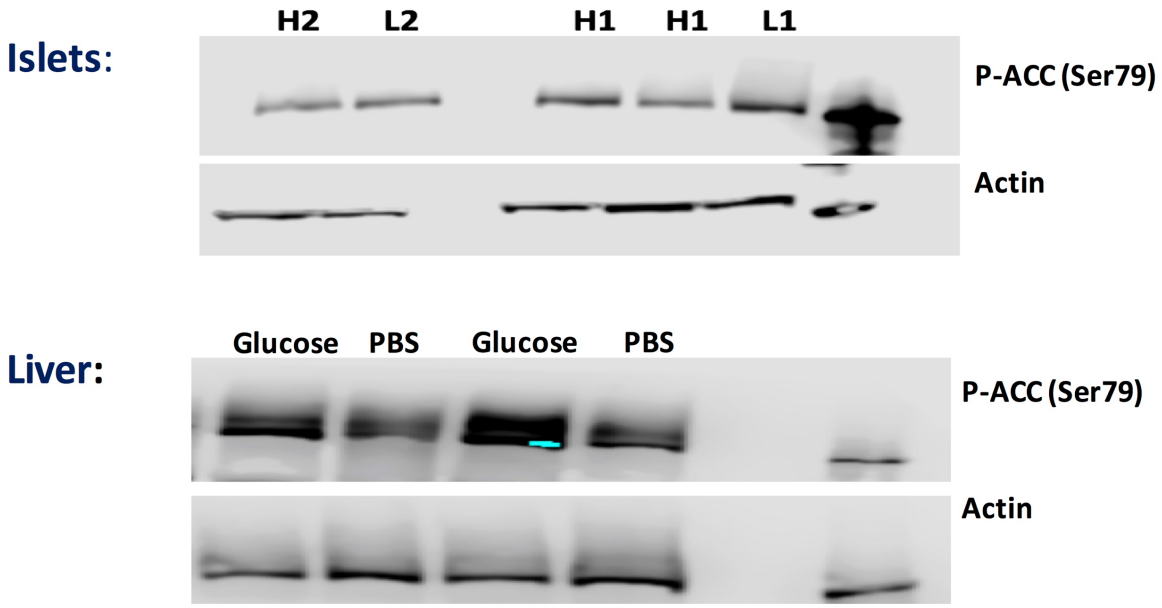


Figure 3-6 ACC179 phosphorylation in response to glucose in wild type islets compared to the liver. Isolated wild type islets were treated with low (2 mmol/l) and high (20 mmol/l) glucose conditions for 1 hour. Wild type mice (C57BL6 background) were fasted overnight, then liver was collected after injecting with glucose (2g/kg) or PBS. 30 μg of proteins was loaded in the gel for each condition. Commercial p-ACC1S79 antibody (Cell Signalling 11818), molecular weight: 269 kDa, was used at 1:1000 dilution, B-Actin (Cell Signalling 8457), molecular weight: 42 kDa, was used as a loading control at 1:100 dilution, and a rabbit HRP conjugated secondary antibody (Cell Signalling 8457) was used at 1:5000 dilution.

Chapter 3.3.3 Testing AMPK Activators Effect on Insulin Secretion and ACC1S79 Phosphorylation in Islets

A much-debated question in the literature is the effect of AMPK activation on insulin secretion. On the one hand, several papers showed that AMPK activators suppress insulin secretion[90,100,101] and suggested that this effect could be due to inhibition of ACC1 pathway[86] (figure 3-7). On the other hand, others showed that AMPK activation enhances insulin secretion; possibly through an AMPK Independent effect[102,103]. We aimed here to see its effect on insulin secretion and to answer the long-lasting question; how much of this effect is due to phosphorylation of ACC1 at S79, using ACC1SKI mouse model. Taking into account that there is a wide range of AMPK activators and that much of the previous literature lacked consistency in terms of the dose used and duration of treatment (which ranged from 1 hour to 72 hours), we designed a series of experiments to test different AMPK activators to establish the optimal dose and duration of treatment that yield firstly the maximal effect on ACC1 phosphorylation at S79, and secondly a consistent effect on insulin secretion on wild type islets.

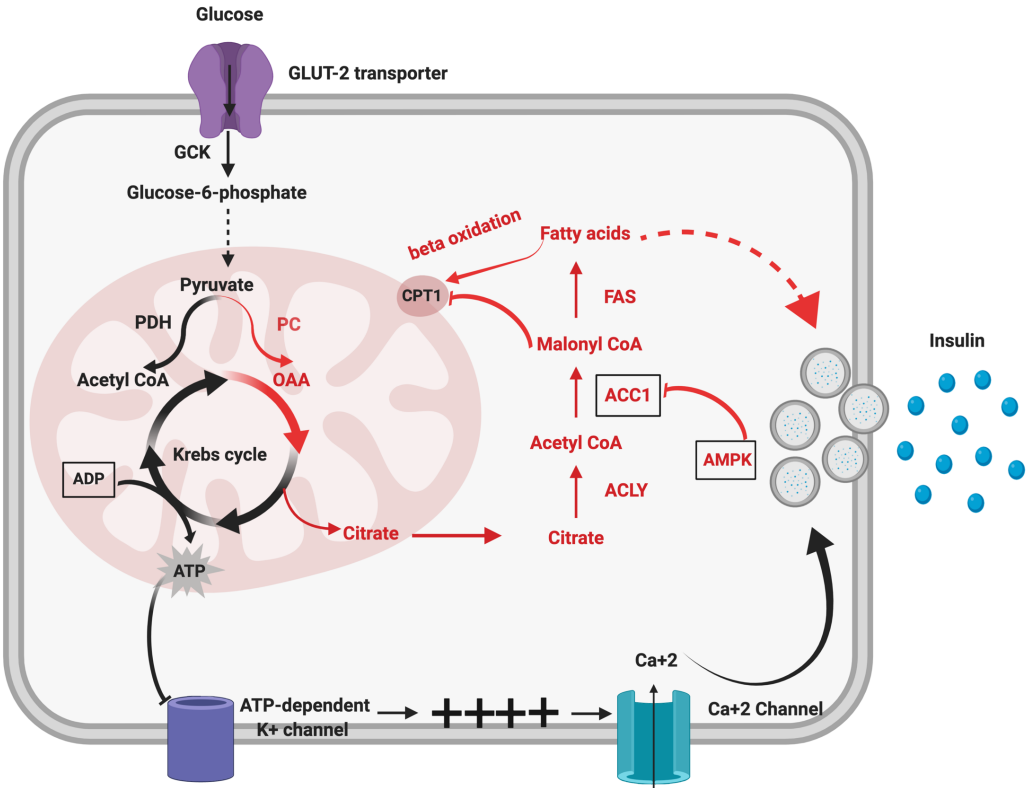
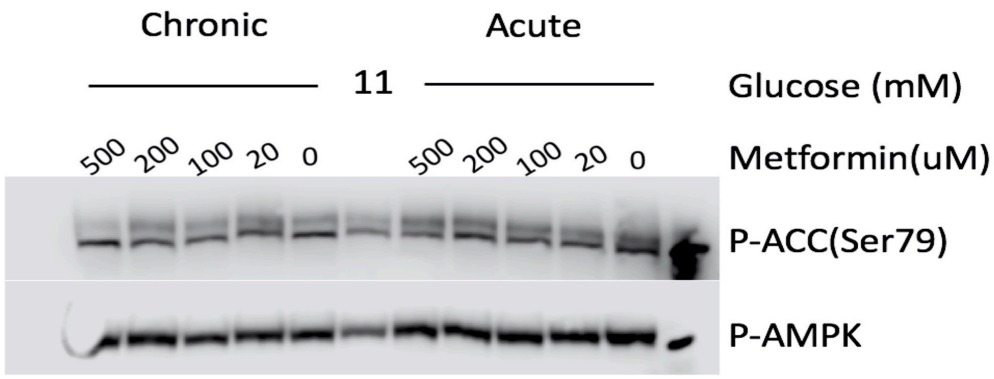


Figure 3-7 The potential regulatory role of AMPK on ACC1 activity and insulin secretion.

We first tested metformin, a well-known AMPK activator that is widely used in treating type 2 diabetes. It activates AMPK indirectly by increasing AMP/ATP ratios through inhibition of complex I of the mitochondrial respiratory chain[104,105]. While metformin primarily increases insulin sensitivity, evidence also suggests that metformin affects the activity of insulin-secreting pancreatic islets[95]. We tested a wide range of metformin doses (20 μM, 100 μM, 200 μM, and 500 μM) acutely for two hours and chronically for 24 hours on wild type islets. As can be seen in figure (3-8), none of these conditions exerted a significant effect on ACC1S79 phosphorylation nor insulin secretion.

A



B

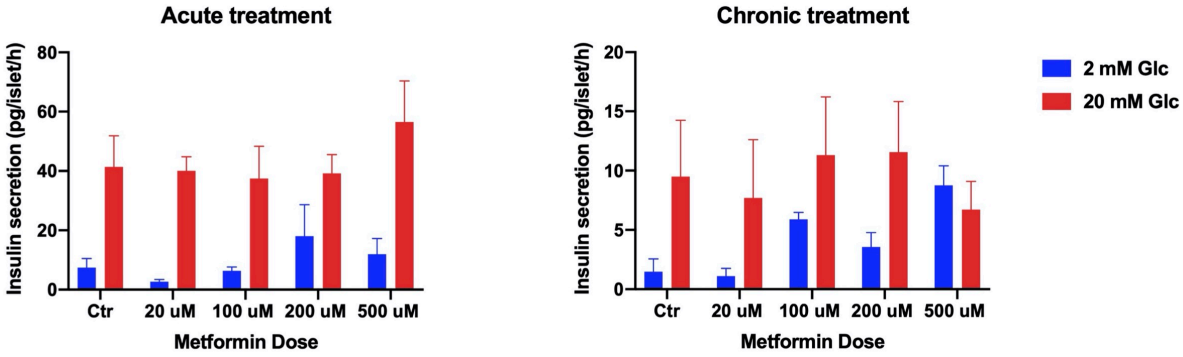
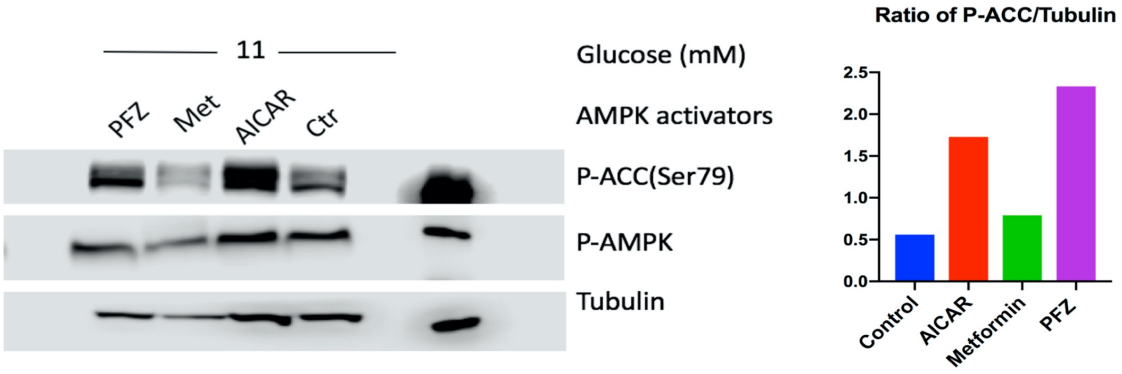


Figure 3-8 Testing metformin effect on ACC1S79 phosphorylation and insulin secretion.
(A) Western blot analysis of islets treated with indicated metformin doses acutely (for two hours) and chronically (for 24 hours). 30 µg of proteins was loaded in the gel for each condition. p-ACC1S79 antibody (Cell Signalling 11818), molecular weight: 269 kDa, was used at 1:1000 dilution. p-AMPK antibody (Cell Signalling 2535), molecular weight: 64 kDa kDa, was used at 1:100 dilution, and a rabbit HRP conjugated secondary antibody (Cell Signalling 8457) was used at 1:5000 dilution. Note: the band in the middle (lane 6) is a leak from the adjacent lane.
(B) Insulin secretion from islets treated with indicated metformin doses acutely and chronically. Data are presented as mean ± SEM.

We subsequently tested another two AMPK activators: 5-Aminoimidazole-4-carboxamide 1-β-D-ribofuranoside (AICAR) and 6-Chloro-5-[4-(1hydroxycyclobutyl) phenyl]-1H-indole-3-carboxylic acid (PFZ), that activate AMPK directly by binding to a specific site within AMPK, leading to conformational changes in the enzyme[10]. Both compounds yielded a significant change in ACC1S79 phosphorylation and enhanced insulin secretion upon one hour of treatment (figure 3-9). In light of these results and given the specificity of PFZ as AMPK activator compared to AICAR, we decided to choose PFZ compound to test ACC1SKI islets in subsequent experiments.

A



B

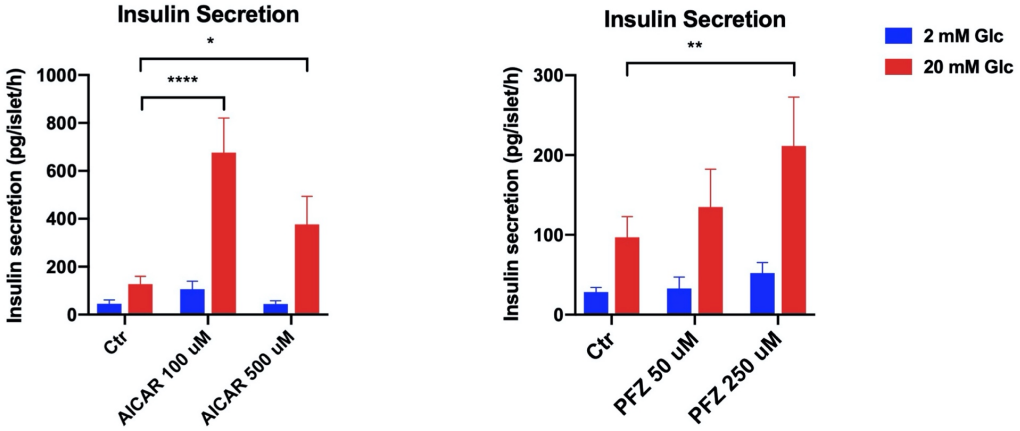


Figure 3-9 Testing AICAR and PFZ compound effects on ACC1S79 phosphorylation and insulin secretion. (A) Western blot analysis of islets treated with different AMPK activators: AICAR (500 μM), Metformin (500 μM), and PFZ compounds (50 μM) for 1 hour, and quantification of band densities using image J (which shows protein levels in each sample relative to the mean control signal. 30 μg of proteins was loaded in the gel for each condition. p-ACC1S79 antibody (Cell Signalling 11818), molecular weight: 269 kDa, was used at 1:1000 dilution. p-AMPK antibody (Cell Signalling 2535), molecular weight: 64 kDa kDa, was used at 1:100 dilution, and a rabbit HRP conjugated secondary antibody (Cell Signalling 8457) was used at 1:5000 dilution. Tubulin was used as a loading control, molecular weight 55 kDa.
(B) Insulin secretion from islets treated with indicated AICAR and PFZ compound doses, n=12 for PFZ experiments and n= 8 for AICAR experiment. Data are presented as mean ± SEM. *p<0.05, **p<0.01 and ***p<0.001. Analysis done using two-way ANOVA with Bonferroni multiple comparisons tests (the test on the graph).

Chapter 3.3.4 The Role of ACC1S79 in Insulin Secretion Ex-*Vivo*

Next, we aimed to assess ACC1SKI islets function *ex vivo*. We observed no significant differences in insulin secretion both at the baseline and in response to glucose stimulation, which is consistent with *in vivo* measurement of circulating insulin levels; suggesting that this phosphosite does not play a role in glucose-induced insulin secretion. After one-hour incubation with PFZ compound, there is an enhancement in insulin secretion in wild type islets. Surprisingly, this enhancement in insulin secretion is reduced in ACC1SKI islets (figure 3-10). Suggesting that this site play a role when AMPK is activated pharmacologically.

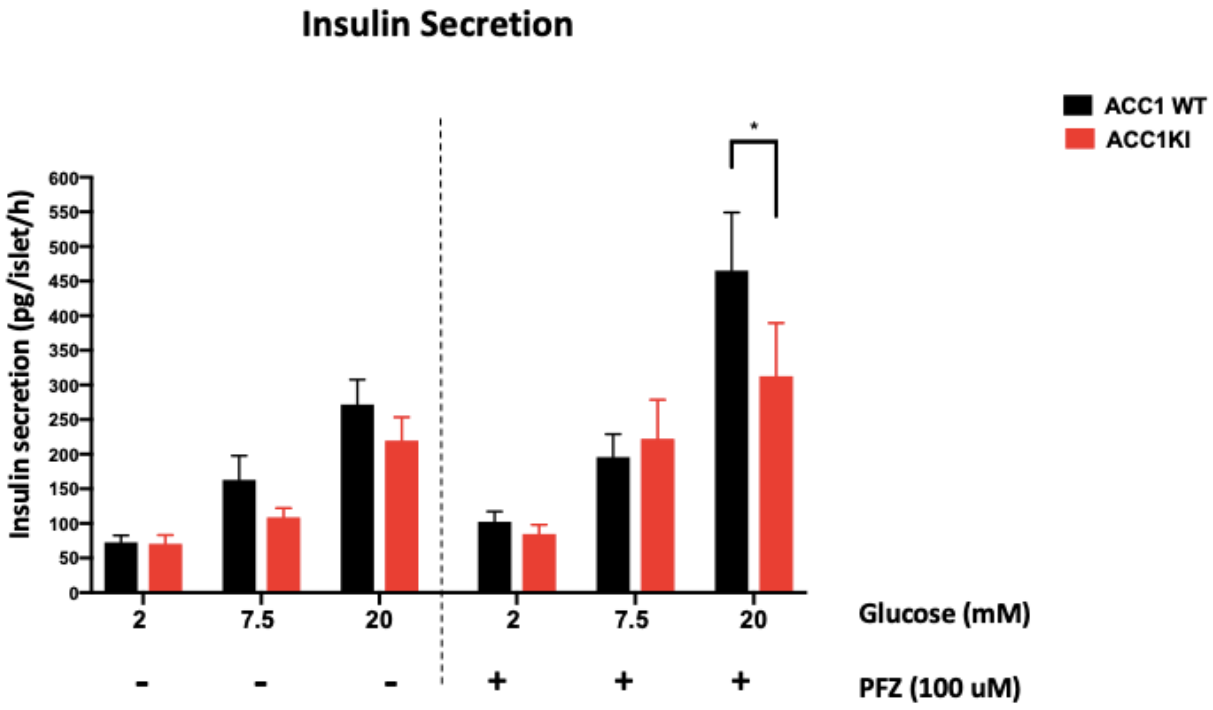


Figure 3-10 GSIS in ACC1SKI islets. Data are presented as mean ± SEM. *p<0.05, **p<0.01 and ***p<0.001. Analysis done using two-way ANOVA with Bonferroni multiple comparisons tests. n ≥ 10 batches of islets collected from 10 independent mice.

Chapter 3.3.5 The Role of ACC1S79 in Glucose Oxidation and DNL

To further assess the role of ACC1S79 in ACC1-coupled pathway in beta cells, we next measured ACC1 activity. Surprisingly, the flux into the lipid pools was impaired in ACC1SKI islets compared to wild type islets at high glucose levels (20 mmol/l) as demonstrated by the impaired flux of d-[U-14C] glucose tracer into total lipid pools (figure 3-11 A). Flux into aqueous pool (figure 3-11 B) and glucose oxidation (figure 3-11 C) were unaffected. We also assessed the impact of pharmacological activation of AMPK on de novo lipogenesis using PFZ: we found that PFZ impaired glucose-flux into lipid pools at high glucose level (20 mmol/l). Remarkably, at high glucose levels PFZ augmented glucose oxidation.

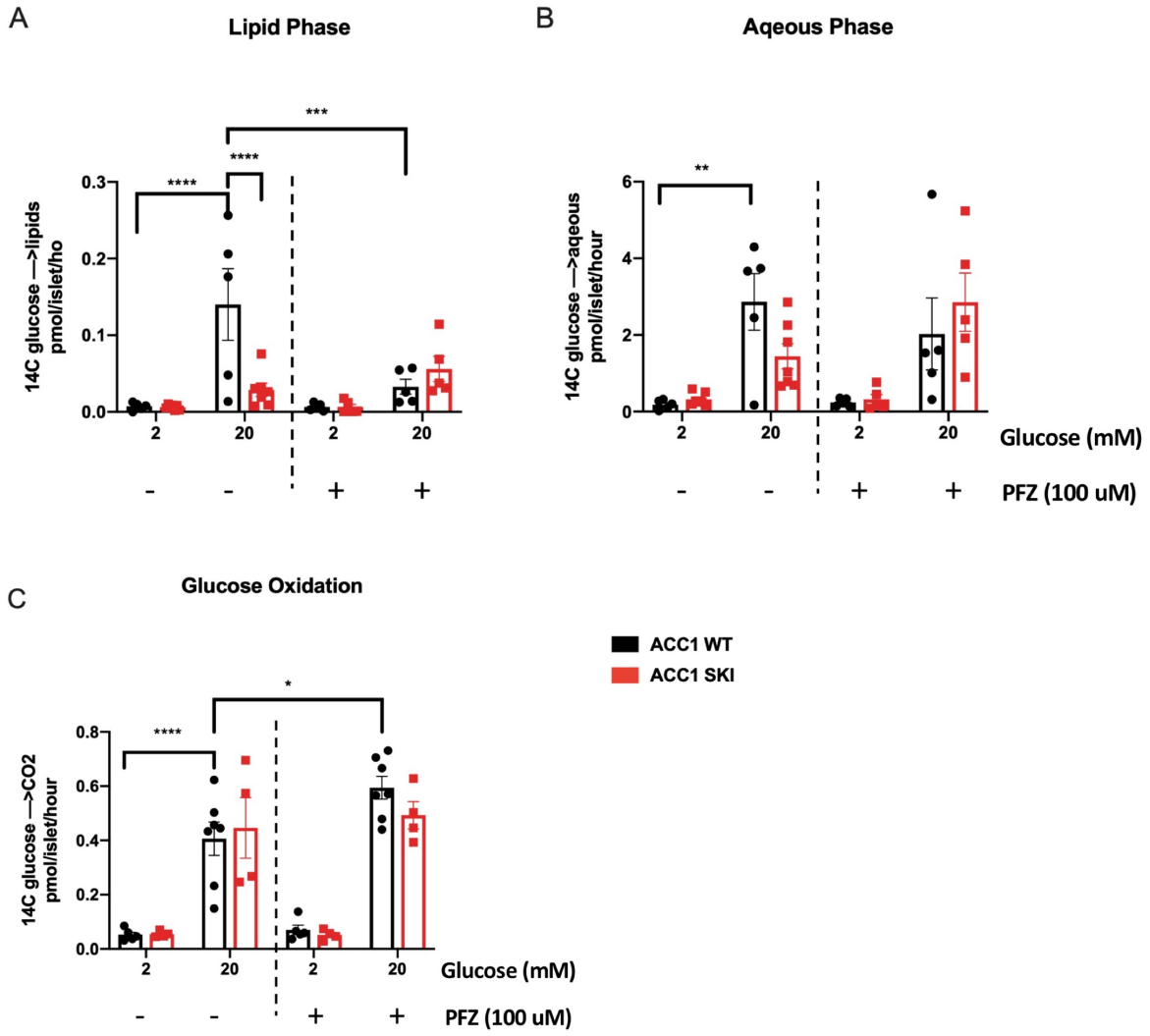


Figure 3-11 De novo lipogenesis and glucose oxidation in ACC1SKI islets. (A) Flux of d-[U-14C] glucose tracer into total lipid pools (B) flux into aqueous pool (C)glucose oxidation. *p<0.05, **p<0.01 and ***p<0.001. Analysis done using two-way ANOVA with Bonferroni multiple comparisons tests. n $\geq$ 4 batches of islets collected from 4 independent mice.

Chapter 3.4 Discussion

The AMPK-ACC1 signalling pathway has been shown to play a critical role in insulin secretion *in vivo* and *ex vivo*. In beta cells, AMPK is activated by stress that depletes cellular ATP (e.g. low glucose level) leading to inhibition of ATP consuming pathways (such as lipid synthesis). Moreover, it has been shown that AMPK activation is associated with cessation of insulin secretion and with a higher level of ACC1 phosphorylation at S79. However, whether this pathway (AMPK-mediated phosphorylation of ACC1 at Ser79) is vital for beta cells function remains unknown. Therefore, the overall aim of this study was to specifically assess the contribution of ACC1S79 phosphorylation in glucose homeostasis and insulin secretion. To this end, we made use of a genetic knock-in mouse model lacking the AMPK phosphorylation site on ACC1(ACC1SKI-Mice). ACC1S79 was mutated to alanine, leaving this enzyme insensitive to inhibition mediated by AMPK.

Chapter 3.4.1 Role Of ACC1S79 In Glucose Homeostasis *In Vivo*

In this study, female ACC1SKI exhibited a normal phenotype. However, the males had lower fasting blood glucose compared to wild type littermate controls. Interestingly, we found no significant difference in serum insulin levels (both at fasting and 30 minutes after glucose injection), GTT and iTT between the two genotypes.

Glucose homeostasis is primarily determined by three factors: the rate of insulin release from the pancreatic beta cells in response to glucose, the sensitivity of the target tissues (e.g. liver, muscles) to insulin, and the levels of circulating counterregulatory hormones (e.g. glucagon, somatostatin). The balance between these factors maintains glucose homeostasis. Our results indicate that the lower fasting blood glucose seen in ACC1SKI males is not due to insulin secretion nor insulin action as there is no difference in serum insulin levels and iTT between the two genotypes, the

observed difference between the two genotypes in fasting blood glucose may be due to a difference in counterregulatory hormones (i.e. glucagon).

The observed difference in the fasting blood glucose between the sexes is possibly due to the compound effect of sex hormones on glucose homeostasis. It is well established that many aspects of glucose metabolism are regulated differently in males and females[106]. For example, insulin sensitivity and capacities for insulin secretion are higher in women compared to men[106]. Furthermore, the role of sex in the incidence and evolution of diabetes, obesity, and metabolic syndrome is well established[107].

In summary, these data suggest that beta-cell ACC1S79 does not play a critical role in insulin secretion nor action *in vivo*.

Chapter 3.4.2 The Role of ACC1S79 in Islets Function Ex Vivo

We also tested the role of ACC1S79 in islet function *ex vivo* as glucose and AMPK regulated phospho-site. Previous studies had shown that pharmacological activation of AMPK was associated with increased (Dews et al. and Navalesi et al.) or decreased (Rutter et al.) glucose-induced insulin secretion. In our hands, acute treatment of islets with PFZ led to an enhancement of glucose-induced insulin secretion under high glucose condition and was associated with an increase in ACC1S79 phosphorylation. Conversely, glucose-induced ACC1S79 phosphorylation was almost unaltered in the absence of PFZ. It can thus be suggested that ACC1S79 does not play a role as a glucose-regulated site (physiological settings) but could be an important site for AMPK action under pharmacological conditions.

The ACC1SKI mouse model provides a means for testing this hypothesis directly: in isolated islets, no differences were found in glucose-stimulated insulin secretion in ACC1SKI islets compared to

wild type islets, confirming our *in vivo* results of serum insulin levels, and further supporting the hypothesis that ACC1S79 does not play a role in insulin secretion under physiological conditions. Surprisingly, PFZ- induced stimulated insulin secretion at high glucose condition was defective in ACC1SKI islets compared to wild types islets, perhaps suggesting a role for ACC1S79 in PFZ enhancement of insulin secretion at high glucose condition.

Furthermore, we demonstrated that PFZ treatment inhibits DNL in wild types islets under high glucose condition. This result suggests that activation of AMPK using PFZ phosphorylates ACC1 and consequently suppresses its activity. Contrary to expectations, in ACC1SKI islets DNL was defective under high glucose conditions compared to wild type islets, although interestingly, these changes did not result in an apparent change in insulin secretion. The reason(s) for this discordance between changes in DNL and insulin secretion could be explained as following: first, the number of samples (n=5) for lipogenic signal is low; moreover, two of these data points did not increase in response to high glucose. Second, ACC1 localisation and/or malonyl Co-A production could be affected in ACC1SKI mice affecting insulin secretion and compensating for the loss of lipogenesis. Third, AMPK can no longer phosphorylate ACC1S79 in ACC1SKI islets, however, it might be more active on other proteins which counteract the impact of loss of lipogenesis

We have considered the possibility of an altered flux through the glucose oxidation pathway as Newgard et al. showed that ACC1 had an essential role in regulating glucose oxidation in the INS1 cell line[96]. However, a recent study by Cantley et al. has shown intact glucose oxidation in ACC1 beta cells-specific null mice[1]. In our present study, we found that glucose oxidation was unaltered in ACC1SKI islets. Contrary to expectations, PFZ augmented glucose oxidation under high glucose condition.

AMPK is active under low glucose condition where insulin secretion is basal, for physiological reasons one may wonder why pharmacological activation of AMPK using PFZ leads to enhancement of insulin secretion and changes in the overall metabolic flux of substrates (i.e. enhancement of glucose oxidation and suppression of lipid synthesis pathway)[102]. It can thus be suggested that when AMPK is activated pharmacologically under high glucose conditions (when it would not normally be active), it promotes glucose oxidation. This mode of controlling the source of energy utilization seems to fit in with AMPK's role as a fuel sensor. This data may provide a mechanistic underpinning for understanding the mechanism by which pharmacological activation of AMPK leads to enhancement of glucose-induced insulin secretion

Chapter 3.4.3 Conclusion

In conclusion, ACC1S79 does not play a role as a glucose regulated site but may be an important site for AMPK action under pharmacological conditions.

Chapter 4 Developing a Phospho-proteomic Workflow to Study ACC1 Phosphorylation

Chapter 4.1 Introduction

Phosphorylation is a crucial post-translational modification that regulates the function of proteins[108]. In order to comprehensively investigate the functional role of ACC1 phosphorylation, it is critical to identify all possible phosphorylation sites on ACC1 and to determine how these sites are regulated under different conditions. Using phosphosite prediction algorithms, there are more than 200 putative sites on ACC1[109]. Given the technical difficulties involved in studying all these sites using traditional methods, we decided to apply state of the art quantitative phosphoproteomics technology. High-throughput phosphoproteomics provides an unbiased and high-efficiency tool to characterise these phosphosites and to perform quantitative measurement of their level of phosphorylation across different biological conditions[110].

For optimal phospho-profiling, it is crucial to purify as much target protein as possible to get optimal protein coverage[111]. To achieve this, we aimed in this chapter to develop a protocol to purify ACC1 from INS1 cells and analyse the protein using a label-free liquid chromatography-tandem mass spectrometry (LC-MS/MS) based proteomics approach.

Our work initially utilised the INS1 cell line, a commonly used insulinoma beta-cell line of rodent origin that is capable of eliciting insulin secretion response following stimulation with glucose, for ACC1 pull down protocol optimisation. While the use of human islets would ideally enable us to have a better understanding of ACC1 regulation in human beta cells, conventional phosphoproteomics requires several milligrams of sample to generate reliable and statistical results, therefore, using human islets would implicate ethical and technical challenges. For

example, variation in islet preparations due to donor genetic/environmental variation and organ handling variation.

Similarly, islets isolated from an individual mouse are numerically limited (less than 300 islets), and pooling islets from several mice will add to sample variability due to inter-individual variability of mouse physiology.

The fundamental concept of our approach to purify ACC1 in sufficient quantities for proteomic analysis, is to use the naturally biotinylated state of the protein (due to its carboxylase activity) enabling ACC1 to bind streptavidin with a strong non-covalent bond (Fig 4.1 A & B). This approach will purify not only ACC1 but all biotinylated proteins in the cells. Therefore, this protocol will ensure that purified proteins are separated using gel electrophoresis, visualised and fixed using Coomassie blue staining (MS Compatible stain). The corresponding ACC1 band is then excised from the gel, digested using trypsin and analysed by LC-MS/MS (Fig 4.1 C).

The aims of this chapter are:

1. To develop a protocol to purify ACC1from INS1 cells that yields high coverage and purity.
2. To identify novel ACC1 phosphosites.

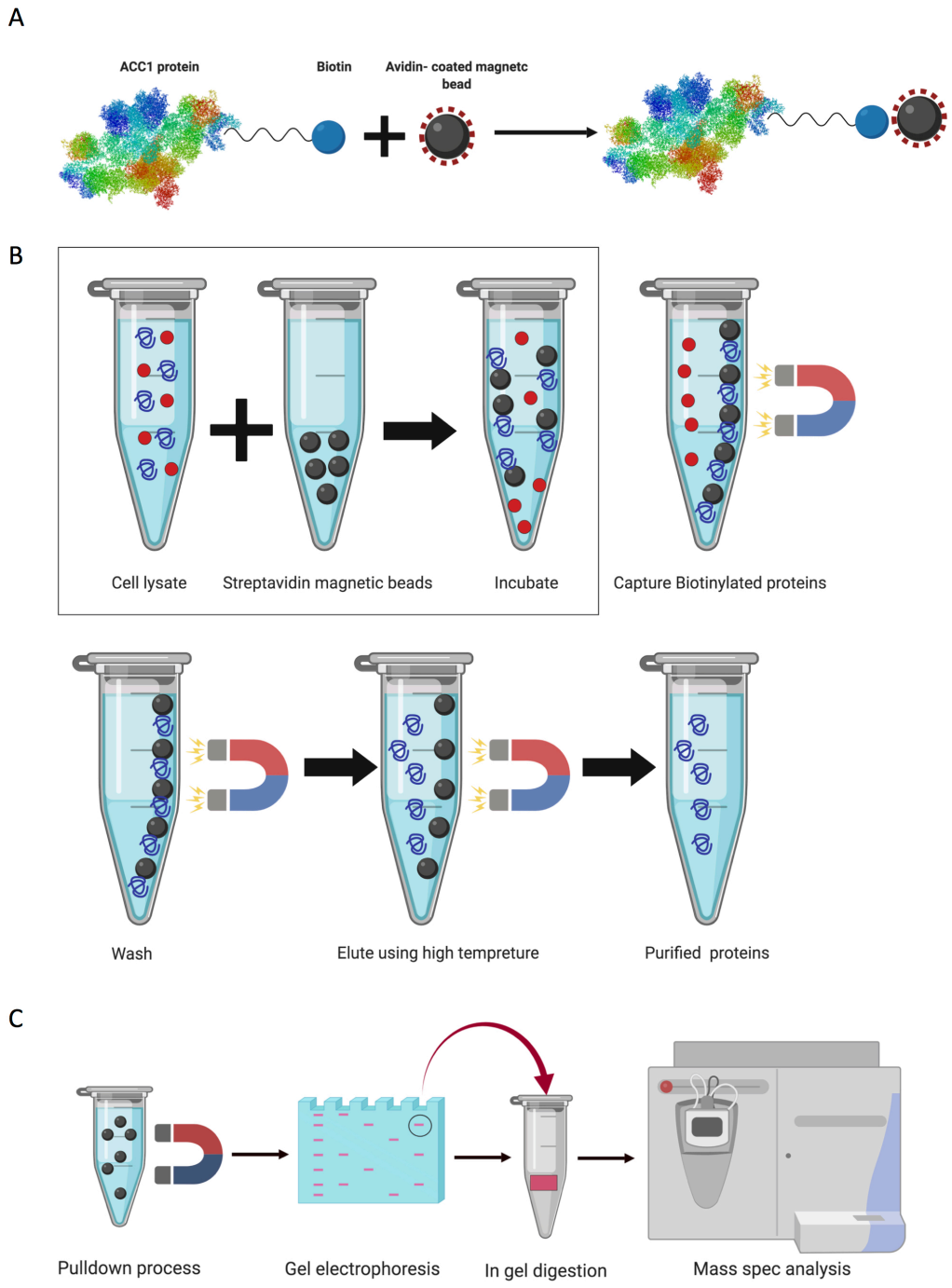


Figure 4-1 ACC1 pull down protocol principle and workflow. (A) ACC1 pull down principle (B) ACC1 pull down protocol workflow, adopted from (abramagnetic beads) (C) Separation of the elute by gel electrophoresis, followed by in gel digestion and LC-MS/MS analysis.

Chapter 4.2 Methods

General methods are described in chapter 6; this section describes the specific methods used in LC-MS/MS analysis.

Chapter 4.2.1 In gel digestion

Proteins were separated using gel electrophoresis, then fixed with coomassie blue staining. Subsequently, gel bands were cut and subjected to in-gel digestion as previously described with either trypsin or chymotrypsin[112]. Briefly, the bands were de-stained using 50% Acetonitrile (ACN), 50 mmol/l AB at 37°C. Then, reduction using (tris(2-carboxyethyl)phosphine (TCEP) and alkylation using Chloroacetamide (CAA) steps were performed. Trypsin (2 ng/µL final concentration) was added to the band and incubated at 37°C. While chymotrypsin (4 ng/µL final concentration) digestion was performed at 25°C. After overnight incubation, supernatants were transferred to fresh tubes and 10% FA was added to extract digestion products remaining in the bands.

Chapter 4.2.2 LC−MS/MS Analysis

After digestion, samples quality and contents were checked first with Linear Trap Quadrupole (LTQ), low resolution instrument. Then, peptides were separated by nano-flow reversed-phase liquid chromatography using an UltiMate 3000 UHPLC system (Dionex Thermo Scientific) coupled to a Q-Exactive Hybrid Quadrupole-Orbitrap mass spectrometer (Thermo Fisher Scientific). In brief, samples were reconstituted in Dimethyl sulfoxide (DMSO) 5% (v/v) and formic acid (FA 5% (v/v) and peptides were loaded on a C18 PepMap100 pre-column (300 µm i.d. x 5 mm, 100Å, Thermo Fisher Scientific) at a flow rate of 12 µl/min in 100% buffer A (0.1% FA in water). Peptides were then transferred to an in-house packed analytical column heated at

45°C (75 µm i.d. x 50 cm, packed with ReproSil-Pur 120 C18-AQ, 1.9 µm, 120 Å, Dr.Maisch GmbH) and separated using a 60 min gradient from 10 to 30% buffer B (0.1% FA in ACN) at a flow rate of 200 nL/min. Q Exactive survey scans were acquired at 70,000 resolution to a scan range from 350 to 1500 m/z, AGC target 3e6, maximum injection time 50 ms. The mass spectrometer was operated in a data-dependent mode to automatically switch between MS and MS/MS. The 10 most intense precursor ions were submitted to Higher-energy collisional dissociation (HCD) fragmentation using an MS/MS resolution set to 17 500, a precursor Automatic Gain Control (AGC) target set to 5e4, a precursor isolation width set to 1.5 Da, and a maximum injection time set to 120 ms.

Chapter 4.2.3 Database Searching, MS Data Analysis and Computational analysis

Raw data files were processed using Mascot software, MaxQuant software version 1.5.0.35 and Perseus version 1.5.5.3 as described previously [113-115]. MS/MS spectra were searched against the rat Uniprot database; precursor mass tolerance was set to 20 ppm and MS/MS tolerance to 0.05 Da. Enzyme specificity was set to either trypsin with a maximum of two missed cleavages or chymotrypsin with a maximum of nine missed cleavages. Phospho (STY), Acetyl (K), Acetyl (Protein N-term), and Oxidation (M) were included as variable modifications. False discovery rate (FDR) for protein and peptide spectral matches was set at 0.01.

Chapter 4.3 Results

Chapter 4.3.1 Optimising Bead Volume for ACC1 Pull Down

1 mg of INS1 cells protein lysates were incubated overnight at 4ºC with escalating concentrations of magnetic beads to determine the optimal bead concentration. Beads were washed with NP-40 lysis buffer to remove proteins that bind non-specifically to the beads. Biotinylated proteins were then eluted using 4X loading dye (contains Sodium dodecyl sulfate, (SDS)) at 95°C.

The elutes then were analysed by gel electrophoresis and stained with Coomassie blue stain (Fig 4.2A). Western blot analysis of the elute was used to confirm if ACC1 is present in the elute (Fig 4.2B).

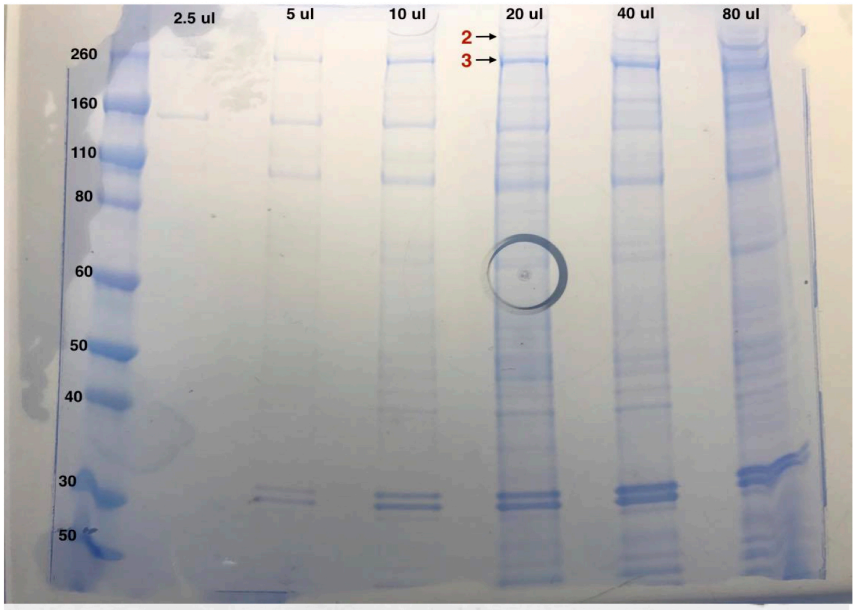
This experiment clearly showed that 20 µl of beads efficiently pulled down ACC1 with a minimum degree of contamination. Two putative ACC1 bands (band 2, band 3) based on a molecular weight for ACC1 of 269 kDa, were excised for LC-MS/MS analysis.

In-gel digestion using trypsin enzyme was performed, before sample injection into an LTQ mass spec (Thermo Fisher), a low-resolution instrument, to check the sample quality and contents. The chromatographic peak of defined bovine serum albumin (BSA) peptides were also checked to monitor the instrument performance regarding sensitivity and peptide fragmentation. The chromatograph of Band 3 is shown in (Fig 4.2 C). Mascot software, a database search algorithm that is usually used to identify proteins from the peptide sequence database, was used to analyse the raw data.

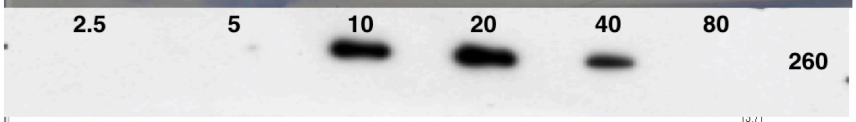
Mascot software analysis for band 3 (Fig 4.2 D) revealed that two proteins were present: ACC1 and the more abundant Myosin-9. The molecular weight of Myosin-9 is 230 kDa, which is very close to ACC1 on the gel, making it very difficult to separate them while cutting the gel band. Myosin does not contain biotin and is most likely binding to the beads through a non-specific

interaction much weaker than the Avidin-Biotin bond: therefore, the next aim was to optimise the pull down to disrupt the weaker myosin interaction and retain ACC1.

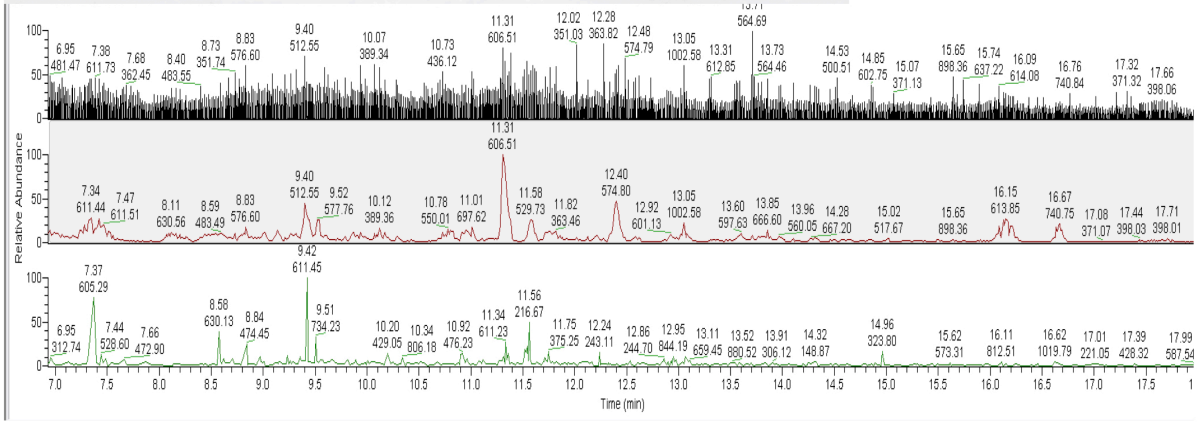
A



B



C



D

MATRIX SCIENCE **MASCOT Search Results**

Protein families 1–10 (out of 11)

Q62812	1205	Myosin-9 OS=Rattus norvegicus GN=Myh9 PE=1 SV=3
Q9JLT0	299	Myosin-10 OS=Rattus norvegicus GN=Myh10 PE=1 SV=1
P11497	184	Acetyl-CoA carboxylase 1 OS=Rattus norvegicus GN=Acaca

Figure 4-2 ACC1 pull down using different beads volume in INS-1 cells. (A) 1 mg of INS1 cells protein lysates were incubated overnight at 4ºC with escalating concentrations of magnetic beads, the elutes then were analysed by gel electrophoresis and stained with Coomassie blue stain (B) Western blot analysis of the elute was used to confirm if ACC1 is present in the elute, 30 μg of proteins was loaded in the gel for each condition. ACC1S79 antibody, molecular weight: 269 kDa, was used at 1:1000 dilution and a rabbit HRP conjugated secondary antibody was used at 1:5000 dilution. (C) Proteins are first converted into peptides by proteolytic digestion, the resulting peptide mixture is then separated by LC and ionized by electrospray before entering the mass spectrometer (top spectrum). A full MS spectrum is acquired for the peptides that are eluted from the LC column into the gradient (middle spectrum). The tandem-MS (MS/MS) spectrum of the peptide ion of interest (bottom spectrum). D) Mascot software search for band 3.

Chapter 4.3.2 Optimising ACC1 Pull Down to Decrease Contaminating Proteins

The pulldown process depends mainly on three factors: (1) Binding conditions, (2) washing conditions, (3) elution conditions. Empirical optimisation for these conditions is required to obtain the desired yield and purity of our target protein. In this experiment, seven different conditions (listed in the paragraphs below) have been tested separately while keeping other conditions exactly the same as in the previous experiment.

Starting with the binding conditions: **1) less protein** (0.5 mg) was tested since excessive protein concentration may force non-specific protein-biotin interactions. **2) Incubation for a shorter period of time** was tested because the Avidin-Biotin interaction is very fast and happens in the first few minutes, longer incubation time might increase the chance for non-specific interactions. **3) Beads were blocked with Bovine serum albumin (BSA)** before incubation with lysate, to block the sites available for non-specific protein binding. Although a small amount of BSA may co-elute with ACC1, its identity and molecular weight (66.5 KDa) are known and far away from ACC1 on the gel, making it less troublesome in downstream analysis.

For the washing conditions, three different washing buffers were tested. **4) NP-40 buffer with higher salt concentration** (1 M NaCl concentration compared to 150 mmol/l in the previous experiment) to reduce nonspecific binding caused by ionic and electrostatic interactions**. 5) Washing buffer with low levels of reducing agents,** 2mmol/l of beta-mercaptoethanol (BME) that can help disrupt non-specific interactions mediated by disulphide bridges or nucleophilic interactions. **6) Washing with 2% SDS**, a strong detergent that may improve specificity by disrupting non-covalent bonds.

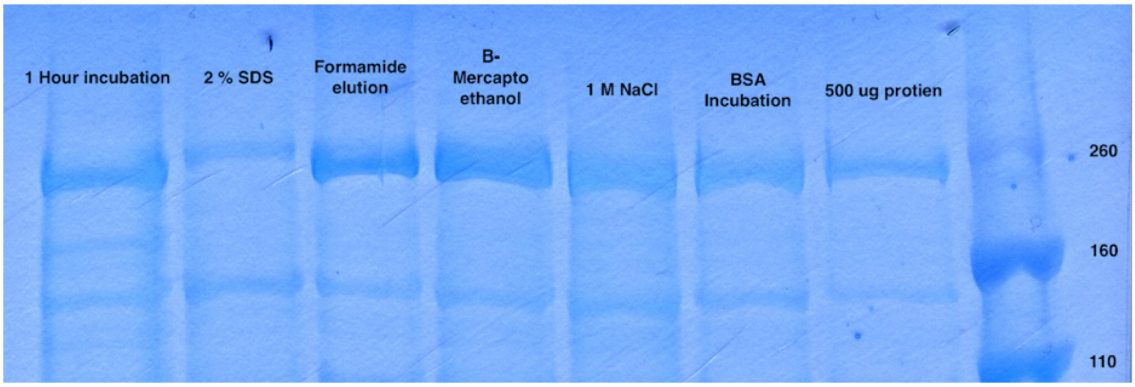
Optimising the elution condition may also be crucial as the loading dye that is used in the previous experiment may not be strong enough to break the Avidin-Biotin bond, potentially resulting in

very small amounts of ACC1 being eluted with the remainder bound to the beads. **7) Therefore, Formamide was tested** as an alternative elution buffer.

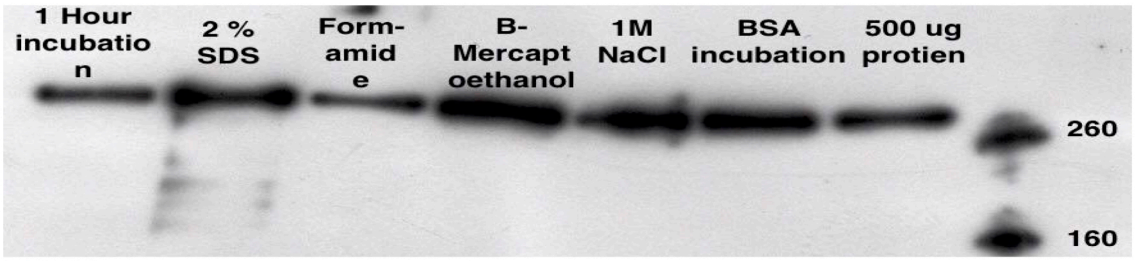
As illustrated with Coomassie blue gel staining (Fig 4.3 A), washing with 2% SDS was the most successful approach, as only the higher ACC1 band is present, indicated that Myosin has been removed. Western blotting analysis for the different conditions is shown in (Fig 4.3 B).

In gel-digestion for the band corresponding to SDS washing condition was performed using trypsin, 3ul of sample digest was checked using LTQ Mass Spec, Mascot software analysis of the data (not shown) was performed and showed that the most abundant protein in the band was ACC1. 40ul of the sample digest was then injected into a High-resolution mass spec (Q Exactive, Thermo Fisher) to identify protein coverage (Fig 4.3 C) and phosphorylation sites (Fig 4.3 D). Protein sequence coverage is 57 % (Detecting enough peptides to show 57% of the sequence of a protein); within this coverage we were able to identify the well-known phosphosite ACC1S79. In addition, two new phosphosites were identified: S29 and S2342. To our knowledge, we are the first to report these phosphosites for ACC1.

A



B



C

MATRIX SCIENCE **MASCOT Search Results**

Protein families 1–10 (out of 162)

|P11497|ACACA_R...	13284	Acetyl-CoA carboxylase 1 OS=Rattus norvegicus GN=Acaca PE=...
D3ZBE2|D3ZBE2_...	604	Protein Acacb OS=Rattus norvegicus GN=Acacb PE=1 SV=2
G3V6P7|G3V6P7_...	5316	Myosin, heavy polypeptide 9, non-muscle OS=Rattus norvegicu...
|Q9JLT0|MYH10_...	1074	Myosin-10 OS=Rattus norvegicus GN=Myh10 PE=2 SV=1

Protein View: sp|P11497|ACACA_RAT

Acetyl-CoA carboxylase 1 OS=Rattus norvegicus GN=Acaca PE=1 SV=1

Protein sequence coverage: 57%

D

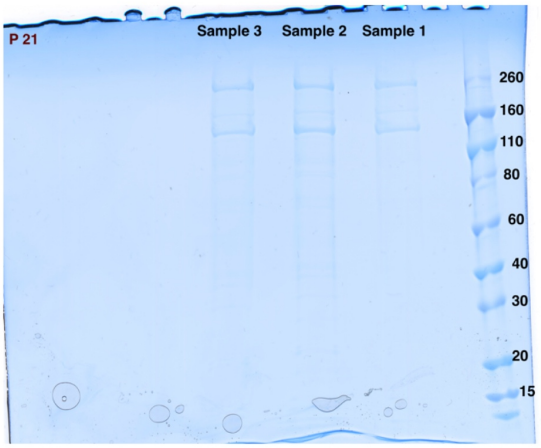
19 – 38	1138.0260	2274.0374	2274.0304	3.07	0	56	5.9e-06	1	U	R.FIIGSVSEDNSEDEISNLVK.L	+ Phospho (ST)
76 – 88	740.3613	1478.7081	1478.7065	1.11	1	44	0.0001	1	U	R.SSMSGLHLVKQGR.D	+ Phospho (ST)
1977 – 2008	821.6895	3282.7289	3282.6748	16.5	1	34	0.0007	1	U	R.LGGIPVGVVAVETRTVELSVPADPANLDSEAK.I	+ Phospho (ST)
2331 – 2345	843.3974	1684.7802	1684.7743	3.48	1	52	1.3e-05	1	U	R.AEVVRILSTMDSPST.-	+ Phospho (ST)

Figure 4-3 Optimising ACC1 pull down to decrease the level of contaminants in INS-1 cells. (A) Coomassie blue staining of the gel (B) Western blot for ACC1 protein, 30 µg of proteins was loaded in the gel for each condition. ACC1S79 antibody, molecular weight: 269 kDa, was used at 1:1000 dilution and a rabbit HRP conjugated secondary antibody was used at 1:5000 dilution (C) Mascot software for SDS washing buffer condition (D) ACC1 phospho-sites detected in this experiment.

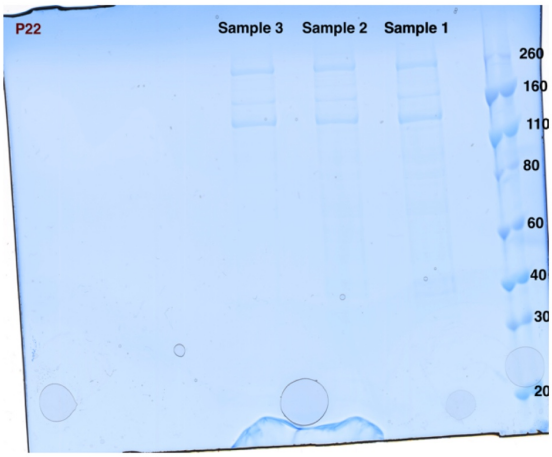
Chapter 4.3.3 ACC1 Pull Down Reproducibility

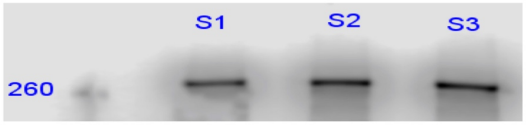
To check the reproducibility of the pull-down process within the same experiment and between two different experiments, which is critical when we compare how different conditions are affecting ACC1, we performed two consecutive experiments using two different cell passages with a triplicate for each experiment (Fig 4.4 A & B). The Coomassie blue stained gels show that the pulldown process is reproducible with minimum variation between the two experiments. To confirm this further, we analysed sample two from each experiment by LC-MS/MS. ACC1 was the most abundant protein in the two samples, the protein coverage was 52 % for the first experiment (Fig 4.4 C) and 57 % for the second experiment (4.4 D).

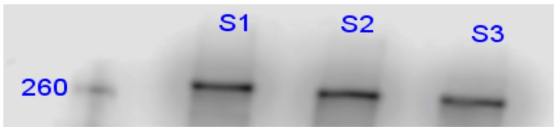
A



B







C

MATRIX SCIENCE **MASCOT Search Results**

Protein families 1–10 (out of 100)

	Score	Mass	Matches	Sequences	emPAI	
sp|P11497|ACACA_RA	14420	266707	991 (722)	226 (190)	39.52	Acetyl-CoA carboxylase 1 OS=Rattus norv...
tr|D3ZBE2|D3ZBE2_R	1096	278544	67 (54)	18 (18)	0.40	Protein Acacb OS=Rattus norvegicus GN=A...

Protein sequence coverage: 52%

76 – 85	577.7686	1153.5226	1153.5202	2.01	0	25	0.0069	1	U	R.SSMSGLHLVK.Q + Phospho (ST)

D

Protein families 1–10 (out of 104)

	Score	Mass	Matches	Sequences	emPAI	
sp|P11497|ACACA_RA	14504	266707	943 (718)	205 (180)	29.44	Acetyl-CoA carboxylase 1 OS=Rattus norv...
tr|D3ZBE2|D3ZBE2_R	930	278544	66 (52)	20 (15)	0.32	Protein Acacb OS=Rattus norvegicus GN=A...

Protein sequence coverage: 57%

19 – 38	759.0216	2274.0430	2274.0304	5.51	0	43	8.8e-05	1	U	R.FIIGSVSEDNSEDEISNLVK.L + Phospho (ST)
76 – 85	577.7674	1153.5203	1153.5202	0.028	0	46	0.00016	1	U	R.SSMSGLHLVK.Q + Oxidation (M); Phospho (ST)
76 – 88	493.9104	1478.7095	1478.7065	2.03	1	29	0.0071	1	U	R.SSMSGLHLVKQGR.D + Phospho (ST)
1247 – 1281	1056.4370	4221.7189	4221.6608	13.8	1	25	0.0049	1	U	R.IFDEVMGCFCDSPPQSPTFPESGHTSLYDEDKVPR.D + Oxidation (M); 2 Phospho (ST)

Figure 4-4 ACC1 pull down reproducibility in INS-1 cells. (A&B) Coomassie blue staining of the gel and western blot for ACC1 protein for 2 consecutive experiments (3 replicates in each experiment). 30 µg of proteins was loaded in the gel for each condition. ACC1S79 antibody, molecular weight: 269 kDa, was used at 1:1000 dilution and a rabbit HRP conjugated secondary antibody was used at 1:5000 dilution (C) Mascot software search for sample 2 from the first experiment (D) Mascot software search for sample 2 from the second experiment.

Chapter 4.3.4 Re-Optimising Bead Volume to Increase Protein Coverage

To improve the protein sequence coverage under this harsh washing buffer and to see if there are new phosphosites in the currently undetected regions of the protein, we re-optimised the concentration of the beads. We used a range of beads concentrations and analysed flow-through, wash buffer and elutes for protein content. Eluted ACC1 peaks with 40ul beads (Fig 4.5 A), so 40ul of beads were used in upcoming experiments. This experiment clearly shows that most contaminants are being washed out in the first wash (Fig 4.5 B).

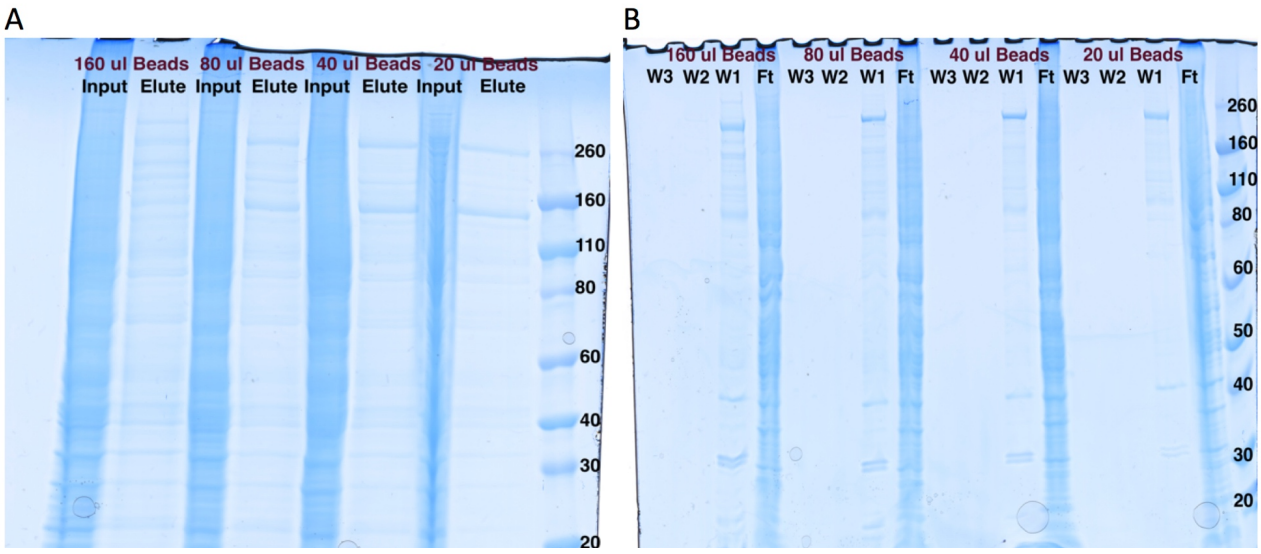


Figure 4-5 Re-optimising beads volume in INS-1 cells. (A) Coomassie blue staining for elutes using different beads concentrations (B) Coomassie blue staining for flow through (Ft) and washes (W).

Chapter 4.3.5 Increasing LC-MS/MS Coverage of ACC1 Protein

The maximum protein coverage we were able to get with all these optimisation steps was 57%. To enhance protein coverage and to see if there are new phosphosites in the currently undetected regions of the protein, we planned to scale up the whole experiment 10-fold and digest the ACC1 protein using a second proteolytic enzyme such as Chymotrypsin.

So far, we have been using trypsin because it is the gold standard for protein digestion, due to its high specificity and efficiency. Moreover, it generates short peptides with a basic residue at the carboxyl terminus of the peptides and that are in the preferred mass range for sequencing. However, some of the tryptic peptides are too short to be ionised and identified by LC-MS/MS. Therefore, it is impossible to cover the whole protein and to identify all phospho-sites in the protein using only trypsin[116].

Trypsin cuts at the C-terminal side of Lysine and Arginine residues while Chymotrypsin cuts at the C-terminal side of tryptophan, tyrosine, phenylalanine and leucine. Because each enzyme has such a distinctive specificity, they generate different sets of peptides; therefore, by exposing the same protein to digestion with multiple proteases in parallel, complementary parts of the protein sequence can be covered[117].

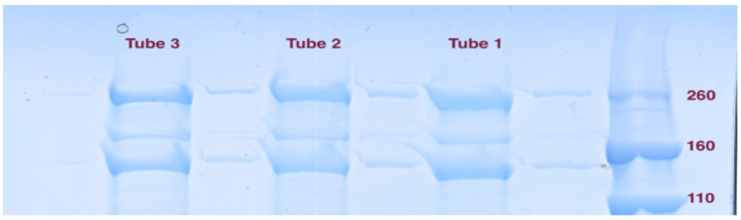
In this experiment, we used 10 mg of cell lysate and 400 µl of beads: the materials (cell lysates and beads) were distributed equally into three tubes and loaded into three different wells, with some unavoidable spillage into the surrounding wells. By inspecting the Coomassie blue stained gel (Fig 4.6 A), we can see that ACC1 bands are much stronger than previous experiments. Trypsin and Chymotrypsin digestion were performed in separate tubes at 37°C overnight. The chromatographic peaks for each digestion are shown in (Fig 4.6 B). For trypsin digestion, the signal intensity is 4.5X stronger than before (2.42E9 in this experiment compared to 5.38E8 in

the previous experiment). For Chymotrypsin digestion, the sequence coverage was only 18 % (Fig 4.6 D).

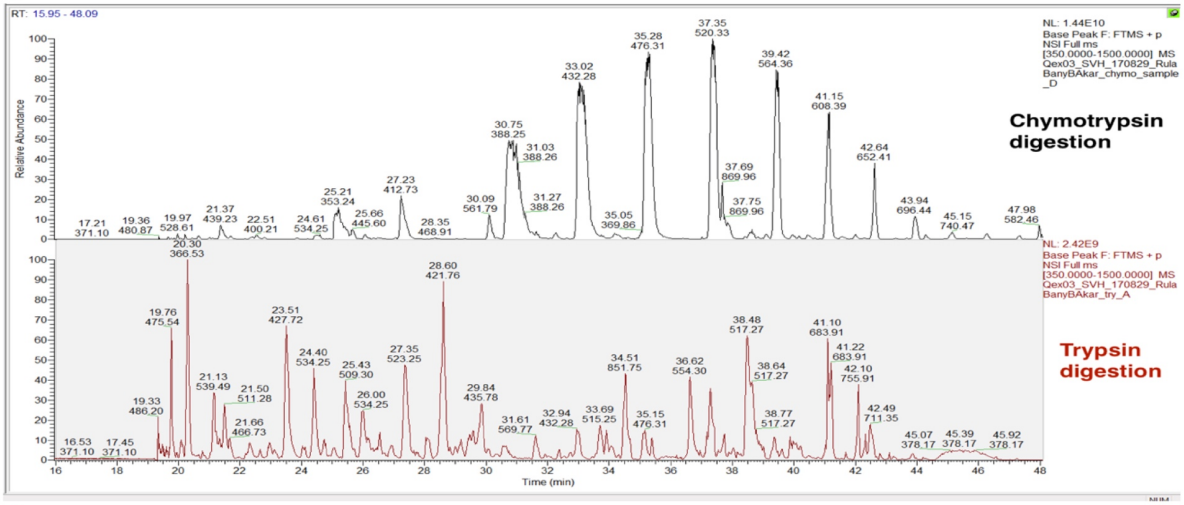
Mascot search results for trypsin digestion (Fig 4.6 C) show that the ACC1 protein score has increased from 14k (in the previous experiment) to 54k. Protein score is defined as the likelihood that the observed match between the experimental data and the database sequence is a random event[118]. So, by scaling up the pull-down process the quality of the data has significantly improved. emPAI, which is an estimated quantitation of the proteins in a mix based on the protein coverage by the peptide matches[118], has also increased from 39 to 66 which confirms that we have more protein in the band[119].

Even though we have such improvement in different parameters, the protein sequence coverage for the band digested using trypsin is only 53%. With this coverage, we were able to identify the well-known phosphosites S77 and S79. In addition, two new phosphosites were identified: S5 and S2342 (Fig 4.6 E). To our knowledge, we are the first to report these phosphosites for ACC1.

A



B



C

MASCOT Search Results

Protein sequence coverage: 53%

	Score	Mass	Matches	Sequences	emPAI	
sp|P11497|ACACA_RA	54469	266678	1996 (1943)	169 (165)	66.38	Acetyl-CoA carboxylase 1 OS=Rattus norvegicus
tr|D3ZBE2|D3ZBE2_R	1874	278497	81 (74)	16 (15)	0.34	Protein Acacb OS=Rattus norvegicus GN=Acacb

D

MASCOT Search Results

Protein sequence coverage: 18%

	Score	Mass	Matches	Sequences	emPAI	
sp|P11497|ACACA_RA	1683	266678	98 (92)	40 (36)	0.80	Acetyl-CoA carboxylase 1 OS=Rattus norvegicus

E

9602	1 – 18	541.2482	2160.9637	2160.9874	-11.0	1	60	3e-06	1	U	-.MDEPSPLAKTLELNQHSR.F + Oxidation (M); Phospho (ST)
5415	76 – 88	499.2440	1494.7102	1494.7014	5.89	1	35	0.0053	1	U	R.SSMSGLHLVKQGR.D + Oxidation (M); Phospho (ST)
2691	76 – 85	577.7683	1153.5221	1153.5202	1.58	0	55	2.7e-05	1	U	R.SSMSGLHLVK.Q + Oxidation (M); Phospho (ST)
2662	2336 – 2345	574.2362	1146.4578	1146.4516	5.46	0	26	0.028	1	U	R.ILSTMDSPST.- + Oxidation (M); Phospho (ST)

Figure 4-6 ACC1 pull down scale up and double digestion. (A) Coomassie blue staining of the gel, one band and a half were used for each trypsin and chymotrypsin digestion (B) Mass spectrometry chromatographs for trypsin and chymotrypsin digestion of ACC1 (C) Mascot software search for trypsin digestion (D) Mascot software search for chymotrypsin trypsin digestion (E) ACC1 phospho-sites detected in the band digested with trypsin.

Chapter 4.3.6 Optimising Chymotrypsin Digestion

To investigate why chymotrypsin digestion is not working, we did a control experiment to make sure that the problem is not in the chymotrypsin stock that we are using. We performed a parallel trypsin and chymotrypsin in-gel digestion on a BSA gel band as a control protein that is known to be digested well using chymotrypsin (results are not shown). Even though the signal was lower in the chymotrypsin chromatogram as compared to the trypsin one, it was clean and resulted in a sequence coverage of 67% for BSA compared to 76% coverage for trypsin digestion. Upon reviewing the literature, we found that the optimal digestion temperature for chymotrypsin is 25°C[117]. To test the effect of temperature on ACC1 chymotrypsin digestion, ACC1 was digested using chymotrypsin at 25°C and 37°C in parallel. The sequence coverage at 37°C was 21% (Fig 4.7 C) compared to 63% at 25°C (Fig 4.7 B). Trypsin digestion was done in parallel (fig 4.7 A), the combined sequence coverage for ACC1 using trypsin and chymotrypsin was 92%. This experiment clearly indicated that 25°C should be used in all subsequent chymotrypsin experiments.

A

Protein sequence coverage: 65%

	Score	Mass	Matches	Sequences	emPAI	
sp|P11497|ACACA_RA	73755	266678	2930 (2869)	218 (215)	67.00	Acetyl-CoA carboxylase 1 OS=Rattus norvegicus GN=Acaca PE=1 SV=1
tr|D3ZBE2|D3ZBE2_R	9033	278497	329 (325)	25 (24)	0.52	Protein Acacb OS=Rattus norvegicus GN=Acacb PE=1 SV=2

B

Protein sequence coverage: 63%

	Score	Mass	Matches	Sequences	emPAI	
P11497	9038	266678	720 (557)	229 (192)	26.68	Acetyl-CoA carboxylase 1 OS=Rattus norvegicus GN=Acaca PE=1 SV=1
Q13085	7277	267095	554 (423)	169 (143)	10.86	Acetyl-CoA carboxylase 1 OS=Homo sapiens GN=ACACA PE=1 SV=2
P11029	5098	264149	367 (284)	109 (88)	4.05	Acetyl-CoA carboxylase OS=Gallus gallus GN=ACAC PE=1 SV=1

C

Protein sequence coverage: 21%

sp|P11497|ACACA_R...	322	Acetyl-CoA carboxylase 1 OS=Rattus norvegicus GN=Acaca PE=1 SV=1

Figure 4-7 Optimising Chymotrypsin digestion. (A) Mascot search for trypsin digestion of ACC1 protein (B) Mascot search for chymotrypsin digestion of ACC1 protein at 25°C (C) Mascot search for chymotrypsin digestion of ACC1 protein at 37°C.

Chapter 4.3.7 Chymotrypsin Digestion Reproducibility

We performed chymotrypsin digestion on three replicates, to test for reproducibility with the modified protocol and to assess the variation within a given condition. The results were analysed by MaxQuant software revealing that the variation between the replicates is minimum in terms of both the sequence coverage (Fig 4.8 A) and the signal intensity of the detected phosphosites (Fig 4.8 B).

A

Sequence coverage Acc Chymo 25C_on_01 [%]	Sequence coverage Acc Chymo 25C_on_02 [%]	Sequence coverage Acc Chymo 25C_on_03 [%]
80.7	78.6	78.9

B

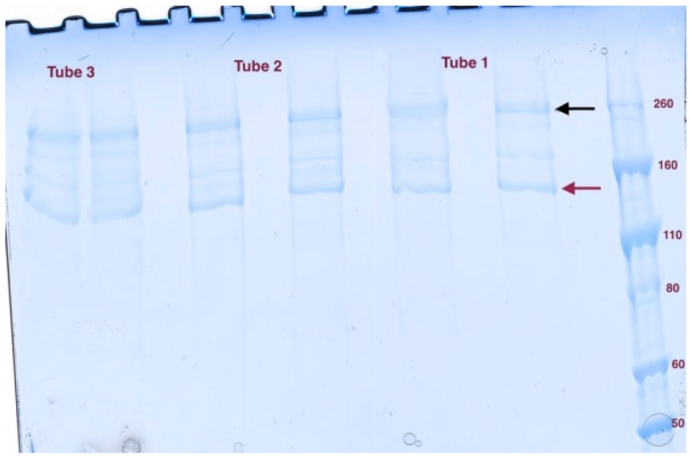
Protein names	Positions within proteins	Number of Phospho (STY)	Amino acid	Intensity Acc Chymo 25C_on_01	Intensity Acc Chymo 25C_on_02	Intensity Acc Chymo 25C_on_03
Acetyl-CoA carboxylase 1;I	5;5	1	S	3.46E+07	3.34E+07	2.09E+07
Acetyl-CoA carboxylase 1;I	23;23	1	S			
Acetyl-CoA carboxylase 1;I	79;79	1	S	4.44E+07	3.56E+07	2.93E+07
Acetyl-CoA carboxylase 1;I	996;1258;1250	1	S	6.14E+07	4.47E+07	2.62E+07

Figure 4-8 Chymotrypsin digestion reproducibility. (A) Sequence coverage for 3 biological replicates (B) Phoshosites detected in these replicates.

Chapter 4.3.8 Phospho-Profiling of PC

By reviewing the pathway described in the introduction and based on the fact that the pull down process will purify not only ACC1 but all biotinylated molecules in the cells, we decided to study PC protein as it primes the cataplerotic ACC1-coupled pathway that we are testing (figure 1-2)[43,120]. However, the phospho-regulation of this enzyme has not been investigated. We excised the band that we expected to be PC (Fig 4.9 A red arrow) based on the expected M.W of 130 kDa[121]. Trypsin digest and LC-MS/MS analysis of this band identified PC with 73% sequence coverage, including novel phosphosites. The combined sequence coverage for PC using trypsin and chymotrypsin was 93 %.

A



B

MATRIX SCIENCE **MASCOT Search Results**

Protein families 1–10 (out of 341)

sp|P52873|PYC_RAT 47553 Pyruvate carboxylase, mitochondrial OS=Rattus norvegicus GN=Pc PE=1 SV=2

	Score	Mass	Matches	Sequences	emPAI	
sp|P52873|PYC_RAT	47553	130436	1888 (1653)	93 (87)	36.85	Pyruvate carboxylase, mitochondrial OS=Rattus norvegicus GN=Pc

Protein sequence coverage: 73%

19 – 30	633.2993	1264.5840	1264.5813	2.18	0	54	9.2e-06	1	U	R.SSTAPVASPNVR.R + Phospho (ST)
329 – 355	627.7081	3133.5040	3133.5081	-1.32	0	44	7.5e-05	1	U	R.LQVEHTVTEEITDVDLVHAQIHVSEGR.S + Phospho (ST)
520 – 542	594.3179	2373.2424	2373.2498	-3.10	0	9	0.13	1	U	K.VSPSPVDPIVPVVPIGPPPAGFR.D + Phospho (ST)
520 – 542	792.0885	2373.2437	2373.2498	-2.57	0	33	0.0039	1	U	K.VSPSPVDPIVPVVPIGPPPAGFR.D + Phospho (ST)
1022 – 1036	578.9280	1733.7623	1733.7662	-2.24	0	27	0.0043	1	U	K.DFTATFGPLDSLNTR.L + Phospho (ST)

Figure 4-9 PC pull down and phospho-profiling in INS-1 cells. (A) Coomassie blue staining of the gel (B) Mascot search for PC band.

Chapter 4.4 Discussion:

Post-translational modification (PTM) of proteins is a key mechanism by which cell function is controlled. Among those, protein phosphorylation is a well-described PTM that plays a critical role in transiently altering protein physical and chemical properties. The biological impact of phosphorylation results from the negatively charged phosphate group, which pulls towards a positively or repels from a negatively charged nearby amino acid residues leading to conformational changes in the protein[110]. The research to date has tended to focus on phosphorylation of ACC1 at S79; however, ACC1 can be a target for several kinases at multiple sites with different dynamics. Thus, it is essential to identify the exact position of phosphorylation and quantify site-specific changes in the level of phosphorylation across different biological conditions[122].

An essential step in characterising phosphorylation in detail is the isolation of the target protein in sufficient quantities for analysis. In this chapter, we have successfully developed a highly effective and robust protocol to purify ACC1. Our results show that this protocol provides more than 95% coverage of the ACC1 protein, with the well-known ACC1S79 phosphosite and identified several novel phosphosites detected. In the next chapter, we will use this pull down and mass spectrometry protocol to investigate the dynamic regulation of these phosphosites in the pancreatic beta cell in response to glucose.

Chapter 5 Label-Free Quantitative Phosphoproteomics

Chapter 5.1 Introduction

MS-based phosphoproteomics provides an unbiased platform to comprehensively and quantitatively analyse protein phosphorylation. Different quantification techniques have been developed over the past few years; these include label-based quantification (chemical and metabolic labelling) and label-free quantification. Label-free quantification provides a high degree of quantitative reproducibility without the need to optimise labelling strategies. The basic principle of label-free quantification is comparing the ion intensity, which is proportional to the phosphopeptide concentration, between two groups [114]. However, one limitation of this strategy is its substantial need for reproducibility of sample preparation and instrument performance[123].

Chapter 5.2 Results

Chapter 5.2.1 Quantification of ACC1 and PC Phospho-Sites upon 30 Minutes of Glucose Treatment

This chapter aimed to quantify the dynamic response of ACC1 novel phosphosites in the presence of high or low glucose concentration. First, we performed a functional integrity test, which showed that INS1 cells exhibited significant insulin secretion in response to 30 minutes of high glucose treatment (15 mmol/l) (figure 5.1 A). Then, we employed the workflow described in (figure 5.1 B) to examine the changes in ACC1 and PC phosphosites. Briefly, INS1 cells were pre-incubated in 2 mmol/l glucose KRBH buffer for 30 minutes to clear any serum effect. Cells were then washed and incubated for 30 minutes with low (2 mmol/l) and high glucose (15 mmol/l) concentration. Subsequently, pulldown (figure 5.1 C), SDS-PAGE and label-free LC-MS/MS analysis were performed, followed by data analysis using MaxQuant software for protein identification and quantification, and statistical analysis using Perseus software. This experiment was performed in biological triplicate for each condition.

Western blot for ACC1S79 was performed to check the phosphorylation of this well-known site under these conditions. Figure (5.1 D) shows no significant change in ACC1S79 phosphorylation upon 30 minutes of glucose stimulation. We also checked the pull down elute for other types of PTMs using pan-malonylation and pan-acetylation antibodies. The blot for acetylation did not show any bands, while the blot for malonylation showed an 80 kDa band (figure 5.1 E).

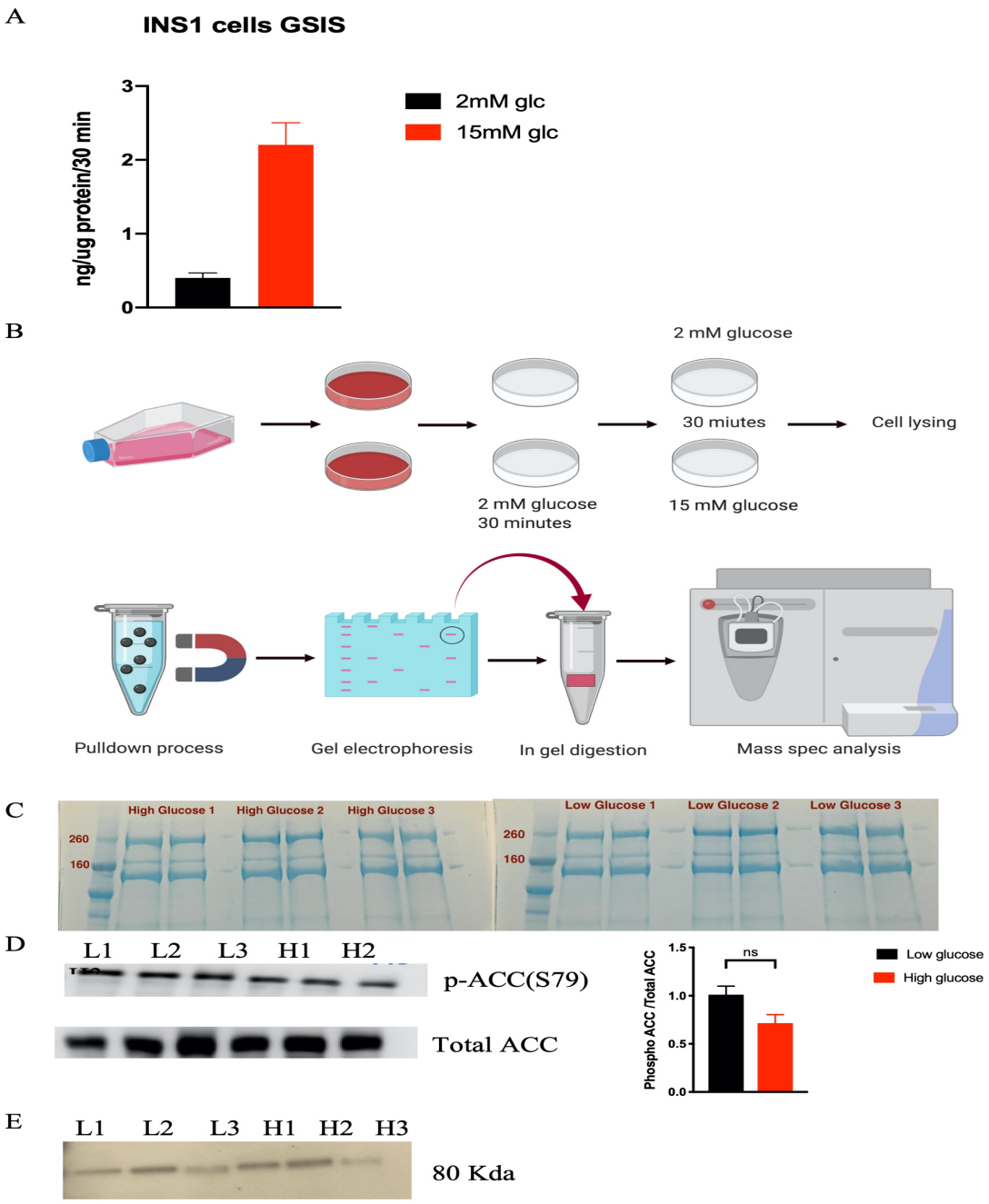


Figure 5-1 Quantitative phosphoproteomics workflow in INS-1 cells. (A) Function of INS1 cells was evaluated with 30 min GSIS (B) Schematic demonstration of the experimental workflow applied to analyse ACC1 phospho-sites (C) Coomassie blue staining of the gel for ACC1 pull down from INS1 cells(D) Western blot for ACC1S79 and total ACC. 30 µg of proteins was loaded in the gel for each condition. p-ACC1S79 antibody, molecular weight: 269 kDa, was used at 1:1000 dilution, total ACC1 antibody was used as a loading control and a rabbit HRP conjugated secondary antibody was used at 1:5000 dilution (E) Western blot using pan-malonylation antibody.

We analysed phosphoproteomic raw data using MaxQuant software then we performed downstream bioinformatics analysis using Perseus software. The MaxQuant analysis showed 92% coverage of ACC1, with 13 sites detected. Table (5-1) shows the positions of these site within the protein, the localisation probability of each site (a score to measure the reliability of site localisation), Andromeda score (a statistical measure of reliability) for each site. Sites that have a score higher than 40 and localisation probability higher than 0.75 are considered class 1 sites (high confidence phosphosites)[124,125].

Table 5-1 ACC1 phospho-sites detected upon 30 minutes of low glucose (2 mmol/l) or high glucose (15 mmol/l) treatment.

Protein	Gene names	Positions within proteins	Localisation prob.	Score	Amino acid
P11497	Acaca	5;5	1	74.611	S
P11497	Acaca	23;23	0.916731	42.384	S
P11497	Acaca	25;25	0.929149	101.6	S
P11497	Acaca	29;29	0.998461	88.239	S
P11497	Acaca	79;79	0.999127	90.913	S
P11497	Acaca	220;482;482	0.526833	44.625	S
P11497	Acacb;Acaca	352;352;352;352;212;212	1	52.862	S
P11497	Acaca	953;1215;1207	0.955743	51.726	S
P11497	Acaca	996;1258;1250	0.999999	137.99	S
P11497	Acaca	1032;1294;1286	1	143.25	T
P11497	Acaca	1503;1765;1757	0.980003	40.968	S
P11497	Acaca	1894;2156;2148	0.956285	89.451	S
P11497	Acaca	2055;2317;2309	0.991111	87.155	S
P11497	Acaca	2080;2342;2334	0.975843	72.928	S

The volcano plots in figure (5-2) show the fold change in ACC1 phosphorylation between high glucose samples and low glucose samples on the $\log^2$ scale (so changes in both directions appear symmetrical) plotted against the negative log scale of the student t-test p-value, thus smaller p-values appear higher up on the scale. Using *p-value* of 0.05 as a cut point for statistical significance, none of the detected sites exhibited a statistically significant response (more than two fold change) upon 30 minutes of low glucose (2 mmol/l) or high glucose (15 mmol/l) treatment.

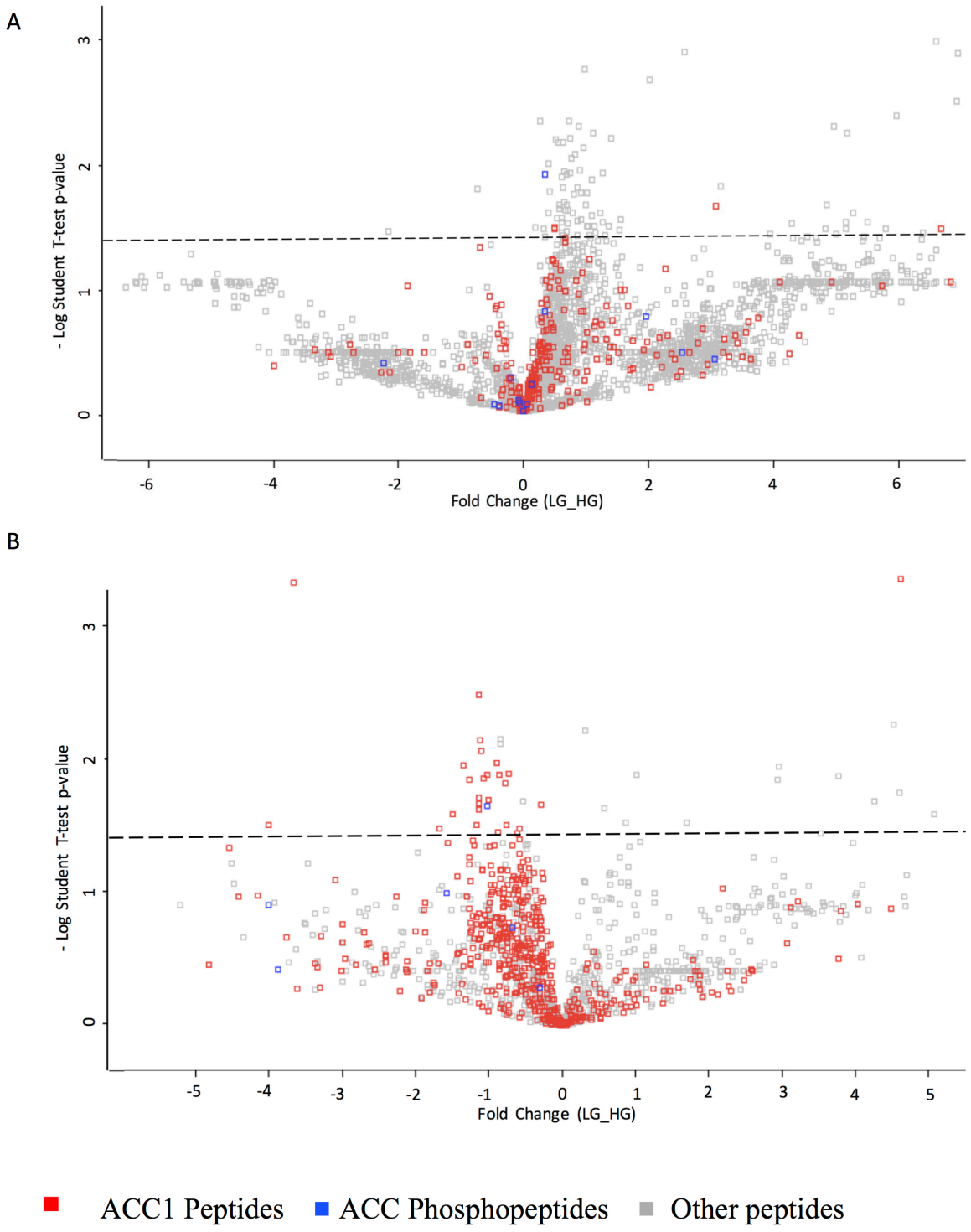


Figure 5-2 Quantification of ACC1 phospho-sites upon 30 minutes of glucose stimulation in INS1 cells. (A) Volcano plot of quantified phospho-sites in ACC1 band digested with trypsin (B) Volcano plot of quantified phospho-sites in ACC1 band digested with chymotrypsin.
The dash lines represent a *p-value* of 0.05

In the same way, we performed PC phosphoproteomics analysis which showed 2 novel class 1 phosphosites (Table 5-2). Similarly, none of these sites exhibited a significant response to 30 minutes of low glucose (2 mmol/l) or high glucose (15 mmol/l) treatment (figure 5-3).

Table 5-2 PC phospho-sites detected upon 30 minutes of low glucose (2 mmol/l) or high glucose (15 mmol/l) treatment.

Proteins	Gene	Positions within proteins	Localization prob.	Score	Amino acid
P52873	PC	411;510	0.772023	46.953	S
P52873	PC	682;781	0.765312	51.475	Y

To this end, we identified novel phosphosites for ACC1 and PC. We observed that none of these sites showed a significant glucose response under our experimental conditions. Given the novelty of the identified ACC1 phosphosites, their dynamic response to glucose is unknown, and it was hard to conclude at that stage that they were not glucose responsive. Thus, further optimisation experiments were needed to elucidate their dynamics and glucose response. Taken into account the cost and time required to study both proteins, we decided to drop out PC from our future experiments and focus on ACC1, the main target of this project. However, this data provides a rational for future hypothesis-driven research to pinpoint, as yet unknown, functional relevance of these sites. Studies of this kind will thereby contribute to our understanding of PC regulation in beta cells and other tissues.

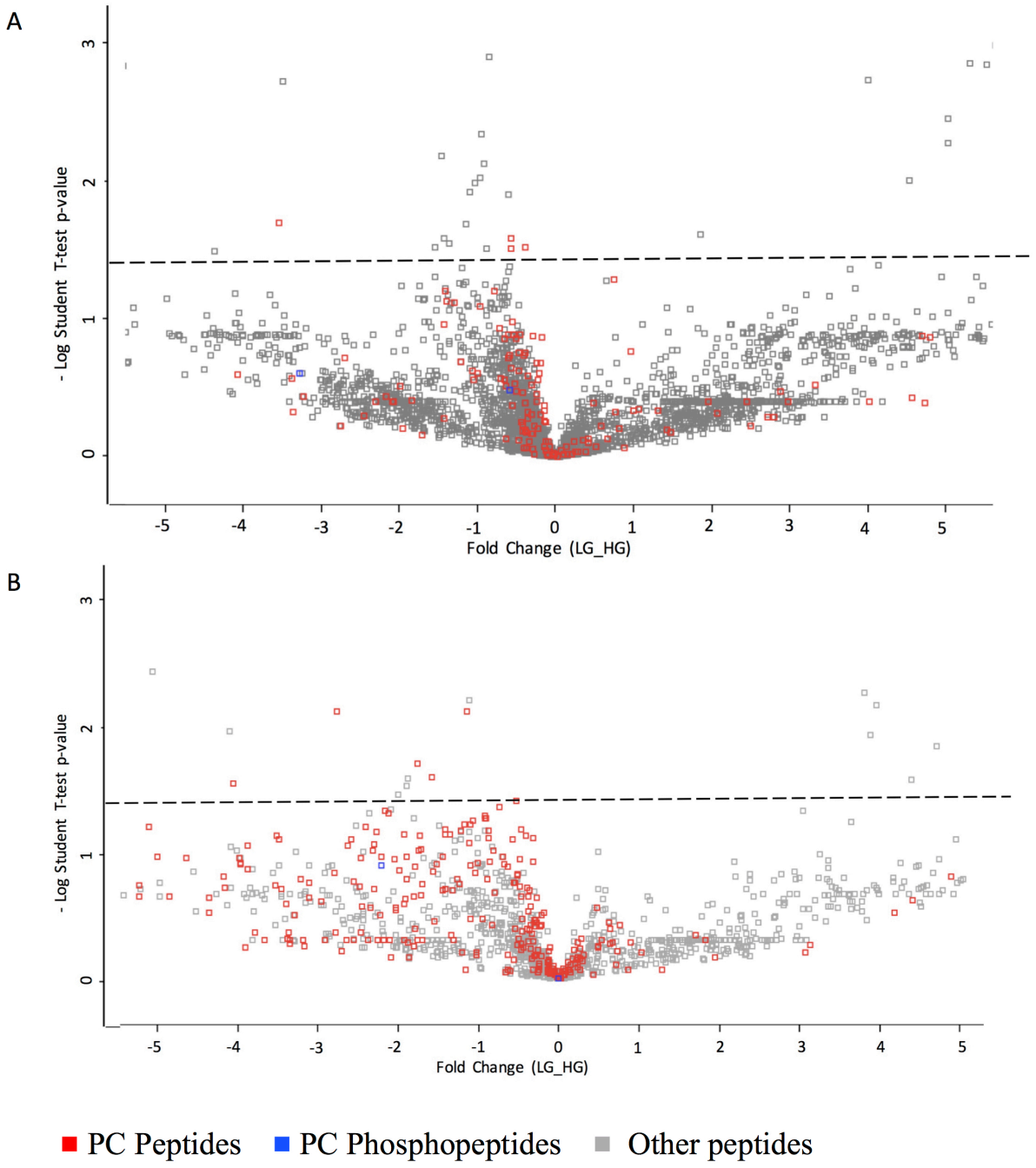


Figure 5-3 Quantification of PC phospho-sites upon 30 minutes of low glucose (2 mmol/l) or high glucose (15 mmol/l) treatment in INS1 cells. (A) Volcano plot of quantified phospho-sites in PC band digested with trypsin (B) Volcano plot of quantified phospho-sites in PC band digested with chymotrypsin. The dash lines represent a *p-value* of 0.05

Chapter 5.2.2 Optimising ACC1 Phosphorylation Model

The experimental model used in the previous experiment (pre-incubation with low glucose for 30 minutes followed by 30 minutes of low glucose (2 mmol/l) or high glucose (15 mmol/l) treatment was chosen to match the validated insulin secretion timeline (figure 5-1 A). One question that remains, however, is whether this is a time point to study ACC1 phosphorylation. We used the well-characterised phosphorylation of ACC1 (S79) as a proxy to investigate this; we reviewed the experimental design focusing on the pre-incubation and incubation steps.

Starting with the pre-incubation step: INS1 cells are cultured in high glucose concentration media (RPMI media containing 11mmol/l glucose), therefore we hypothesised that changing the cells' media abruptly to low glucose KRBH might cause changes in kinase and phosphatase activity. Taking into consideration that this step is essential to clear any serum effects, we decided to test whether pre-incubation with 11 mmol/l glucose KRBH buffer (keeping glucose concentration the same as in the media) would make a difference in ACC1 phosphorylation (figure 5-4 A).

Western blot analysis (figure 5-4 B) shows a comparison in ACC1S79 phosphorylation between two models for the pre-incubation step: basal model (2 mmol/l glucose) and high model (11 mmol/l), keeping the incubation step the same as in the previous experiment. The high model evoked marginally more ACC1S79 phosphorylation in response to low glucose (figure 5-4 C).

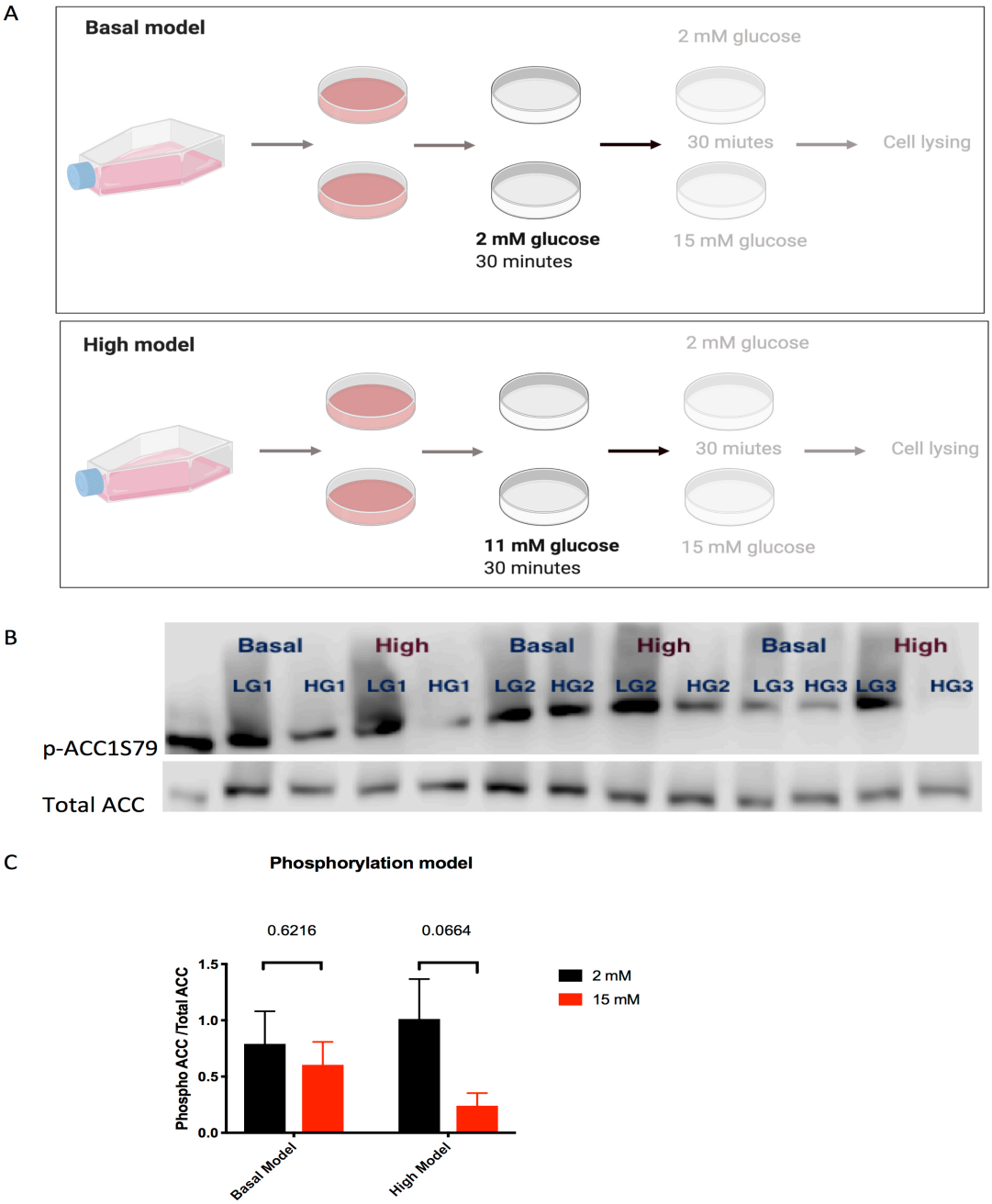


Figure 5-4 Optimising the pre-incubation step in INS1 cells. (A) Experimental design for the basal (2 mmol/l glucose) and high model (11mmol/l glucose) in INS1 cells (B) Western blot for ACC1S79 phosphorylation to test the difference in phosphorylation between two models for the pre-incubation step: basal model (2 mmol/l glucose) and high model (11mmol/l glucose), 30 µg of proteins was loaded in the gel for each condition. p-ACC1S79 antibody, molecular weight: 269 kDa, was used at 1:1000 dilution, total ACC1 antibody was used as a loading control and a rabbit HRP conjugated secondary antibody was used at 1:5000 dilution (C) Quantification of ACC1S79 phosphorylation in both models using image J software.

Next, we investigated the extent of ACC1 phosphorylation at different time points in response to glucose. In view of the previous results, cells were pre-incubated with KRBH 11mmol/l glucose then treated with low glucose KRBH (2mmol/l glucose) for 10, 20, 30, 60 and 120 minutes (figure 5-5 A). Figure (5-5 B) show that there is more prominent phosphorylation after 60 minutes of low glucose (2mmol/l) compared to the baseline (figure 5-5 B & E).

Furthermore, we explored the dephosphorylation timeline in response to glucose by incubating the cells with low glucose RPMI (2 mmol/l glucose) overnight, cells were then pre-incubated with low glucose KRBH (2mmol/l glucose) for 30 minutes, followed by incubation with high glucose KRBH (15mmol/l glucose) for 10, 20, 30, 60 and 120 minutes (figure 5-5 C). The maximum dephosphorylation was observed after 30 minutes of high glucose (2mmol/l) (figure 5-5 D & E).

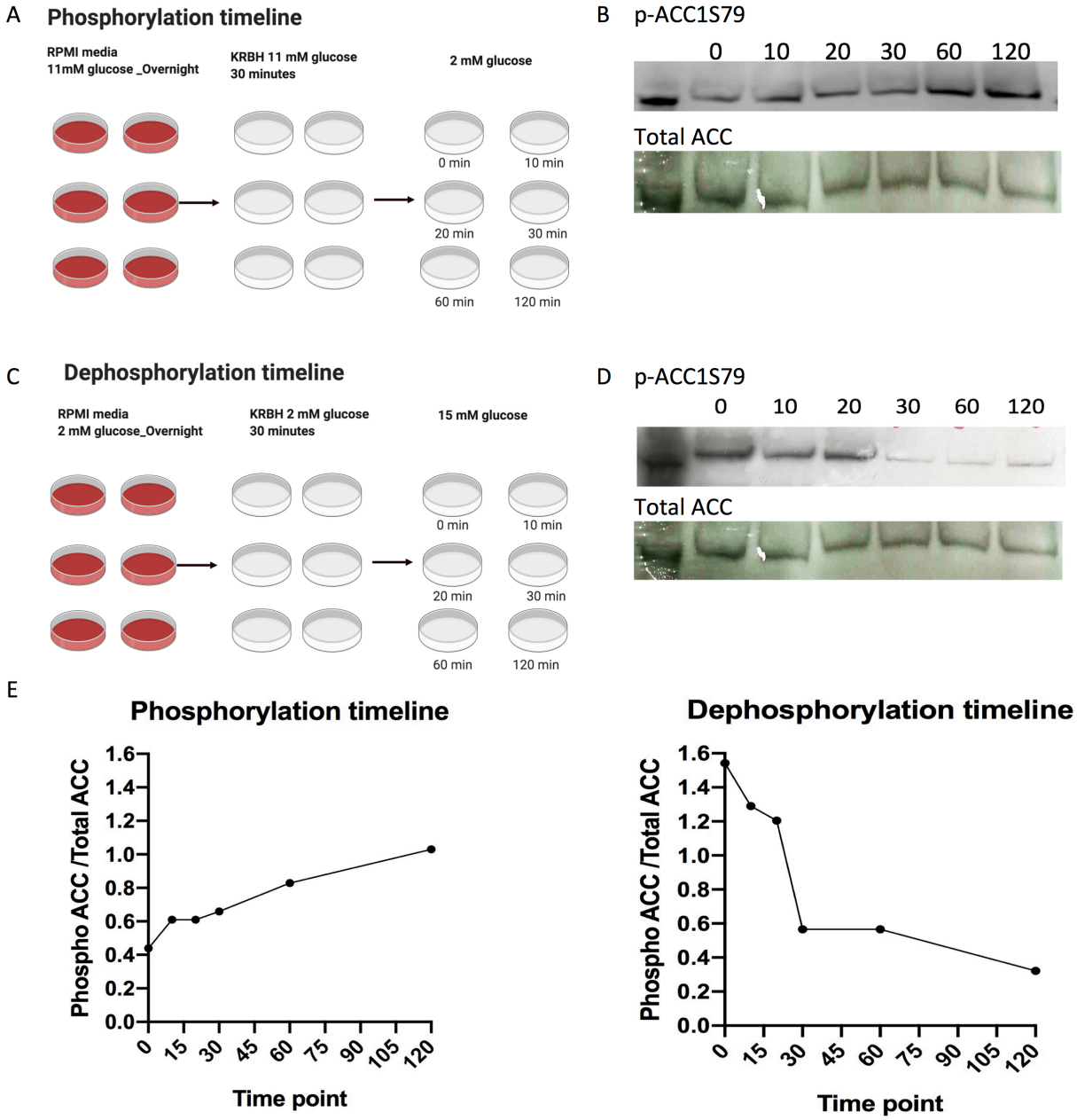


Figure 5-5 ACC1S79 phosphorylation and dephosphorylation timeline in INS1 cells. (A) ACC1 phosphorylation experimental design (B) Western blot for ACC1S79 phosphorylation at different time points (C) ACC1 dephosphorylation experimental design (D) Western blot for ACC1S79 dephosphorylation at different time points. (E) Quantification of ACC1S79 phosphorylation and dephosphorylation using image J plotted against time points.

Chapter 5.2.3 Validating the New ACC1 Phosphorylation Model

To evaluate the modified ACC1 phosphorylation model, we performed an experiment in which cells were pre-incubated with 11mmol/l glucose for 30 minutes, followed by 60 minutes or 120 minutes of low glucose (2mmol/l) or high glucose (15mmol/l). As shown in figure (5-6 A & B), ACC1S79 phosphorylation in response to low glucose was more prominent after 120 minutes compared to 60 minutes of low glucose. Moreover, we assessed potential changes in total protein phosphorylation levels using pan-p-(Ser/Thr) antibody, which is capable of quantitatively detecting phosphorylated Serine and Threonine residues in the cell lysates, upon treating the cells for 120 minutes with low glucose (2mmol/l) or high glucose (15mmol/l).

Next, we performed pull down for the cells treated with glucose for 120 minutes to further test the phosphorylation status of ACC1 using pan-p-(Ser/Thr) antibody. Remarkably, there is more pan-phosphorylation in ACC1 under these conditions (figure 5-6 C).

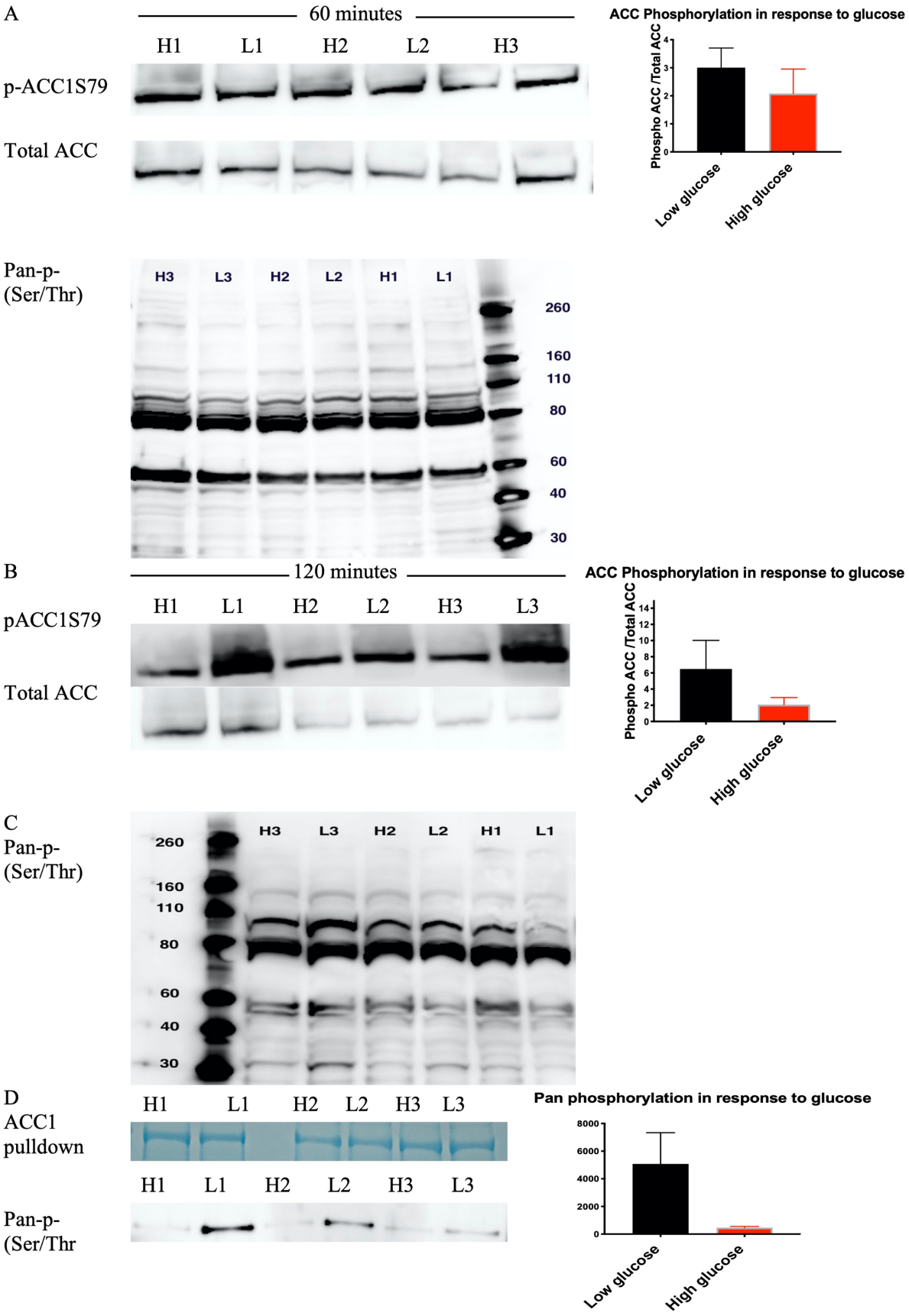

A
60 minutes
H1
L1
H2
L2
H3
p-ACC1S79
Total ACC
ACC Phosphorylation in response to glucose
Phospho ACC /Total ACC
Low glucose
High glucose
Pan-p-
(Ser/Thr)
H3
L3
H2
L2
H1
L1
260
160
110
80
60
40
30
B
120 minutes
pACC1S79
Total ACC
H1
L1
H2
L2
H3
L3
ACC Phosphorylation in response to glucose
Phospho ACC /Total ACC
Low glucose
High glucose
C
Pan-p-
(Ser/Thr)
D
ACC1
pulldown
Pan-p-
(Ser/Thr
Pan phosphorylation in response to glucose
Low glucose
High glucose

Figure 5-6 Evaluating the modified ACC1 phosphorylation model in INS1 cells. (A)Western blot for ACC1S79 phosphorylation and pan-p-(Ser/Thr) upon 60 minutes of low glucose (2mmol/l) or high glucose (15mmol/l) treatment (B) Western blot for ACC1S79 phosphorylation and pan-p-(Ser/Thr) upon 120 minutes of low glucose (2mmol/l) or high glucose (15mmol/l) treatment (C) ACC1 pulldown followed by western blot for pan-p-(Ser/Thr). 30 μg of proteins was loaded in the gel for each condition. p-ACC1S79 antibody, molecular weight: 269 kDa, was used at 1:1000 dilution, total ACC1 antibody was used as a loading control and a rabbit HRP conjugated secondary antibody was used at 1:5000 dilution. Quantification of ACC1S79 phosphorylation in both models using image J software.

Chapter 5.2.4 Quantification of ACC1 Phospho-Sites upon 120 Minutes of Glucose Treatment

In light of these dynamic experiments, we decided to perform label-free LC-MS/MS analysis to quantify changes in the novel ACC1 phosphorylation sites upon 120 minutes of low glucose (2mmol/l) or high glucose (15mmol/l) treatment. This experiment was performed in four independent biological replicates (figure 5-7), exhibiting high quantification accuracy and reproducibility, with Pearson correlation coefficients between 0.679 and 0.961 (figure 5-8).

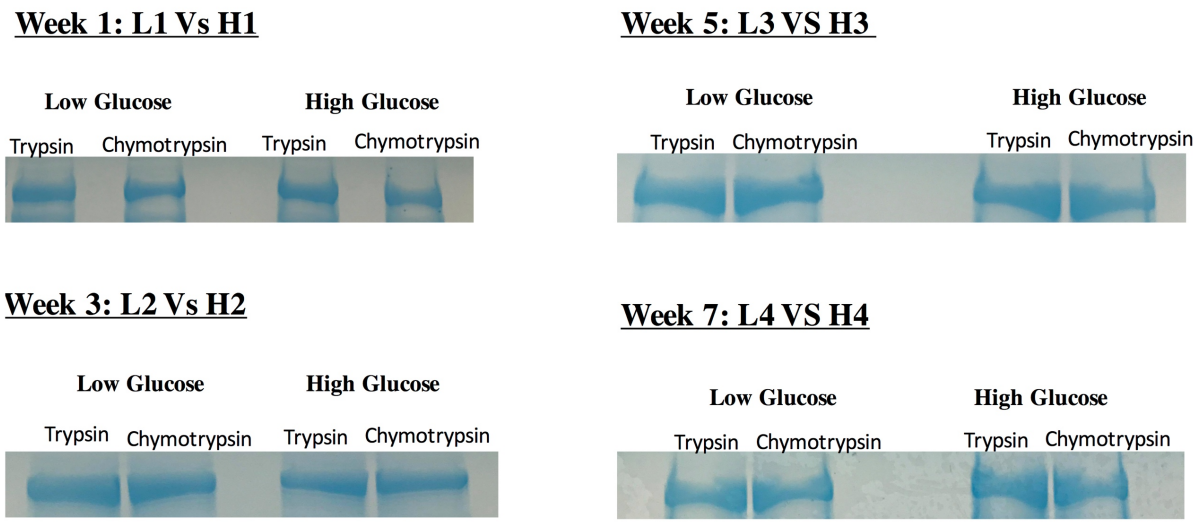


Figure 5-7 Label-free quantification upon 120 minutes of low glucose (2mmol/l) or high glucose (15mmol/l) treatment in INS1 cells: experiment's time line

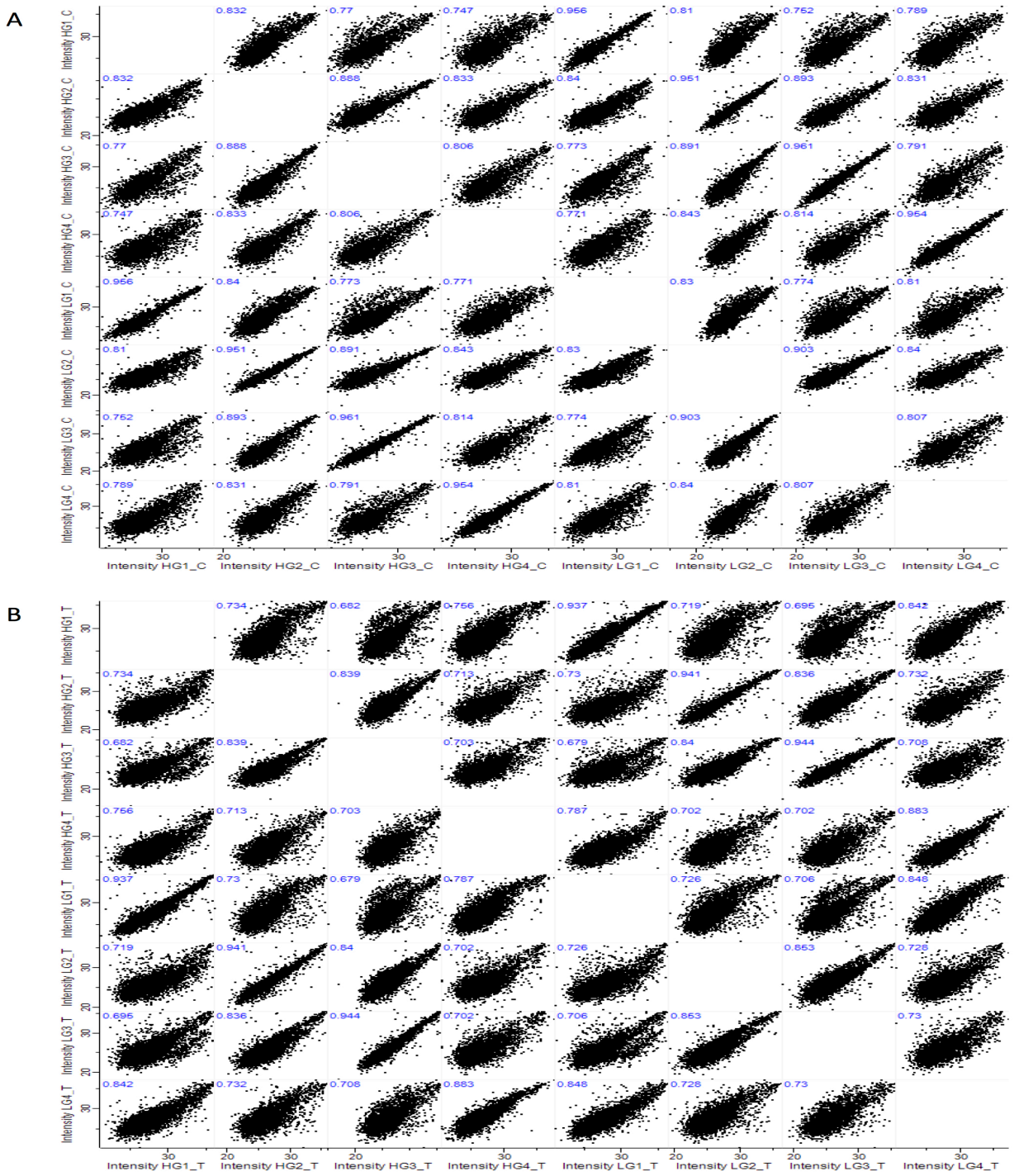


Figure 5-8 Pearson correlation coefficients. Scatter plots showing Pearson correlation coefficients between the different biological replicates for samples digested with chymotrypsin (A) and trypsin (B).

After applying Andromeda score filter of 40 (class 1 phosphosites), we identified twenty phosphosites (Table 5-3), which are localised to one amino acid with high confidence (class 1 sites). We compared this data to www.uniprot.org; a database that incorporates large-scale phosphoproteomics data from human, mouse, and rat studies. We found that seven of these sites (S23, S25, S29, S77, S79, S1215, S1200, S1262) had been identified previously using targeted biological applications. Moreover, eight of these sites have been identified using only large-scale mass spectrometry studies, that involved different types of tissues across three different species. However, it is difficult to assess the data quality in these kinds of datasets. Finally, five of these sites (S95, T510, T1174, S2305, S2317, T1252) are novel and to our knowledge have not been reported.

Table 5-3 ACC1 Phospho-sites detected upon 120 minutes of low glucose (2mmol/l) or high glucose (15mmol/l) treatment. List of ACC1 phosphosites identified via quantitative phosphoproteomics: The location of each site, localisation probabilities and identification scores (characterised using MaxQuant search software).

Residue number	Localization probability	Identification Score							
		LG1	LG2	LG3	LG4	HG1	HG2	HG3	HG4
Ser5	1.000								51.98
Ser5‡	0.998				49.49				42.50
Ser23	0.999	129.85	52.898	96.848	54.103	85.849	106.35	52.185	69.19
Ser25	0.998		90.475	53.453	125.11	130.49	101.75	92.792	133.41
Ser29	1.000	120.32	59.539	99.078	173.55	128.88	108.5	67.88	194.75
Ser29‡/Ser25‡, Ser23‡	0.998/0.779, 0.221				60.35				64.62
Ser29‡/Ser25‡, Ser23‡	0.998/0.501, 0.501								64.62
Ser47‡/Ser49‡	0.999/0.997				51.97	93.23			55.59
Ser77/Ser76	0.700/0.208								65.23
Ser79	0.999	41.24	42.84	50.35	58.40			41.32	52.58
Ser79‡	1.000	81.92	65.88	67.21	91.69		60.64		
Ser95	0.988				67.01				
Thr510/Ser511	0.537/0.462	63.87	41.615			57.142			
Thr832/Ser834	0.500/0.500	53.45							
Thr1174	1.000					48.29			
Ser1200	0.910	82.33		43.56		61.59			
Ser1203/Thr1211	0.536/0.248	61.87	58.53	83.57	193.40	52.20			
Thr1211	0.760	108.01	52.20	64.17	146.03	52.20			
Ser1215	0.992	110.32		99.99	86.93	88.30		52.64	
Ser1215‡	0.995	86.32	102.39	87.10	162.61	48.63			80.37
Ser1217/Ser1215	0.590/0.409					88.30		52.64	
Ser1258‡/Ser1262‡, Thr1264‡	1.000/0.942, 0.046	50.08			62.03	43.63			86.03
Ser1258‡/Ser1262‡, Thr1264‡	1.000/0.802, 0.198	69.22	69.28	51.57	36.79	56.04	69.58	49.59	96.24
Ser1258	1.000	108.90		70.06	137.66	88.54	91.15	63.91	153.86
Ser1258/Ser1262	0.974/0.973			48.80				58.43	
Ser2156	0.937								45.61
Ser2305	1.000		114.15				67.83	159.46	
Ser2317	0.998	111.18		99.319	79.054	103.42	86.54		55.77
Ser2326/Thr2328	0.743/0.224				73.758			47.61	
‡Chymotrypsin									

Figures (5-9 & 5-10) show the volcano plots for samples digested with chymotrypsin and trypsin, respectively. As described previously, in these plots X-axis represents the fold change (the difference in the means of signal intensities between low glucose and high glucose samples; LG-HG) in ACC1 phosphorylation on the log^2 scale (sites that are upregulated in low glucose appears on the positive side of the axis, while sites that are upregulated in high glucose appear on the negative side of the axis). Y-axis represents the negative log scale of the student t-test p-value; thus, smaller p-values appear higher up on the scale.

In MaxQuant software, there are two ways to analyse the changes in phosphorylation; The first one is by looking at the changes in each individual phosphopeptide (panel A in figures 5-9 & 5-10). The second way is by looking into the phosphorylation sites table generated by the software. In this table, quantitative information for each site is derived from all peptides that are phosphorylated at this site and meet the given FDR, Andromeda score and delta score (panel B in figures 5-9 & 5-10)[114].

As shown in these plots, ACC1S1215 exhibits a strong and statistically significant response (upregulated in low glucose) upon 120 minutes of low glucose (2mmol/l) treatment. ACC1S79 shows slight yet significant glucose response (upregulated in low glucose). Interestingly, ACC1S49 and ACC1S25 are significantly upregulated under high glucose conditions (15mmol/l). To our knowledge, we are the first to report the glucose response of these sites.

Representative spectra for these glucose responsive sites are shown in figure (5-11).

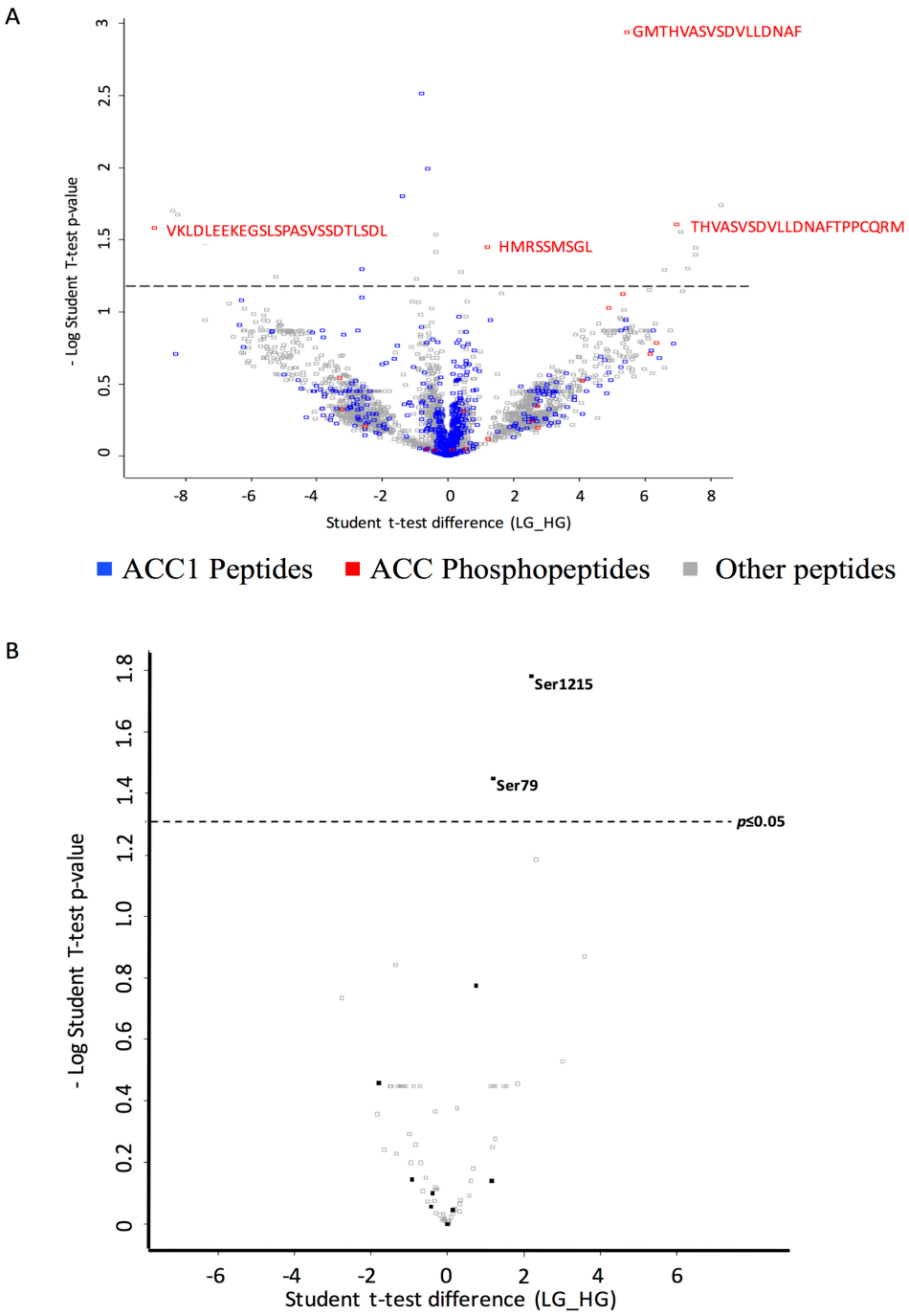
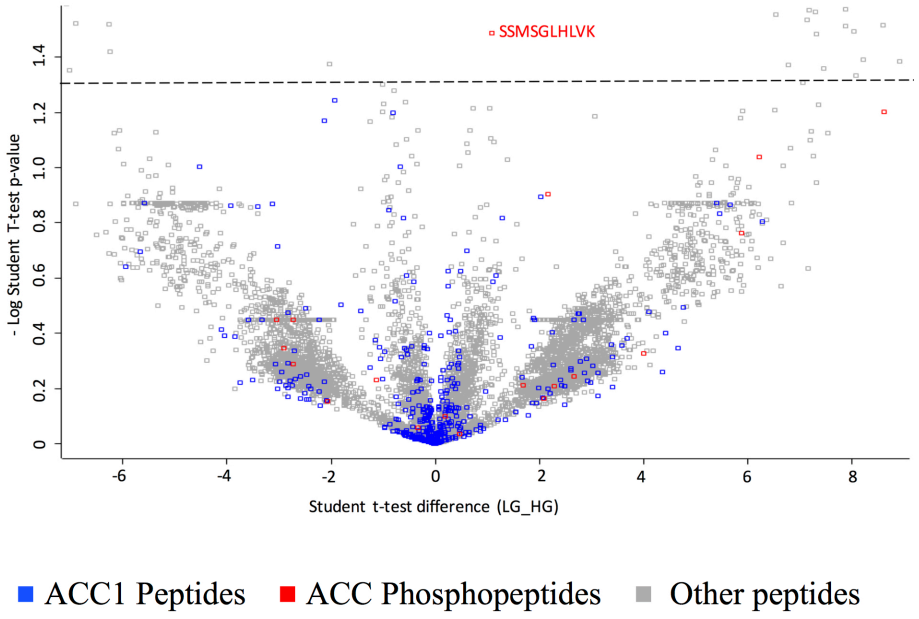


Figure 5-9 Quantification of ACC1 phospho-sites upon 120 minutes of low glucose (2mmol/l) or high glucose (15mmol/l) treatment in samples digested with chymotrypsin. A) Volcano plot for ACC1 phosphopeptides detected in the band digested with chymotrypsin (B) Volcano plot of the corresponding phospho-sites. The dash lines represent a *p*-value of 0.05

A



B

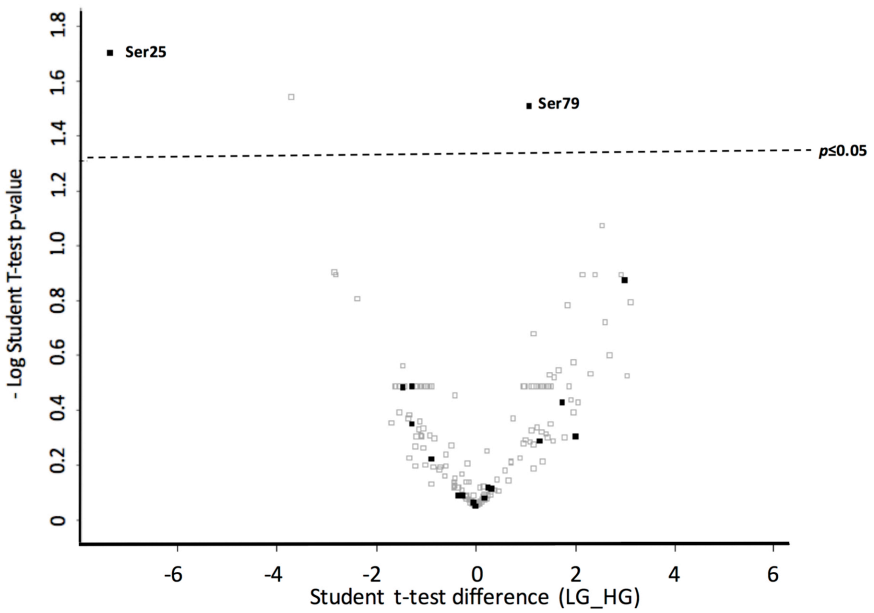
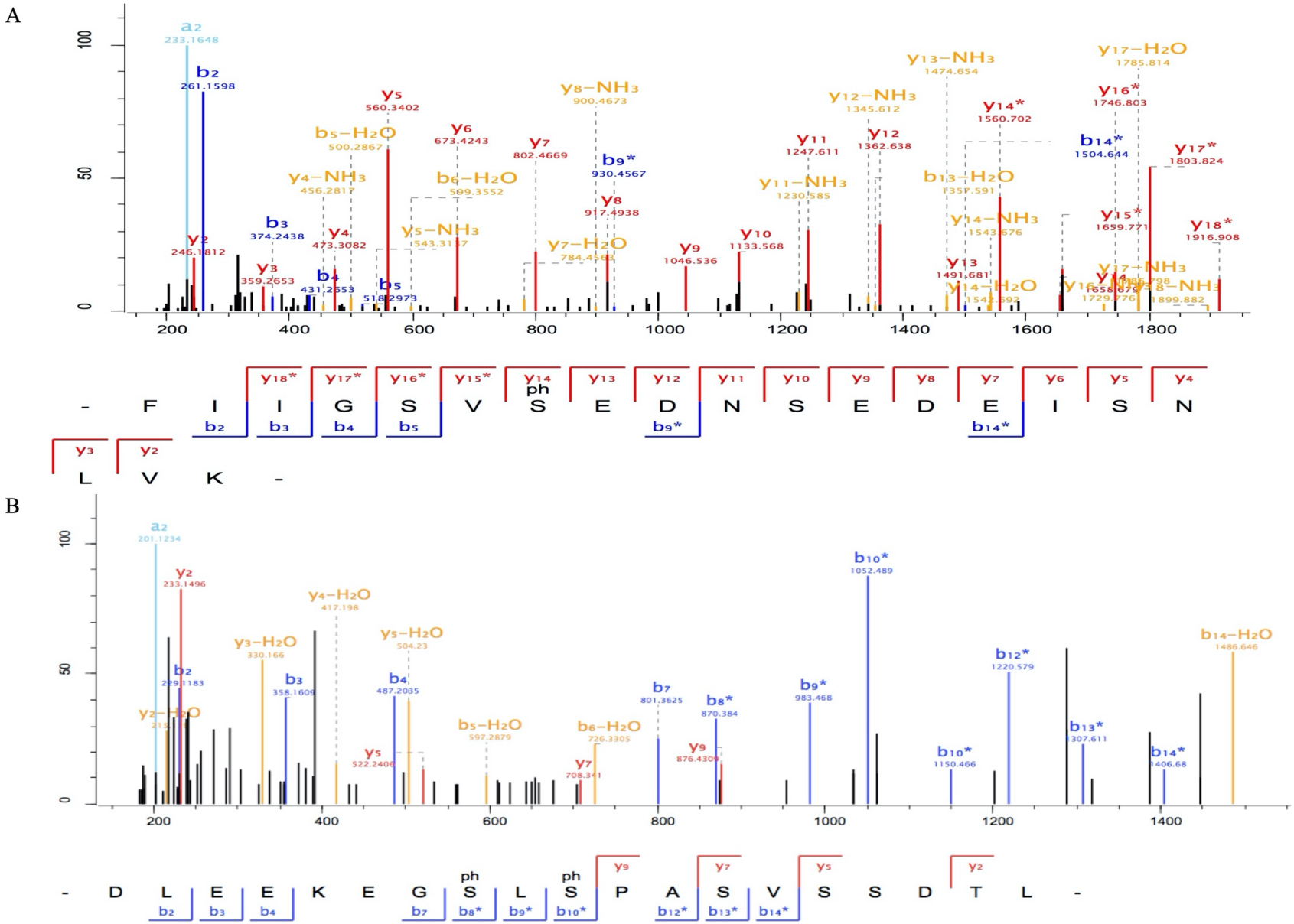


Figure 5-10 Quantification of ACC1 phospho-sites upon 120 minutes of low glucose (2mmol/l) or high glucose (15mmol/l) treatment in samples digested with trypsin. (A) Volcano plot for ACC1 phosphopeptides detected in the band digested with chymotrypsin (B) Volcano plot of the corresponding phospho-sites. The dash lines represent a *p*-value of 0.05


A
a2 233.1648
b2 261.1598
y5 560.3402
b5−H2O 500.2867
y6 673.4243
y8−NH3 900.4673
y7 802.4669
b9* 930.4567
y4−NH3 456.2817
b6−H2O 599.3552
y8 917.4938
b3 374.2438
y4 473.3082
y5−NH3 543.3137
y2 246.1812
y7−H2O 784.4563
y3 359.2653
b4 431.2653
b5 518.2973
y9 1046.536
y10 1133.568
y11 1247.611
y12−NH3 1345.612
y12 1362.638
y13−NH3 1474.654
y14* 1560.702
y11−NH3 1230.585
b13−H2O 1357.591
y17−H2O 1785.814
y16* 1746.803
b14* 1504.644
y17* 1803.824
y14−NH3 1543.676
y15* 1699.771
y18* 1916.908
y13 1491.681
y14−H2O 1542.592
y17−NH3 1768.798
y16−NH3 1729.776
y18−NH3 1899.882
- F I I G S V S E D N S E D E I S N
y18* y17* y16* y15* y14 ph y13 y12 y11 y10 y9 y8 y7 y6 y5 y4
b2 b3 b4 b5 b9* b14*
L V K -
y3 y2
B
a2 201.1234
y2 233.1496
y4−H2O 417.198
y3−H2O 330.166
y5−H2O 504.23
b2 229.1183
b3 358.1609
b4 487.2085
y2−H2O
b5−H2O 597.2879
b6−H2O 726.3305
y5 522.2406
y7 708.341
b7 801.3625
b8* 870.384
y9 876.4309
b10* 1052.489
b9* 983.468
b12* 1220.579
b14−H2O 1486.646
b13* 1307.611
b10* 1150.466
b14* 1406.68
- D L E E K E G S L S P A S V S S D T L -
ph ph
y9 y7 y5 y2
b2 b3 b4 b7 b8* b9* b10* b12* b13* b14*

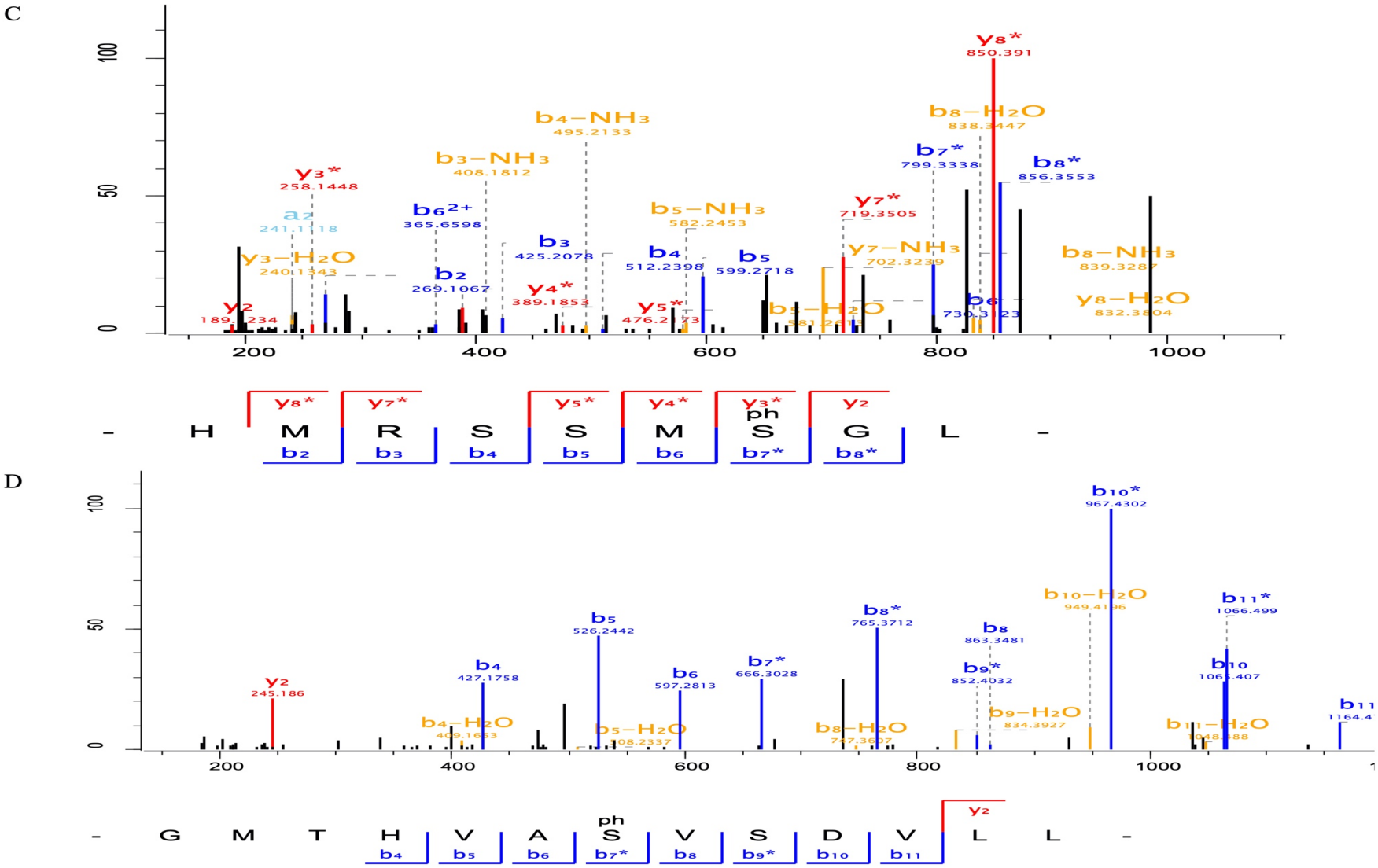


Figure 5-11 Representative spectra of ACC1glucose responsive phospho-sites. (A) ACC1S25 (B) ACC1S49 (C) ACC1S79 (D) ACC1S1215.

Chapter 5.2.5 Looking into other Types of PTMS

Using our mass spectrometry data, we also analysed other types of PTMs; including acetylation (lysine residue), malonylation (lysine residue), and hydroxylation (proline residue). We found that there are no acetylation and malonylation sites for ACC1; which is consistent with the western blot shown in figure (5-1). Interestingly, we found several hydroxylation sites for ACC1 (table 5-4). Overall, these sites are not glucose-responsive.

Table 5-4 ACC1 Hydroxylation sites detected upon 120 minutes of low glucose (2mmol/l) or high glucose (15mmol/l) treatment. List of ACC1 Hydroxylation sites identified via quantitative proteomics: The location of each site, localisation probabilities and identification scores (characterised using MaxQuant search software).

Proteins	Positions within proteins	Localization prob	Score
P11497;P11497-2	255;255	1	167.55
P11497;P11497-2	258;258	1	167.55
A0A0G2K5G8;D3ZRA3;P11497;P11497-2	1360;1216;1478;1470	0.999669	127.76
A0A0G2K5G8;D3ZRA3;P11497;P11497-2	1109;965;1227;1219	1	110.31
A0A0G2K5G8;D3ZRA3;P11497;P11497-2	1110;966;1228;1220	1	110.31
A0A0G2K5G8;D3ZRA3;P11497;P11497-2	507;363;625;625	1	108.9
A0A0G2K5G8;D3ZRA3;P11497;P11497-2	328;184;446;446	0.999982	106.45
A0A0G2K5G8;D3ZRA3;P11497;P11497-2	1366;1222;1484;1476	0.997025	91.637
A0A0G2K5G8;D3ZRA3;P11497;P11497-2	632;488;750;750	0.998878	81.565
A0A0G2K5G8;D3ZRA3;P11497;P11497-2	1784;1640;1902;1894	1	79.974
A0A0G2K5G8;D3ZRA3;P11497;P11497-2	638;494;756;756	0.632623	79.089
A0A0G2K5G8;D3ZRA3;P11497;P11497-2	1958;1814;2076;2068	1	77.744
A0A0G2K5G8;D3ZRA3;P11497;P11497-2	226;82;344;344	0.999329	73.841
A0A0G2K5G8;D3ZRA3;P11497;P11497-2	2193;2049;2311;2303	1	72.928
A0A0G2K5G8;D3ZRA3;P11497;P11497-2	1920;1776;2038;2030	1	72.34
A0A0G2K5G8;D3ZRA3;P11497;P11497-2	2074;1930;2192;2184	1	69.122
A0A0G2K5G8;D3ZRA3;P11497;P11497-2	1553;1409;1671;1663	1	63.454
A0A0G2K1F2;E9PSQ0;D3ZBE2;A0A0G2K5L6	1511;1516;1514;1509	1	62.823
A0A0G2K5G8;D3ZRA3;P11497;P11497-2	1533;1389;1651;1643	1	57.836
A0A0G2K5G8;D3ZRA3;P11497;P11497-2	1448;1304;1566;1558	0.999978	54.776
A0A0G2K5G8;D3ZRA3;P11497;P11497-2	1847;1703;1965;1957	1	52.716
A0A0G2K5G8;D3ZRA3;P11497;P11497-2	792;648;910;910	1	47.288
A0A0G2K5G8;D3ZRA3;P11497;P11497-2	1550;1406;1668;1660	1	42.904
A0A0G2K1F2;E9PSQ0;D3ZBE2;A0A0G2K5L6;A0A0G2K5G8;D	2128;2133;2131;2125;1901;1757;2019;2011	1	42.711
A0A0G2K5G8;D3ZRA3;P11497;P11497-2	704;560;822;822	0.795196	41.514

Chapter 5.3 Discussion

This study was undertaken to expand our understanding of ACC1 regulation in beta cells. To this aim, we have identified and systematically characterised twenty phosphosites for ACC1 (class 1 sites). Moreover, we quantified changes in the phosphorylation status of these sites upon 120 minutes of low glucose (2mmol/l) or high glucose (15mmol/l) treatment. Additionally, we looked for other types of PTMs; Acetylation, Malonylation, and Hydroxylation. To the best of our knowledge, this is the first study providing an in-depth, targeted and unsupervised assessment of ACC1 PTMs. The most striking results to emerge from our data is that ACC1S1215 shows dramatic upregulation in low glucose conditions compared to ACC1S79. In addition, ACC1S25 and ACC1S49 are upregulated in response to high glucose conditions.

The significant glucose response for ACC1S1215 might suggest a crucial role in ACC1 activity. This observation is in contrary to several earlier findings[93,94] but in agreement with others [126-129].

The first discussions and analysis for the role of S1215 in ACC1 activity emerged during the 1990s with Hardie et al. study on ACC phospho-regulation[94]. The authors in this study observed that phosphorylation of Sl200 and S1215 (located in the central region of ACC1) does not affect ACC activity while phosphorylation of S77 and S79 (located in the N-terminal region of ACC1) is crucial for ACC activity. Briefly, in this study the authors hypothesised that the marked ACC inactivation caused by AMPK compared to the inactivation caused by PKA is due to the presence of an additional phosphorylation site for AMPK (i.e. S1215). To test this hypothesis, the authors made use of the observation that incubating ACC with PKA followed by AMPK would restrict phosphorylation by AMPK to S1215. Based on this, they measured ACC activity in four conditions; **Control**, **ACC incubated with AMPK** (which leads to ACC phosphorylation at S79, S1200 & S1215), **ACC incubated with PKA** (which leads to ACC phosphorylation at S77 &

S1200), **ACC incubated with PKA then AMPK** (which leads to ACC phosphorylation at S1215 only) (figure 5-12). They found that phosphorylation of S1215 did not produce any change in enzymatic activity above the moderate inactivation caused by PKA. Thus, they concluded that the difference in the kinetic effects of PKA and the AMPK are due to their different sites of phosphorylation within the N-terminal region (i.e. Ser77/Ser79), and not due to phosphorylation of S1215 by AMPK. They supported their conclusion further based on the observation that limited proteolysis with trypsin leads to protein activation by selectively removing the amino-terminal region containing S79 leading to protein activation and reversing the effect of phosphorylation by AMPK and PKA, suggesting that the amino-terminal region is the regulatory domain.

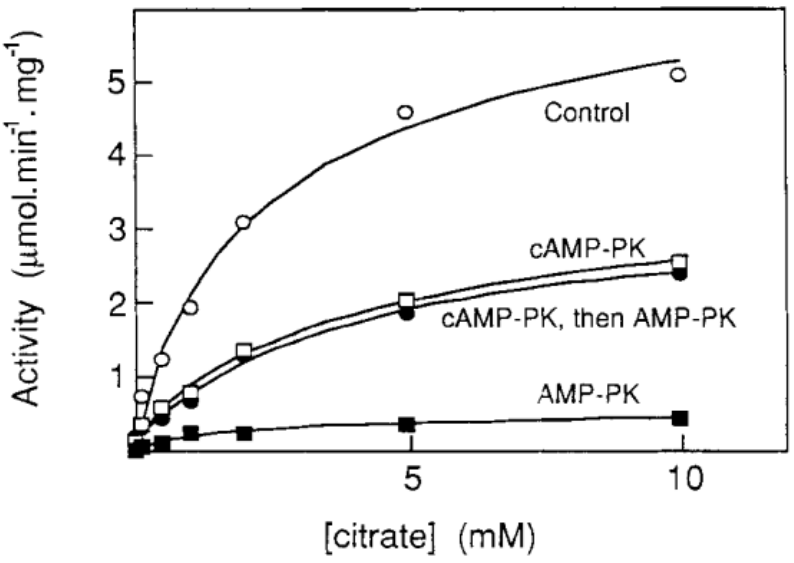


Figure 5-12 ACC activity measured across four different conditions in Hardie et al. study[94].

Several questions regarding the method used in this study remain to be addressed. Firstly, ACC1 activity was assessed by incubating ACC1 purified from lactating rat mammary gland, with AMPK/PKA purified from rat liver for 30 minutes in test tubes. This *in vitro* assessment of ACC1 activity might not reflect ACC1 activity in cells. Secondly, the authors observed that S1215 is phosphorylated slower than S79, yet they did not modify the experimental condition based on this observation (i.e. 30 minutes incubation with AMPK might not be enough to cause a change in S1215 phosphorylation status, thus not affecting ACC1 activity, and this is in line with our observations). Thirdly, the source of purified ACC1 is lactating mammary gland: according to www.proteinatlas.org there is substantial expression of ACC2 in this tissue; nevertheless, the authors did not distinguish between the two forms of ACC in their study. We ran a sequence alignment between ACC1 and ACC2, and we found that ACC1S79 is conserved between the two forms, the location of the equivalent phosphosite is ACC2S212, while S1215 is not conserved (figure 5-13).

To understand why the authors did not distinguish between the two isoforms in their study we searched the literature and found that while ACC1 was discovered in 1959, it was only until 1989 for ACC2 to be discovered and recognised as a unique isoform of ACC enzyme[58].

Finally, their conclusion that proteolysis activates the enzyme by removing the N-terminal region (which contains S79) was criticised later by Kim et al. in 1994, because in many cases partial proteolysis leads to enzyme activation by itself[93].

Kim et al. in this study attempted to localise critical phosphorylation sites that affect ACC1 activity using site directed mutagenesis (SDM) technique to mutate different phosphorylation sites and assess the impact of that on ACC1 activity in Hela cell line. In this study, Kim et al. agreed with Hardie et al. on the effect of S1215 on ACC1 activity. However, he disagreed regarding the effect

of S1200 on ACC1 activity. Overall, there has been confusion in the literature regarding ACC1 critical phosphorylation sites.

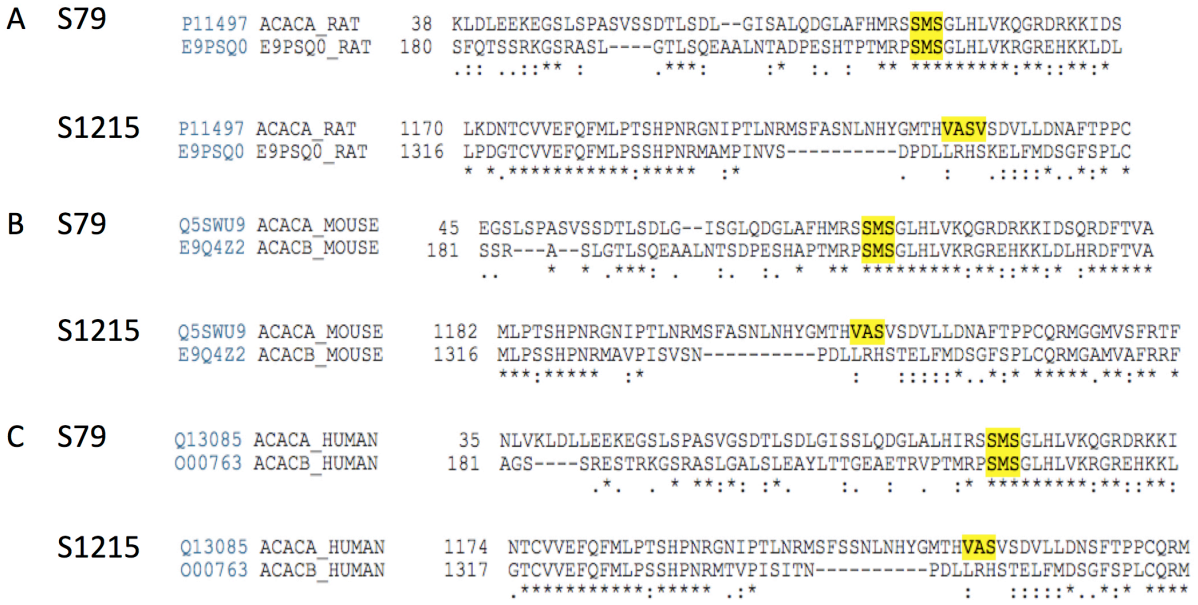


Figure 5-13 Sequence alignment between ACC1 and ACC2 S79 and S1215. (A) rat (B) mouse (C) human. Sequence alignment was performed using https://www.uniprot.org .

For many years, ACC1S1215 was neglected by molecular biologists based on these studies. Only in the past five years, researchers in the field of structural biology have addressed this issue again. Cryo-electron microscopic studies showed that ACC1 central region is located at the sides of the protein and acts as a scaffold to position BC and CT domains (crucial domains for ACC1 activity) correctly for catalysis. Moreover, they found that yeast ACC1 is directly phosphorylated by the SNF1 protein kinase at residue S1157 (which is well conserved with S1215 phosphorylation site in rat ACC1), resulting in potent inhibition of ACC1. Phosphorylation of ACC1 at this site in yeast has been shown to cause dramatic conformational changes. Furthermore, these studies have shown that mutating this site to alanine increased ACC1 enzymatic activity [126-129].

Given this inconsistency in the literature about the effect of ACC1S1215 on ACC1 activity and in light of the novel ACC1S25, ACC1S25 and ACC1S49 glucose response, we aimed in the next chapters to explore their effect further, to perform further validation experiments, to look into possible kinases that regulate these sites, and to do tissues comparison as these sites could be also critical in other tissues (e.g liver).

Chapter 6 Phosphoproteomics Data Validation

Chapter 6.1 Introduction

While the use of MS technology for analysis of protein phosphorylation has become a valuable tool in the field of biological sciences, several limitations still have to be addressed in order to generate robust and reliable data. In a typical high-throughput phosphoproteomics experiment, peptides are first generated from digestion of the denatured proteins using proteolytic enzymes. before ionisation and analysis in the mass spectrometer to generate MS/MS spectra. The subsequent identification of proteins from the MS/MS spectra depends on the bioinformatic software and database search engines used, and is prone to false matches leading to false-positive results [130,131]. Among those are Identification errors (i.e. false identification of phosphopeptides) and localisation error (i.e. false localisation of the phosphorylation site). The localisation of site-specific modifications is a particularly challenging task especially when candidate sites are in close proximity in the peptide sequence[130,132]. Even though phosphoproteomics as a field has generated a variety of experimental, informatics and statistical means to avoid potential false-positive results[130,133], validation of these data remains quite essential.

In this project, the applied phosphoproteomic workflow and MS analysis yielded a global view of ACC1 phosphoregulation with accurate quantification of changes in tens of phosphosites between two conditions: low and high glucose. As explained in detail in the previous chapter, three phosphosites, ACC1S25, ACC1S49 and ACC1S1215, showed substantial and significant changes in phosphorylation in response to glucose. Although every effort has been made to produce robust, reproducible and statistically significant results (see chapters 4 & 5), these data require further validation using an alternative approach. Thus, we aimed to validate our phosphoproteomics data using western blotting with phospho-specific antibodies against ACC1S1215, ACC1S25 and

ACC1S49. At the time of conducting this study, the ACC1S25 antibody was not ready due to some technical issues, so we worked with ACC1S1215 and ACC1S49 antibodies.

These antibodies are valuable tools to explore the dynamics of ACC1 phosphorylation in beta cells, not only in response to glucose but also many nutrients and hormones. Moreover, they can be used in a wide range of *in vivo* studies of ACC1; some of which are not easily performed by mass spectrometry[134]. Examples of future experiments include studying putative kinases that regulate these sites (using activators and inhibitors) to elucidate new molecular mechanisms in beta-cell function; analysing ACC1 phosphorylation in other tissues that have a high level of ACC1 expression (e.g. liver, adipocytes); and most importantly studying these sites in primary mouse and human islets to extend our findings from the INS1 cell line to a more physiological setting.

Another limitation of the phosphoproteomics work, is the limited mechanistic insights into the functional role of these phosphorylation sites. Furthermore, it has been suggested that some phosphorylation events could be non-functional by-products of kinase activity [135]. Therefore, further functional studies are required to pinpoint the mechanisms by which these phosphosites and their responsible kinases may affect ACC1 activity and hence, beta-cells function. To this end, we aimed to generate ACC1KO INS1 cells lines, to mutate these phosphosites to alanine (phospho-null) or aspartate (phospho-mimetic) using site-directed mutagenesis, overexpress these mutated constructs in INS1 cells using transient transfection, and assess the effect on GSIS and ACC1 activity.

The aims of this chapter are:

1- Generation of ACC1S25, ACC1S49 and ACC1S1215 phospho-specific antibodies.

2- Validate the glucose response in ACC1S1215 and ACC1S49 in INS1 cells.

3- Use a bioinformatics approach to predict the kinases targeting these sites.

4- Exploring the dynamics of these sites in other tissues.

5- Generation of ACC1KO INS1 cell line using CRISPR-CAS9.

6- Mutant and wild type ACC1 overexpression in INS1 cell line to assess functional role of key phosphosites.

Chapter 6.2 Methods

General methods are described in chapter 2; this section describes the specific methods used in generating ACC1KO INS1 cell lines using CRISPR technology.

Chapter 6.2.1 Dot blot

PVDF membrane (polyvinylidene difluoride, Invitrogen, pore size: 0.45 µm, catalogue number LC2005) was used for dot blot. A pencil was used to draw a grid to indicate the region for the blot. Using narrow-mouth pipette tip, 2 µl of samples was loaded onto the membrane. The membrane was left to dry for one hour. Then it was blocked by soaking in 5% BSA in TBS-T for one hour at room temperature. The membrane was then incubated with primary antibody (1:1000 dilution) dissolved in BSA/TBS-T for one hour at room temperature. The membrane was washed three times with TBS-T (3 times for 5 minutes). Then it was incubated with secondary antibody conjugated with HRP (1:5000 dilution) for one hour at room temperature. The membrane was washed three times with TBS-T (3 times for 5 minutes).

Chapter 6.2.3 Genomic DNA extraction

Genomic DNA was extracted from cells for genotyping using QIAamp DNA Mini Kit (Qiagen Hilden, Germany, catalogue number 51304). According to the manufacturer's cells were cultured in 6-well plate (5 x 10^6 cells) then detached from the culture flask by trypsinisation:
the medium was aspirated and cells were washed with PBS, PBS were aspirated, and 0.10–0.25% trypsin was added. After cells have detached from the dish or flask, they were collected in medium, and transferred to a 1.5 ml microcentrifuge tube. Cells were then centrifuged for 5 min at 300 x g. The supernatant was then removed completely and discarded, with cautions not to disturb the cell pellet. Cell pellet were then resuspended in PBS to a final volume of 200 µl. Then 20 µl proteinase

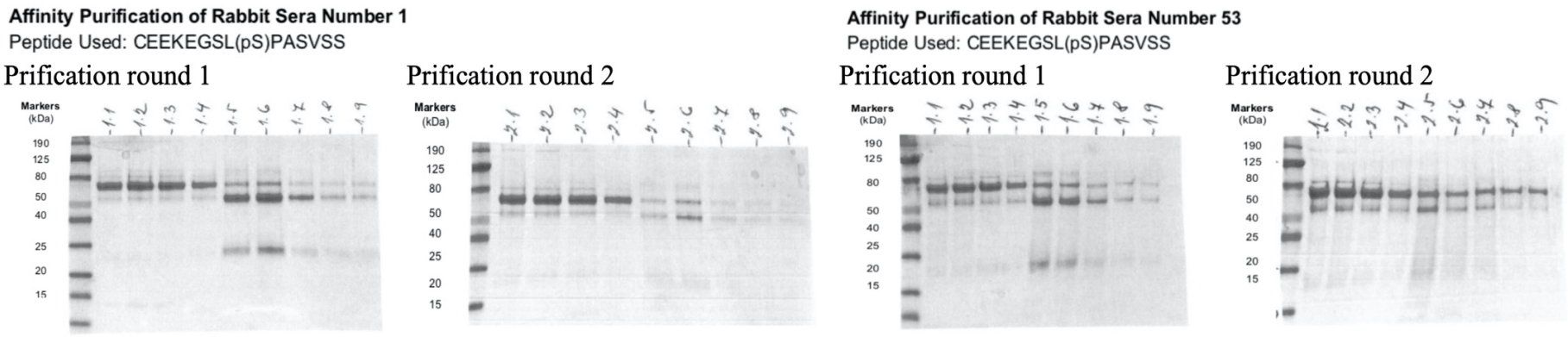
K were added. 200 µl of Buffer AL was added to the sample, mixed by pulse vortexing for 15 seconds, incubated at 56°C for 10 min. Then, the 1.5 ml microcentrifuge tube was briefly centrifuged to remove drops from the inside of the lid. 200 µl ethanol (96–100%) was added to the sample, and mixed again by pulse-vortexing for 15 seconds. After mixing the 1.5 ml microcentrifuge tube was briefly centrifuged to remove drops from the inside of the lid. The mixture was carefully applied to the QIAamp Mini spin column (in a 2 ml collection tube) without wetting the rim, and centrifuged at 6000 x g (8000 rpm) for 1 min. Then, the QIAamp Mini spin column in was placed a clean 2 ml collection tube, and the tube containing the filtrate was discarded. 500 µl of Buffer AW1 was added and centrifuge at 6000 x g (8000 rpm) for 1 min. QIAamp Mini spin column was placed in a clean 2 ml collection tube and the collection tube containing the filtrate was discarded. 500 µl Buffer AW2 was added and the tubes were centrifuged at full speed (20,000 x g; 14,000 rpm) for 3 min. Finally, 200 µl Buffer of buffer AE was added and the samples were incubated at room temperature (15–25°C) for 1 min, and then centrifuge at 6000 x g (8000 rpm) for 1 min.

Chapter 6.3 Results

Chapter 6.3.1 Generation of ACC1S1215 and ACC1S49 Phosphospecific Antibodies

To validate the glucose response in ACC1S1215 and ACC1S49, phospho-specific rabbit polyclonal antibodies against these phosphosites were custom-made (DC Biosciences, Dundee). For each antibody two rabbits were immunised with synthetic site-specific phosphopeptides, two rounds of purifications have been carried out and nine fractions have been collected (figure 6-1). We performed a series of western blot analyses to test these fractions and to validate their specificity for phospho-peptides. We used 1:1000 antibody dilution as a starting point. In agreement with our phosphoproteomics data, fraction number 1.8 purified from rabbit number 53 for ACC1S49 antibody, showed that ACC1S49 was upregulated with high glucose condition compared to low glucose condition (figure 6-2A). Similarly, fraction number 1.8 and fraction number 1.9 purified from rabbit number two for ACC1S1215 antibody showed that ACC1S1215 was upregulated in cells treated with low glucose for two hours and in cells treated with 500 μM AICAR (AMPK activator) (figure 6-2B). Moreover, the non-specific bands detected in these fractions (fraction 1.8 for ACC1S49, fraction 1.8 & 1.9 for ACC1S1215) were less compared to other fractions (suggesting high purity of our target antibody) so we selected these fractions for use in future experiment.

ACC1S49 Antibody:



ACC1S1215 Antibody:

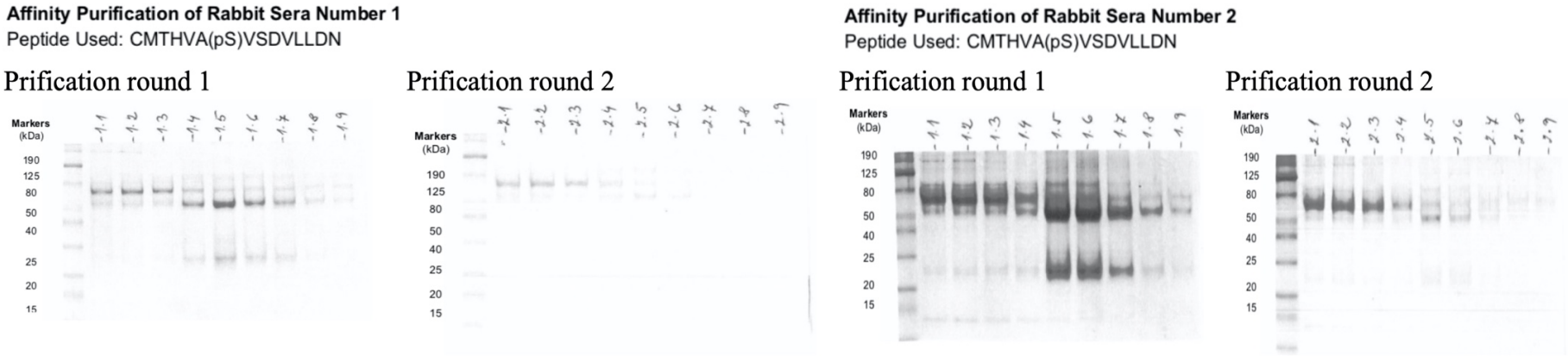


Figure 6-1 Generation of ACC1S49 and ACC1S1215 phospho-specific antibodies. SDS-PAGE protein gels showing elution of Igg chains. For each antibody two rabbits were immunised with site specific phospho-peptide, two rounds of purifications have been carried out using by immunoaffinity chromatography and nine fractions have been collected. Each fraction is assigned with an identification code consisting of 2 numbers; the first one is the purification round number and the second one is the fraction number (for example 1.3: purification round number 1, fraction number 3). Source: (DC Biosciences, Dundee)

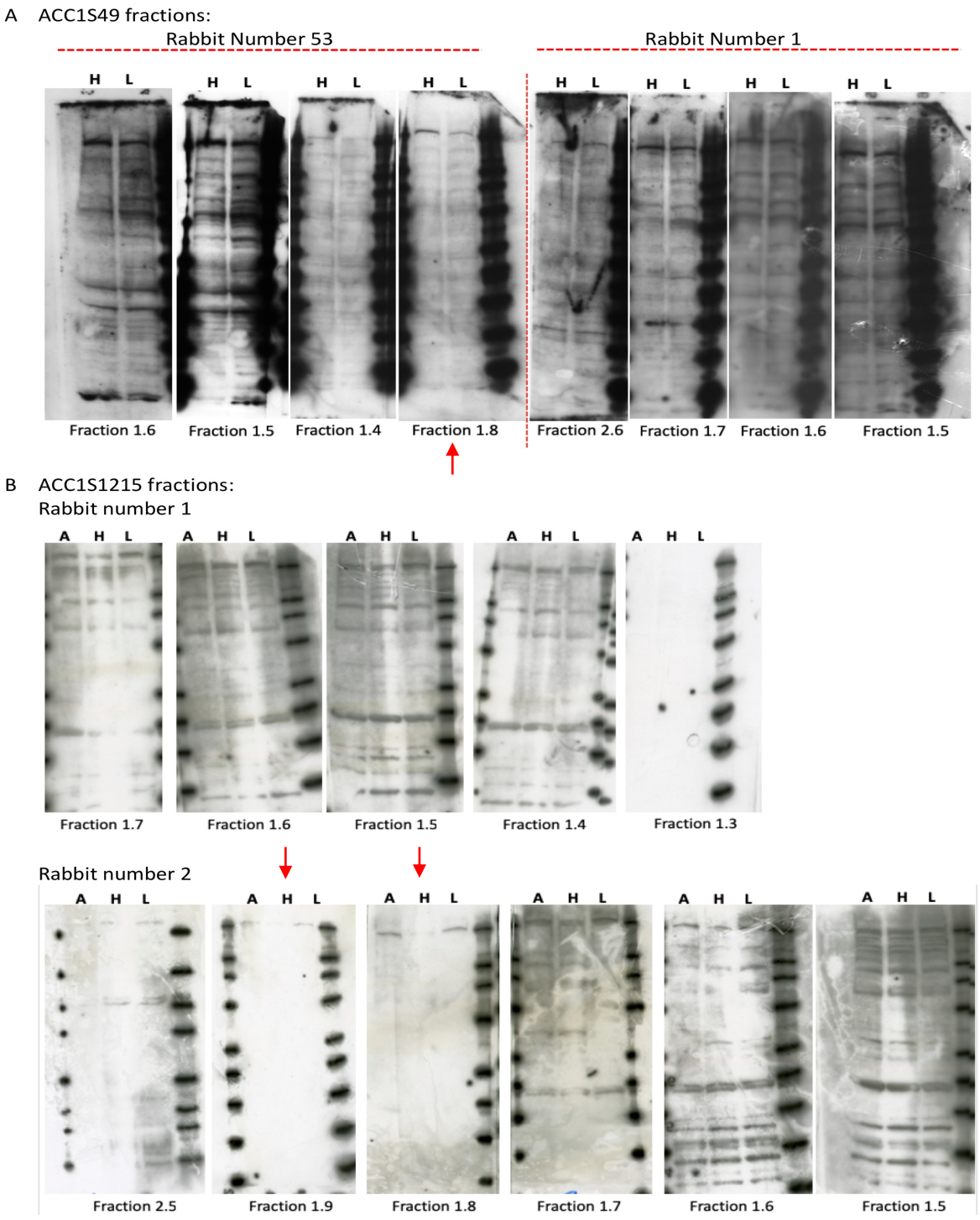


Figure 6-2 Testing different fractions for ACC1S49 and ACC1S1215. Western blot analysis of INS-1cells treated with the corresponding condition for two hours. L: low glucose (2 mmol/l), H: high glucose (15 mmol/l), A: AICAR (500 µM). Fraction 1.8 for ACC1S49 (A) and fraction 1.8 & 1.9 for ACC1S1215 (B) clearly show the glucose response in these sites. 30 µg of proteins was loaded in the gel for each condition. ACC1S79 antibodies, molecular weight: 269 kDa, were used at 1:1000 dilution and a rabbit HRP conjugated secondary antibody was used at 1:5000 dilution..4-12% gradient gel was used.

Chapter 6.3.2 Validating the Glucose Response in ACC1S1215 and ACC1S49 in INS1 Cells.

Next, we aimed to test whether these antibodies are ACC1-selective, reproducible, and phosphorylation-specific (i.e. recognise only the phosphorylated forms of ACC1). We employed dot blot assays to test the reaction of each antibody to the phospho-peptide (used in the generation of these antibodies), to the unmodified peptide, and INS1 cells lysates treated with low and high glucose for ACC1S1215 and ACC1S49, respectively. As can be seen from figure (6-3 A & B), both antibodies detected the phospho-peptide and had minimum reactivity to the non-phosphorylated peptide.

To increase the reliability of these antibodies, we performed western blotting for INS1cells pre-incubated with 11 mmol/l glucose for 30 minutes and treated with low glucose (2 mmol/l) or high glucose (15 mmol/l) for two hours, the same conditions as used for mass spec experiments, in addition to cells treated with AICAR (500 μM on top of high glucose 15 mmol/l). Each condition was tested in triplicate. Cell lysates were blotted for ACC1S1215, ACC1S49 and ACC1S79 antibodies (figure 6-3C). A single band at the known molecular weight for ACC1 was detected by ACC1S1215 and ACC1S49 antibodies, corresponding to the band detected by ACC1S79 antibody (Cell signalling, catalogue number 3676), a previously validated and commercially available antibody[136]. In accordance with the phosphoproteomics data, ACC1S1215 showed a striking glucose response (upregulated in low glucose condition), while ACC1S49 showed marginal glucose response (upregulated in high glucose condition). Similarly, ACC1S79 showed a minor glucose response (upregulated in low glucose condition). Interestingly, AICAR enhanced ACC1S1215 phosphorylation, suggesting that it is phosphorylated by AMPK site.

To further confirm that these antibodies are ACC1-selective and the glucose response is reproducible, we purified ACC1 using ACC1 pulldown method from INS1 cells treated with low and high glucose on different days; then we performed western blotting using these antibodies. The results, as shown in figure (6-3D), indicate that these antibodies bind to ACC1 as apparent from the single band detected at the known molecular weight for ACC1. Furthermore, it confirms the glucose response in ACC1S1215 and ACC149.

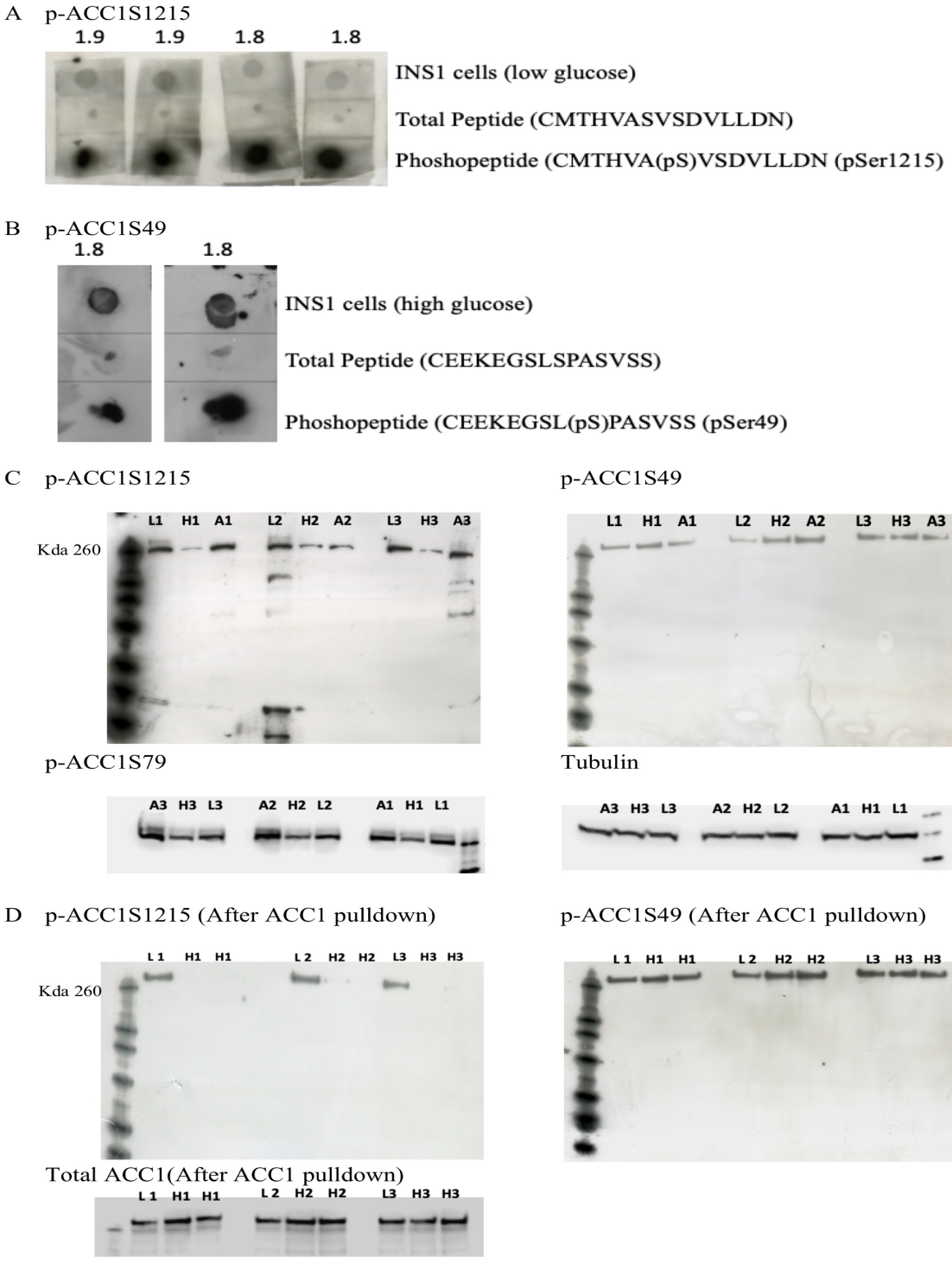


Figure 6-3 Validating ACC1S1215 and ACC1S49 antibodies and testing the glucose effect in INS-1 cells.(A) dot blot assay for ACC1S1215 (B) dot blot assay for ACC1S49 (C) western blot for cell treated with low (L) (2 mmol/l), high (H) (15 mmol/l) and 500 μM AICAR (A) for two hours.(D) western blot performed after ACC1 pulldown for cell treated with low (L) (2 mmol/l) and high glucose (H) (15 mmol/l). 4-12% gradient gel was used, primary antibodies were diluted 1:1000, rabbit HRP conjugated secondary antibody was used at 1:5000.

Chapter 6.3.3 Exploring the Dynamics of ACC1S1215 and ACC1S49 Phosphosites in Alpha Cell and the Liver.

Next, we aimed to investigate the phosphorylation states of these sites and their glucose response in other endocrine cells (alpha cells). Additionally, we aimed to examine ACC1 phosphorylation profile in the liver, which has a high level of ACC1 expression.

10-week old male mice were fasted for 16 hours then injected with normal-saline or glucose. The livers were then harvested 15, 30, 60, and 120 minutes post injection. After tissue homogenization, proteins were analysed by western blotting (fig 6-4A). 16 hours of fasting led to ACC1 phosphorylation in the liver while glucose injection led to ACC1 dephosphorylation at S79 and S1215. Differences in ACC1 phosphorylation were most prominent 15 minutes post normal-saline/glucose injection compared to other time points. Interestingly, only very faint bands were detected using ACC1S49.

The alpha cell line (aTC9)[137] was treated with low and high glucose condition for two hours. As can be seen in figure (6-4B) there was almost no change in ACC1S79 phosphorylation in response to glucose. On the other hand, ACC1S49 phosphorylation was upregulated in high glucose condition. The blot for ACC1S1215 was not conclusive in this experiment as there was only few bands detected in the second replicate.

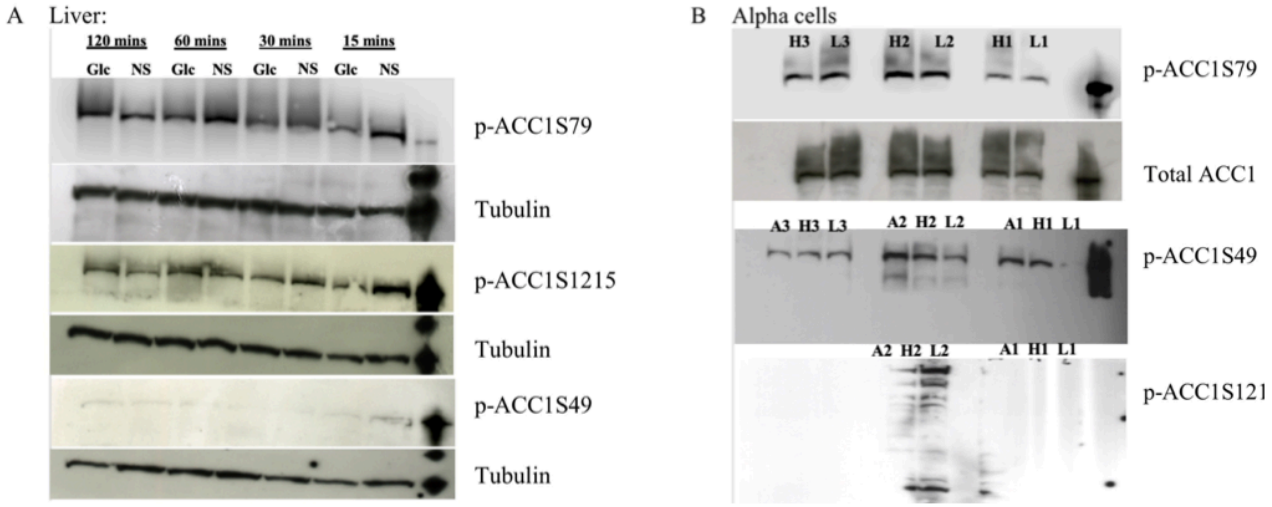


Figure 6-4 ACC1 phosphorylation profile in the liver and alpha cells. (A) Time line for ACC1S79, ACC1S1215 and ACC1S49 phosphorylation in the liver in response to glucose. 10-week old male mice were fasted for 16 hours then injected with normal saline (NS) or glucose (Glc). The livers were then harvested 15, 30, 60, and 120 minutes post injection. Tubulin was used as a loading control for each membrane. (B) ACC1 phosphorylation profile in alpha cell line. Alpha cell line was treated with 500 μM AICAR (A), low (L) (2 mmol/l) and high (H) (15 mmol/l) glucose condition for two hours. 4-12% gradient gel was used, primary antibodies were diluted 1:1000, rabbit HRP conjugated secondary antibody (Cell Signalling 8457) was used at 1:5000.

Chapter 6.3.4 Applying Bioinformatic Tools for Kinase Prediction and Test them Using ACC1S1215 and ACC1S49 Phosphospecific Antibodies

The next aim in this study was to identify the kinases responsible for phosphorylation of these sites (S25, S49 and S1215). To address this, we used several bioinformatic tools; Scansite[138] (https://scansite4.mit.edu/4.0), Netphos[139] (http://www.cbs.dtu.dk/services/NetPhos/) and Phospho.Elm[140](http://phospho.elm.eu.org) (table 5). We chose these tools out of dozens of tools available as they represent three distinctive strategies used in predicting the kinases responsible for phosphorylation of a specific site. Phospho.Elm prediction strategy depends on the presence of an exact consensus motif (amino acid sequence) surrounding the phosphorylation site; the phospho-site that has the consensus motif of a given kinase is predicted to be a substrate of that kinase[141,142]. However, the ideal peptide motifs alone might not be adequate to precisely predict the kinase[143]. On the other hand, Scansite uses sequence similarity-based clustering strategy; by comparing a set of features of the site to be predicted (e.g. evolutionary conservation and surface accessibility) to the features of known phosphorylation sites obtained from *in vitro* experiments, which allow more flexible definitions of consensus motifs[143,144]. Netphos is a machine-learning algorithm that is used to develop a sequence motif for each kinase based on its recognised *in vivo* substrates[145].

As shown in table 5, different kinases have been predicted for each site; this could be due to the different ways these prediction tools work, the partial overlapping specificity for some kinases[142] or the fact that some kinases are relatively flexible and do not require their substrates to have a highly strict recognition site [105].

Table 6-1 Bioinformatics tools for kinase prediction

Phospho-site	Kinase-prediction tool	Kinase	Score
ACC1S25	Netphos 3.1	CK2 cdc2	0.684 0.459
	Scansite 4.0	N/A	N/A
	Phospho.Elm	CaM-K2	N/A
ACC1S49	Netphos 3.1	GSK3 p38MAPK	0.497 0.486
	Scansite 4.0	Erk1	0.498
	Phospho.Elm	N/A	N/A
ACC1S79	Netphos 3.1	CaM-2 GSK3	0.460 0.437
	Scansite 4.0	AMPK	0.341
	Phospho.Elm	AMPK	-
ACC1215	Netphos 3.1	CaM-2 GSK3	0.469 0.443
	Scansite 4.0	N/A	N/A
	Phospho.Elm	AMPK	N/A
ACC1S29	Netphos 3.1	CK2	0.714
	Scansite 4.0	CK2	0.410
	Phospho.Elm	CK2	N/A

While *in silico* methods for kinase prediction provide useful and complementary information about kinase-substrate interaction, both false positive and true negative predictions are possible. Therefore, we used ACC1S1215 phospho-specific antibody to investigate *in vivo* which kinase is responsible for ACC1S1215 phosphorylation. Three kinases were predicted for ACC1S1215: Ca2+/calmodulin-dependent protein kinase (CaM-2) and Glycogen synthase kinase 3 (GSK3) (by Netphos 3.1) and AMPK (by Phospho.Elm). As a starting point, we sought to follow the Phospho.Elm result because it predicted ACC1S79 to be an AMPK site, which is in line with many previous *in vivo* studies, making this tool more reliable than Netphos 3.1.

As shown in figure (6-3C) in the previous section, treatment of INS1 cells with AICAR (500 μM, on top of high glucose (15 mmol/l) for two hours), when AMPK activity would normally be suppressed, led to increasing ACC1 phosphorylation at ACC1S79 confirming that this site is an

AMPK site. Similarly, AICAR increased ACC1 phosphorylation at S1215, suggesting that ACC1S1215 is an AMPK site.

Interestingly, while looking into other possible kinases that interact with other sites on ACC1, S29 was suggested to be phosphorylated by Casein Kinase 2 (CK2). It was the only site predicted to be phosphorylated by the same kinase using the three different kinase-prediction algorithms. Therefore, we sought to study this kinase and site further.

To test this *in vitro,* we performed western blot using phospho-CK2 substrates antibody for purified ACC1 from INS1 cells treated with low and high glucose for two hours (figure 6-5A). Two bands were detected at 260 kDa, one of them could be ACC1S29 band. Both bands did not show any changes in response to glucose, which is in line with the phosphoproteomics data as ACC1S29 did not show any response to glucose. In parallel, we examined the role of CK2 in beta cell function: cells were transfected with siRNA targeting CK2 transcript or siControl (siRNA sequence with no known gene homology), and following 48 hours in culture GSIS was measured. As shown in figure (6-5B), cells treated with CK2 siRNA showed an enhancement in insulin secretion at 15 mmol/l glucose compared to cells treated with siControl; indicating that CK2 may play a role in regulating GSIS.

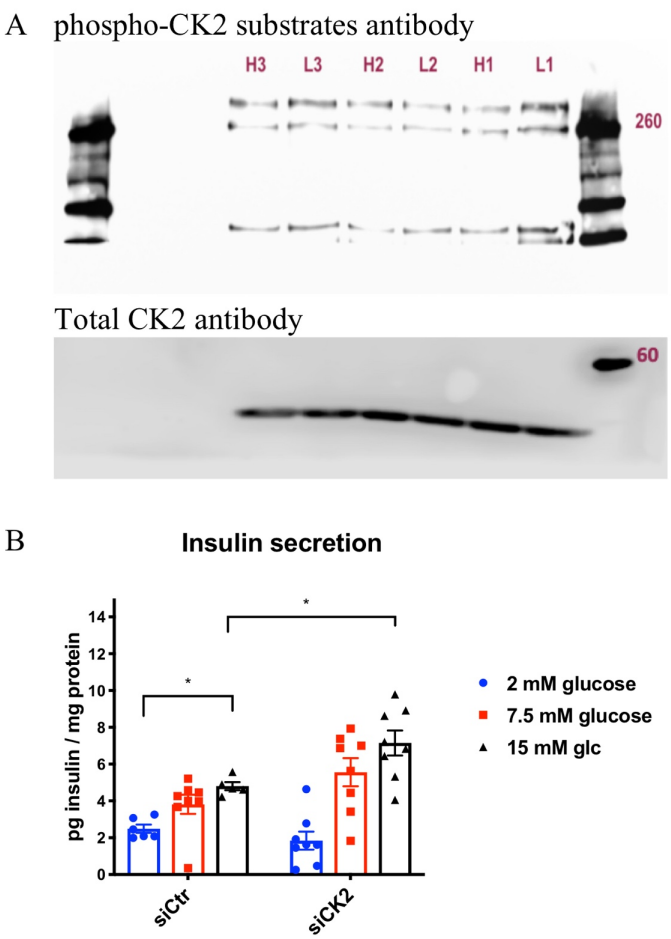


Figure 6-5 ACC1S29 in INS1 cell line. (A)Western blot using phospho-CK2 substrates antibody for purified ACC1 from INS1 cells treated with low (L) (2 mmol/l) and high glucose (H) (15 mmol/l) for two hours, total CK2 antibody was used as a loading control. 4-12% gradient gel was used, primary antibodies were diluted 1:1000, rabbit HRP conjugated secondary antibody was used at 1:5000. (B) The role of CK2 in GSIS: cells were transfected with siCK2 or siControl; GSIS was measured following 48 hours of transfection. Data are presented as mean ± SEM. *p<0.05, **p<0.01 and ***p<0.001 (two-way ANOVA with Bonferroni multiple comparisons test).

In summary, by using ACC1S1215 and ACC1S49 phospho-specific antibodies we were able to validate and confirm the glucose response in ACC1S1215 and ACC1S49. The next part of this project was concerned with the functional role of these site and the mechanism by which these sites affect ACC1 activity.

Chapter 6.3.5 CRISPR-Cas9-Mediated Knockout of ACC1 in INS1 Cell

CRISPR-Cas9 genome editing technology allows knockout (KO) of target genes and study of their biological function in cell lines. We used this technology to induce ACC1-targeted double-strand breaks at the genomic locus in INS1 cells. Figure (6-6A) demonstrates the ACC1 gene map and our targeting strategy. Briefly, we designed four guide RNAs (gRNA) targeting the ACC1 central domain (ACC1C), an essential domain for ACC1 activity. Two of these gRNA (gRNA1, gRNA2) were on the sense strand, while the other two (gRNA3, gRNA4) were on the antisense strand (figure 6-6B). We used non-homologous end-joining DNA repair (NHEJ) to introduce an indel, resulting in a shorter non-functional gene (figure 6-6C).

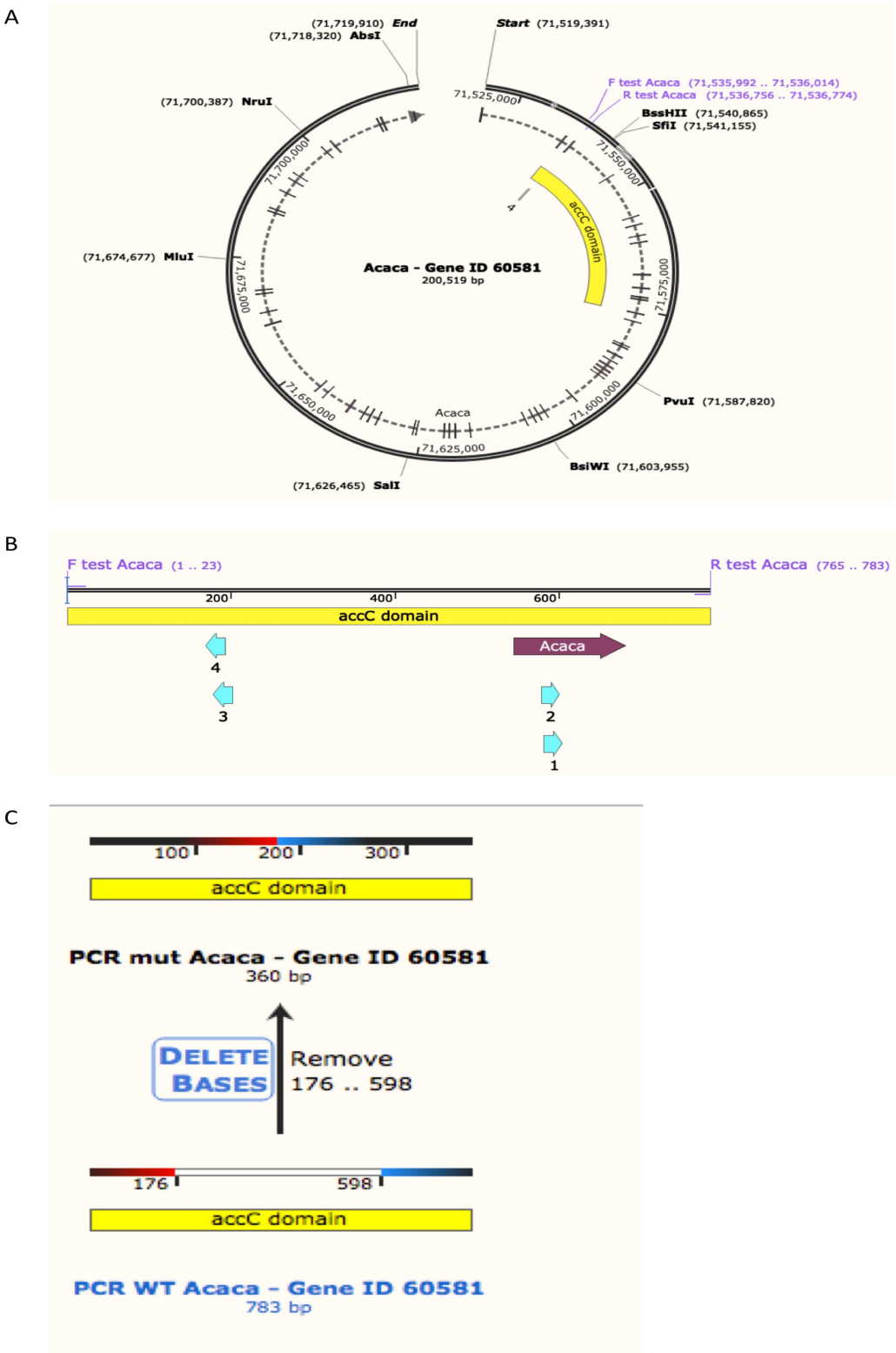


Figure 6-6 CRISPR/Cas9-mediated knock out of ACC1 in INS1 cells. (A) Schematic diagram of ACC1 gene. (B) Targeting ACC1C domain using 4 different gRNA. (C) ACC1 mutant gene is 423 bp shorter than ACC1 wild type gene. Diagrams are created using Snap gene viewer.

Figure (6-7A) illustrates our workflow to generate ACC1KO INS1 cell line. We transfected INS1 cells with Cas-9-gRNA complex using nucleofection; an electroporation-based transfection method that enables the DNA to enter directly to the nucleus[146]. This method of transfection was used due to the high transfection efficiency compared to other methods like plasmid transfection[146].

We tested four different combinations of gRNAs. After nucleofection, cells were left to recover for 48 hours, then genomic DNA was extracted, and the target region was PCR amplified. DNA gel showed that gRNA2-gRNA4 combination resulted in modification of the target site (ACC1) with indel, as apparent from the two bands on the gel (figure 6-7B). The higher band on the gel is the wildtype band (780 bp) while the shorter one is the mutant band (360 bp). To confirm the results further, we re-genotyped the cells transfected with gRNA2-gRNA4 (figure 6-7C) and sequenced the two bands to confirm the deletion.

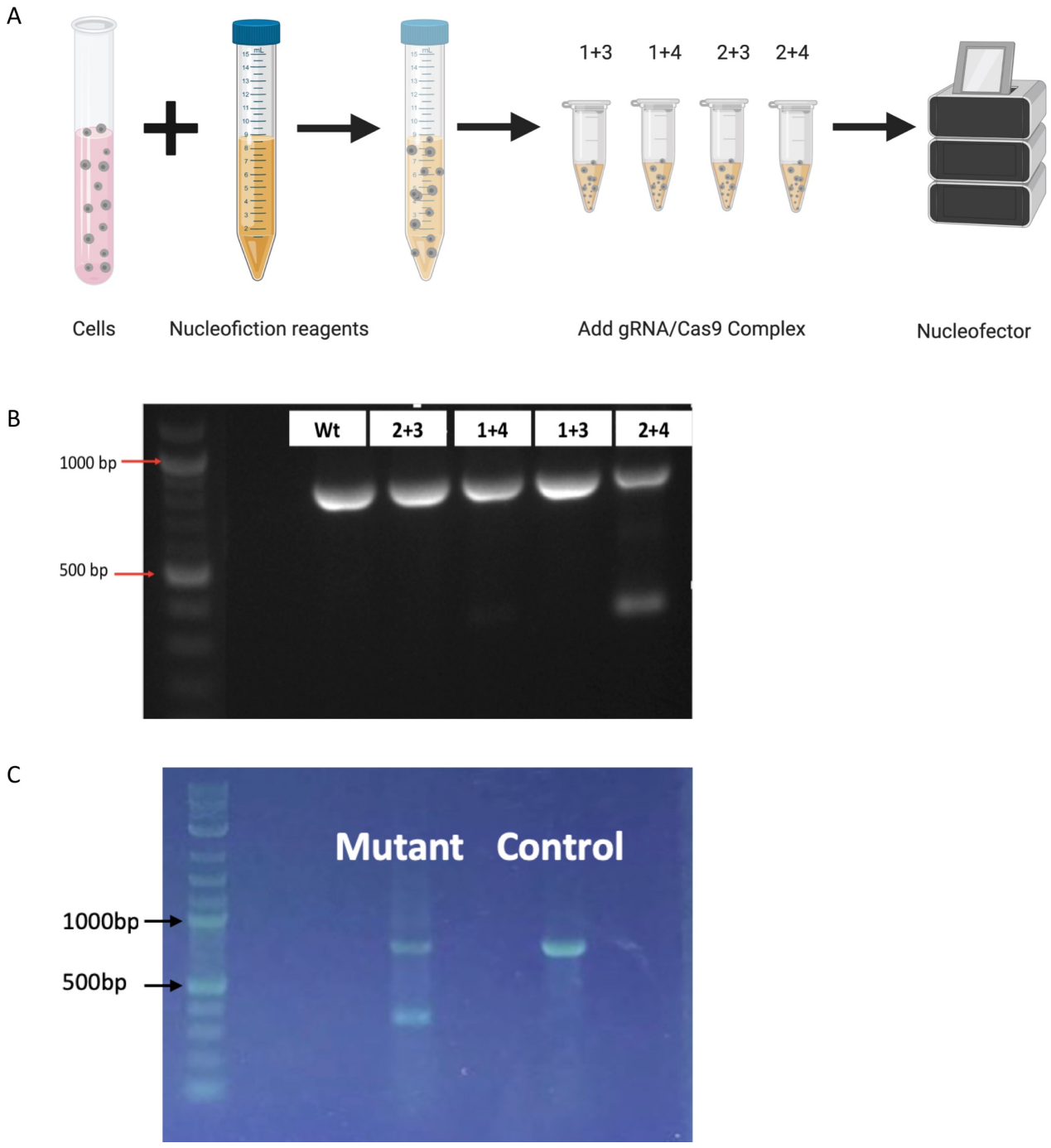


Figure 6-7 CRISPR/Cas9-mediated knock out of ACC1 in INS1 cells. (A) Workflow for generation of ACC1KO INS1 cell line. (B) PCR analysis of INS1 cells transfected with four different combinations of gRNA (1.5% gel stained with Midori green stain and visualised with UV light. (C) Re-genotyping cells transfected with gRNA (2+4) to confirm the result and to sequence the bands.

The cells transfected with (gRNA2-gRNA4) were heterogenous at this stage (i.e. contained a mixed population of ACC1KO cells and ACC1wt cells). Flow cytometry was used for single-cell sorting (figure 6-8A). Single cells were then expanded for three weeks to form colonies (genome-targeted monoclonal cell colonies). Figure (6-8B&C) show the colonies seven and fourteen days after sorting. Seventeen colonies were subsequently genotyped, as shown in (Figure 6-8D). Heterogeneity was evident in post sorted cell populations. Western blotting was attempted to demonstrate the absence of the protein or the degree of knockdown in these colonies (figure 6-8E). It showed that none of these colonies had a complete knock out of ACC1, however, colony 3, 6 and 8 had ACC1 knockdown with approximately more than 60% reduction in ACC1 expression compared to protein-matched wild type colonies (4 and 5).

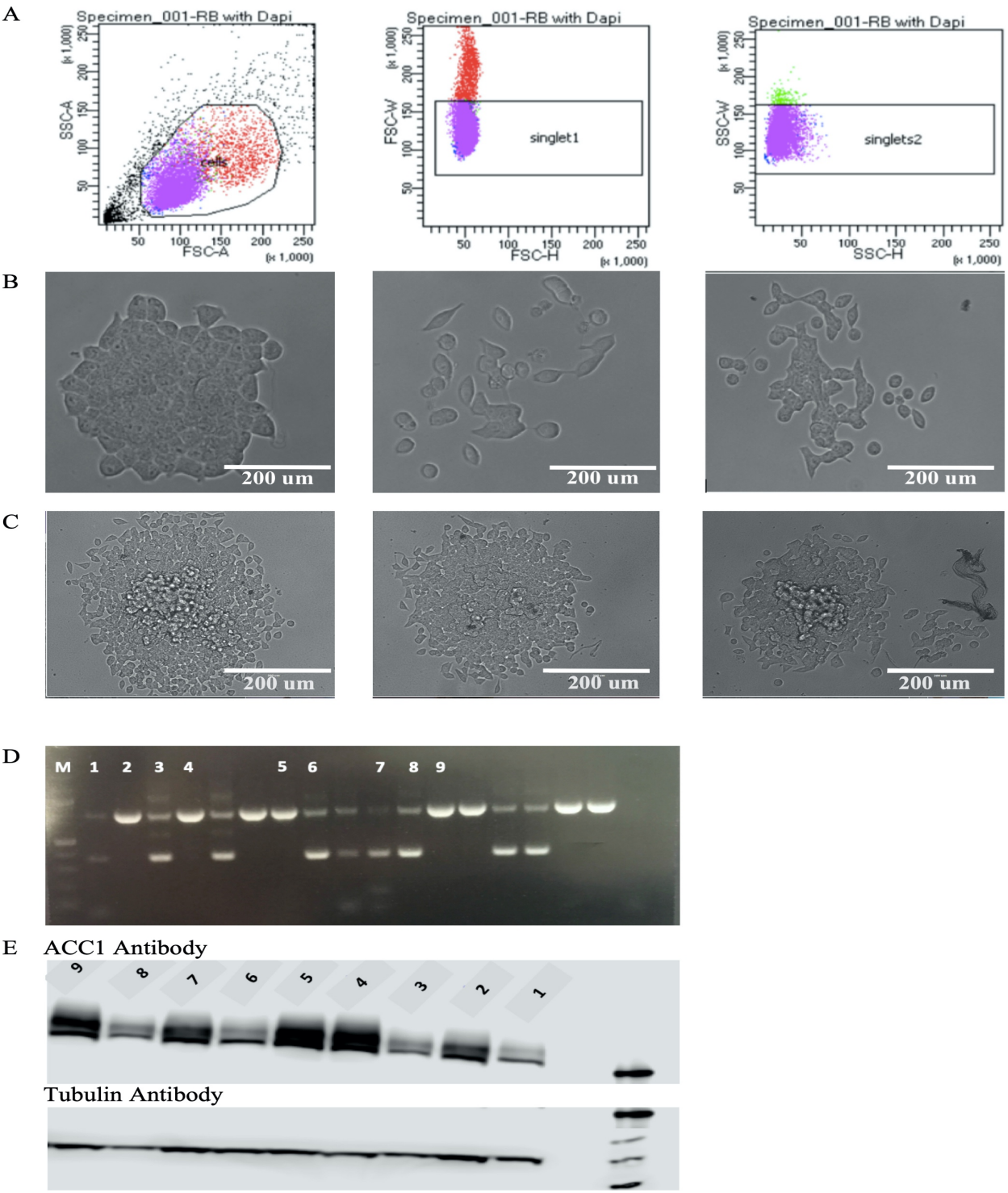


Figure 6-8 Single cells sorting to generate genome-targeted monoclonal cell colonies. (A) Single cells sorting using flow cytometry (B) Colonies seven days after sorting (C) Colonies fourteen days after transfection (D) PCR analysis of seventeen colonies for genotyping (E) Western blotting to assess ACC1 expression on the protein level. (B & C: phase contrast imaging using Evos 4300 microscope (AMF 4300). Scale bar: 200 μm.

Chapter 6.3.6 ACC1 Overexpression in INS1 Cell Line

INS1 cell line is relatively difficult to transfect compared to other cell lines such as HEK cells. So, we worked on optimising a transfection protocol in parallel to our work in generating ACC1KO INS1 cell line. We tested two commercially available transfection reagents for their utility in delivering ACC1 plasmid to INS1 cells to drive ACC1 overexpression: lipofectamine 2000 and lipofectamine 3000. This type of transfection, known as cationic lipid transfection depends on the formation of nucleic acid-cationic lipid reagent complexes via electrostatic interactions between the negatively charged nucleic acid and the positively charged head group of the synthetic lipid reagent. These complexes are believed to be taken up by the cell, then the transfected DNA is translocated to the nucleus to be expressed by a yet unknown mechanism[147].

We used a GFP plasmid as a control to monitor cellular toxicity of different transfection reagents, the transfection efficiency and to optimise different factors in the transfection process. Figure (6-9A&B) shows the cells expressing the GFP plasmid visualised by fluorescence microscopy 24 hours post-transfection using lipofectamine 2000 and lipofectamine 3000. In this experiment, DNA: lipid ratio (1:1 ratio) was determined empirically. As shown in the figure, cellular toxicity was lower in cells transfected with lipofectamine 3000 compared to cells transfected with lipofectamine 2000; however, transfection efficiency was less than 20% in both conditions. Western blotting was performed for cell lysates collected 48 hours and 72 hours after transfection to assess the transfection efficiency on the protein level (figure 6-9C). It showed no increase in ACC1 expression compared to control un-transfected cells and cells transfected with GFP plasmid.

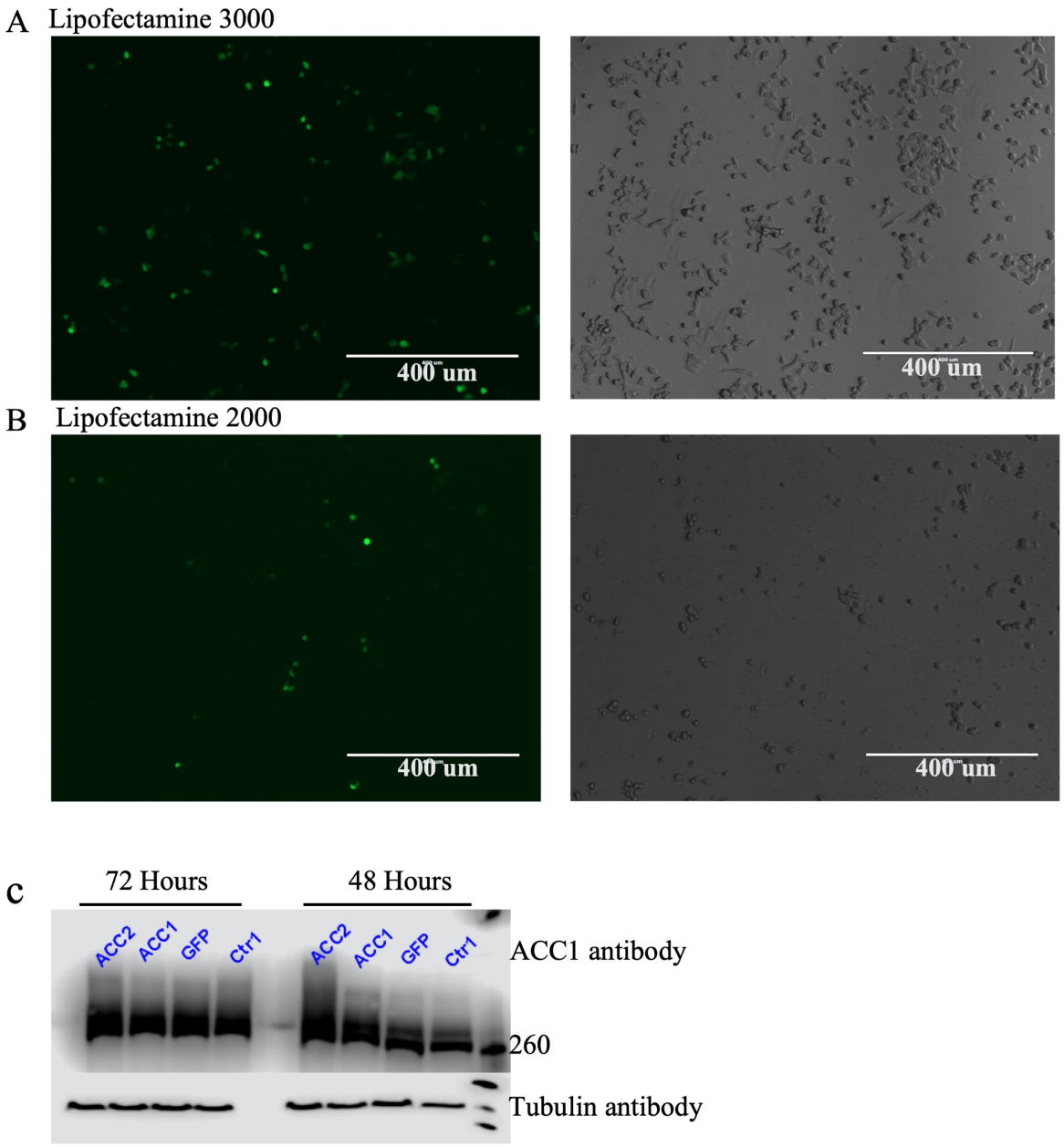


Figure 6-9 ACC1 overexpression using lipofectamine 2000 and lipofectamine 3000. (A) Cells expressing GFP plasmid transfected with lipofectamine 3000 visualised by fluorescence microscopy 24 hours after transfection (B) Cells expressing GFP plasmid transfected with lipofectamine 2000 visualised by fluorescence microscopy 24 hours after transfection (C) Western blot to assess transfection efficiency on the protein level for cells transfected with lipofectamine 3000. 4-12% gradient gel was used, primary antibodies were diluted 1:1000, rabbit HRP conjugated secondary antibody (Cell Signalling 8457) was used at 1:5000. (A & B visualised by Evos 4300 microscope (AMF 4300)). Scale bar: 400 μm.

To improve the transfection efficiency, we sought to optimise the transfection process. We transfected INS1 cells with a higher amount of DNA compared to the previous experiment (4 μg DNA/well) and with varying amounts of lipofectamine to explore the optimum ratio of lipofectamine to DNA. Taking into account the cellular toxicity caused by the transfection process, we cultured cells with media containing double the amount of serum (10%) for 48 hours before the transfection. As shown in figure (6-10A), the transfection efficiency for GFP plasmid has improved significantly for both lipofectamine reagents (lipofectamine 2000 & lipofectamine 3000), and with minimum cellular toxicity for cells transfected with DNA: lipid ratio of 1:3.

Unfortunately, but not unexpectedly given the size of the ACC1 gene, western blot for cells transfected with lipofectamine 2000 showed no increase in ACC1 expression at the protein level (figure 6-10B).

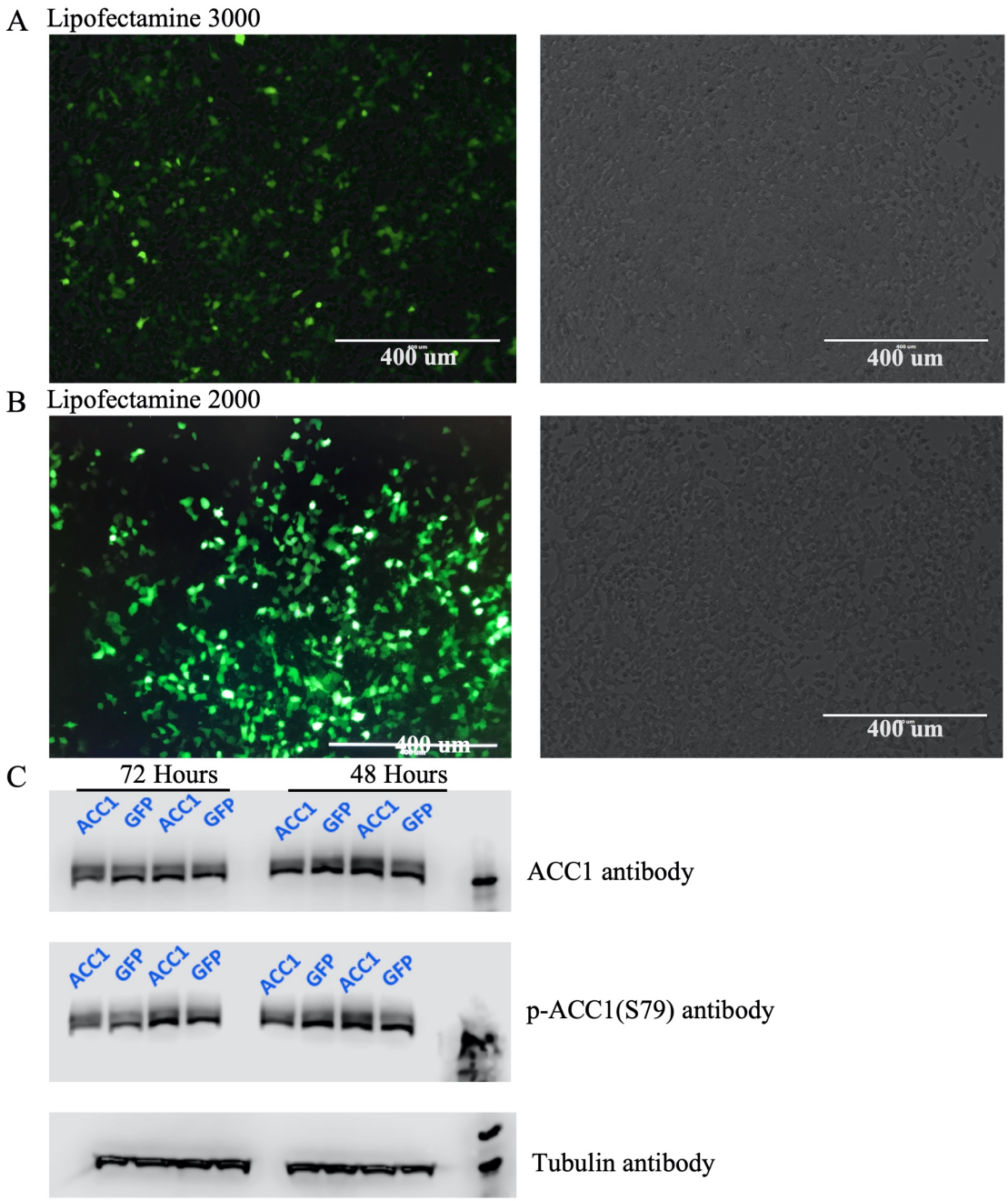


Figure 6-10 Optimising ACC1 overexpression protocol. (A) Cells expressing GFP plasmid transfected with lipofectamine 3000 using DNA: lipid ratio of 1:3 visualised by fluorescence microscopy 24 hours after transfection (B) Cells expressing GFP plasmid transfected with lipofectamine 2000 using DNA: lipid ratio of 1:3 visualised by fluorescence microscopy 24 hours after transfection (C) Western blot to assess transfection efficiency on the protein level for cells transfected with lipofectamine 2000. 4-12% gradient gel was used, primary antibodies were diluted 1:1000, rabbit HRP conjugated secondary antibody (Cell Signalling 8457) was used at 1:5000. (A & B visualised using Evos 4300 microscope (AMF 4300). Scale bar: 400 μm.

Chapter 6.4 Discussion

The present study was designed to validate the glucose response observed in ACC1S1215 and ACC1S49 in INS1 cells using phosphoproteomics (chapter 5). To this end, ACC1S1215 and ACC1S49 phospho-specific rabbit polyclonal antibodies were custom-made (DC Biosciences, Dundee), then western blotting was used to investigate these sites further and examine the phosphorylation profile of these sites in other tissues. While the use of monoclonal antibodies might be better than polyclonal antibodies in studying these phospho-sites due to their high specificity, since they recognise only a single epitope of a protein of interest, they can be challenging to produce and work with when studying modified peptides (e.g. phosphorylated peptides). In contrast, polyclonal antibodies are cheaper and enable greater binding than monoclonal antibodies against the same target as they bind to multiple epitopes of the modified peptide[148]. To improve the specificity of ACC1S1215 and ACC1S49 antibodies (i.e. to increase specificity to the phosphorylated peptide, and to minimise reactivity with the unphosphorylated peptide), immunogen affinity columns were used during the purification process.

Antibodies are a commonly used research tool to study proteins of interest, and can be used in a wide range of applications (e.g. immunohistochemistry, western blotting, and ELISA). Therefore, they can provide a wide range of critical information about a specific protein across different biological conditions. However, antibodies directed at phosphorylated sites on individual proteins could be non-specific; recognising both phosphorylated and non-phosphorylated forms of the target protein or identifying other proteins that contain the phosphorylated residue[134]. Furthermore, several reports have shown the lack of target specificity for some antibodies. For instance, a prior study evaluating 1124 new antibodies, using consistent protocols across five different labs, showed that only 452 antibodies recognised their intended target in HEK cell lysate[149]. Another study

tested 49 commercially available antibodies against 19 subtypes of G protein-coupled receptors (GPCR), found that none of them were selective and, interestingly, concluded that the lack of selectivity is the rule rather than the exception with GPCR antibodies [150]. These issues can potentially drain research time and money spent in an attempt to reproduce data or proceed with a project that is based on imprecise conclusions. Thus, it is imperative to thoroughly validate newly developed antibodies by establishing their specificity, selectivity and reproducibility across experiments. Notably, validating antibodies that recognise proteins with post-translational modifications, such as phosphorylation, is a far more complicated task[148]. Phosphorylation events in cells are of dynamic behaviour; a typical protein kinase target becomes phosphorylated with rapid kinetics of few minutes following kinase activation[151]; subsequently, de-phosphorylation by phosphatases terminates the phosphorylation events. Therefore, highly specific and sensitive antibodies are required to capture the full range of phosphorylation events in cells [152].

In this chapter, we aimed initially to systematically validate these new antibodies. First, we showed that these antibodies are specific (i.e. recognise only the phosphorylated form of the peptide) using dot blot assay. Second, we confirmed that they are ACC1-selective, as a single band was observed at the correct molecular weight for ACC1 in western blots performed for the purified ACC1 (using ACC1 pulldown). In parallel, we compared the blots for these antibodies to the previously validated and commercially available antibody ACC1S79: the detected ACC1 band corresponding to the bands detected by ACC1S1215 and ACC1S49 antibodies in term of the size, confirming further that this band is ACC1 band. One limitation that should be addressed here is the lack of a negative control (i.e. ACC1KO cells, tissues or islets), which is required to confirm specificity for ACC1. Unfortunately, such a control was not available. However, it could have been replaced by cell lines where ACC1 protein has been knocked down using the RNAi technique.

Third, we demonstrated that data obtained using these antibodies are reproducible across experiments and over time. Western blots performed in two independent experiments for INS1 cells treated with low glucose (2 mmol/l) and high glucose (15 mmol/l) with three biological replicates for each condition in each experiment; showed that ACC1S1215 phosphorylation was strikingly upregulated at low glucose conditions while ACC1S49 phosphorylation was marginally upregulated at high glucose. These results are in line with our MS-based phosphoproteomics data, moreover, a strength of our data is that it is supported by two different technical approaches (mass spec and western blotting). Thus, these data provide strong and robust basis for future research to study these sites further.

Next, we sought to examine the phosphorylation profile of these sites in other endocrine cells (alpha cells) and other tissues that have a high level of ACC1 expression (liver). In alpha cells, we did not observe a significant change in ACC1S79 phosphorylation in response to glucose, while western blot result for ACC1S1215 was not conclusive. Conversely, ACC1S49 phosphorylation was upregulated in high glucose condition. In the liver, ACC1S1215 and ACC1S79 phosphorylation were reduced upon 15 minutes of glucose injection, while ACC1S49 phosphorylation was barely detected. The findings of this study suggest that ACC1S49 might be specific to endocrine cells. However, these results need to be interpreted with caution as this experiment was a pilot study and was performed with one biological replicate for each time point. These tissues (i.e. liver, endocrine tissues) and other mammalian tissues exhibit unique physiology despite sharing similar genome and transcription profile[135]. PTMs (phosphorylation in particular) provide an additional layer of functional control of the gene products in a cell [153]. Phosphorylation can influence protein localisation, activity, and interaction with other proteins, controlling biochemical characteristics of a given tissue [135,153]. Moreover, kinases and phosphatases, that

tightly regulate phosphorylation status of proteins are themselves regulated by phosphorylation and have different expression levels across tissues, forming complex regulatory pathways that are tuned to fit specific tissue's physiology [46,154]. Thus, comparing ACC1 phosphorylation sites among tissues could be a critical first step in delineating the unique mechanisms by which ACC1 is regulated in each tissue, thus enabling us to understand the basic biology of ACC1 signalling pathways and presenting a useful resource for future exploration of drug targets for dysfunctional signalling pathways.

In order to decode ACC1 signalling pathways and phosphorylation networks, it is also essential to identify the kinases responsible for specific phosphorylation sites. Predictive bioinformatics tools that create in silico predictions of kinase-substrate relationships have been used for kinase annotation. These tools are inexpensive and fast compared to experimental methods and can be used to generate a focused list of predictions that can then be examined by further experimental testing[155]. Using three different tools, Scansite, Netphos and Phospho.Elm that have distinctive strategies of prediction, we found that ACC1S1215 is predicted to be phosphorylated by AMPK in INS1 cells; we confirmed this finding by western blot using AICAR (AMPK activator). AMPK inhibitor like compound C and other AMPK activators like PFZ compound could be used to confirm this further. ACCS25 and ACC1S49 were predicted to be phosphorylated by multiple kinases, but due to the time limit, we were unable to confirm this experimentally.

Interestingly, ACC1S29 (which did not show any glucose response in phosphoproteomics data) was consistently predicted to be phosphorylated by CK2 using these three tools. We examined its role in GSIS and found that it enhanced insulin secretion at high glucose level, This is in line with previous studies that reported a crucial role for CK2 in regulating ACC-induced insulin secretion

via regulating the transcription factor SP1, a critical regulator of ACC1. However, these studies did not establish a direct interaction between CK2 and ACC1[156,157].

While there is growing evidence that reversible protein phosphorylation in beta cells is implicated in the control of insulin secretion and affecting a large number of biological processes linked to insulin biosynthesis[158], the role of the kinases responsible for these events in beta cells function is not well established[159]. For example, CK2 plays a critical role in many physiological processes such as differentiation and cell cycle regulation[157]. Moreover, CK2 activity is elevated in most cancer cells and has a well-established role in tumorgenesis[157]. In β-cells, it has been reported that down regulation of CK2 activity leads to an elevated level of insulin[160]. On the other hand, another study showed that increased activity of the CK2 kinase is correlated with an enhanced insulin secretion[161]. These studies, however, have failed to address the mechanism by which CK2 affects insulin secretion. Therefore, there is a pressing need for comprehensive and systematic identification of the molecular mechanisms by which these kinases affect beta cells function, not only for a deep understanding of this process but also for the characterization of existing and development of new effective therapeutics targeting diabetes.

The final aim of this chapter was to investigate whether the identified phosphorylation sites are genuinely functional. To this end, we attempted to generate an ACC1KO-INS1cell line using CRISPR technology. The strategy we followed was successful in inducing the mutation at the ACC1 locus. However, the biggest challenge was to isolate the cells that have this mutation from wild type cells. The method we used was single-cell sorting using FACS: it depends on dispensing one cell at a time from a heterogeneous mixture of biological cells. There are some limitations with this strategy: firstly, INS1 cells are healthy when they are in close proximity and contact with each other; culturing from a single-cell might not be compatible with their survival or

differentiation. Secondly, there is a high risk of contamination from wild type cells either during the sorting process or during the clonal expansion stage. We were able to overcome the first challenge by growing the cells in a double amount of the serum used in standard settings. Interestingly, However, we were unable to overcome the second challenge and all the clones in our experiment were heterogeneous. It worth mentioning that there is a possibility that the cloning was successful but the cloned cells contained some unmodified alleles (Heterozygous clone). To explore this, we could have done a second round of sorting for the mixed clones to confirm if the subsequent clones were heterogenous or heterozygous.

Even though we were unable to generate complete ACC1KO-INS1 cells in this project, we established the sites and sequences of gRNA that were successful in inducing the mutation at the ACC1 locus with high transfection and knockout efficiency. Thus, these could be used in future studies generate ACC1KO cells perhaps using other cell lines more suited to cloning. Taking into account the challenge we faced in sorting cells, a different method that allows selection of cells expressing the mutation could be used. A recent study has established an efficient protocol to CRISPR/Cas9 gene knockout using transfection of stem cells with fluorescently labelled CRISPR/Cas9–gRNA RNP complexes, thus the gene-edited cells would be fluorescent, making it easier to isolate mutant cells by flow cytometry (fig 6-11) [162].

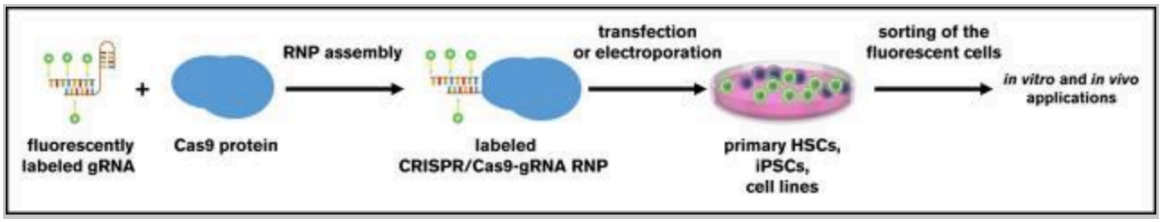


Figure 6-11CRISPR/Cas9–gRNA RNP labelling and cell transfection. Adopted from Nasri et.al 2019

Chapter 7 General Discussion and Summary

Acetyl CoA Carboxylase 1 (ACC1) is an enzyme that couples glucose metabolism with de novo lipid synthesis in lipogenic tissues, by converting acetyl-CoA to malonyl-CoA. In beta cells, ACC1 plays a critical role in beta cell growth and insulin secretion[1]. However, very little is known about how ACC1 activity is regulated in beta cells.

Post-translational modification of proteins introduces changes in mass and charge to proteins; altering their structure and confirmation, thus affecting their activity, binding properties, stability, and /or subcellular localization[134]. While hundreds of protein modifications are known, protein phosphorylation is one of the most prevalent types of post-translational modifications[163].

In order to comprehensively investigate the functional role of ACC1 phosphorylation, it is critical to identify all possible phosphorylation sites on ACC1 and to determine how these sites are regulated under different conditions.

Chapter 7.1 Achievement of Objectives and Aims

The aims of the current project were to assess the role of the AMP-activated protein kinase phospho-site serine 79 (ACC1S79) in beta-cell function and whole-body glucose homeostasis and to screen for novel phospho-sites that may regulate ACC1 activity in beta cells.

We have shown using in vivo studies, that ACC1S79, the well-known phosphosite, does not play a critical role in insulin secretion nor action in vivo. We also have shown that ACC1S79 does not play a role in islets function ex-vivo as a glucose-regulated site but maybe an important site for AMPK action under pharmacological conditions.

Moreover, we have developed a phosphoproteomic workflow to study ACC1 and we have identified twenty phospho-sites on the ACC1 protein in beta cells. ACC1S1215 was highly phosphorylated at 2 mmol/l glucose and showed a marked and highly significant reduction in

phosphorylation in response to 15 mmol/l glucose, contrary to the more modest changes in phosphorylation of ACC1S79. In contrast, phosphorylation of ACC1S25 and ACC1S49 was lower at basal glucose and increased upon glucose stimulation. Validation by Western blotting confirmed that ACC1S1215 phosphorylation was highly-regulated by glucose, with ACC1S79 phosphorylation more subtle.

Chapter 7.2 The Role of ACC1S79 in Beta Cell Function

This study has been informative in terms of clarifying the role of ACC1S79 in beta-cell function and whole-body glucose homeostasis. It has shown that global ACCS79A knock-in (ACC1SKI mice) results in almost a normal phenotype characterised by normal glucose-stimulated insulin release in vivo, normal serum insulin levels, normal body mass and normal peripheral insulin sensitivity. Interestingly, ACC1SKI male mice had lower fasting blood glucose compared to wildtype littermate control; that may be due to a difference in counterregulatory hormones (i.e. glucagon).

To test the function of ACC1SKI beta cells, we performed GSIS on isolated islets. Consistent with the in vivo data, the in vitro insulin secretion from isolated ACC1SKI islets in response to glucose was unaltered compared to control islet GSIS.

According to these data, we can infer that ACC1S79 does not play a critical role in beta cells function.

Chapter 7.3 Phosphoproteomics Analysis of ACC1

We have developed in this thesis a phosphoproteomics workflow to study ACC1 regulation in pancreatic beta cells. To the best of our knowledge, this is the first study providing an in-depth, targeted and unsupervised assessment of ACC1 PTMs. The most striking results to emerge from our data is that ACC1S1215 shows dramatic upregulation in low glucose conditions compared to ACC1S79. In addition, ACC1S25 and ACC1S49 are upregulated in response to high glucose conditions.

The striking glucose response observed in ACC1S1215 suggests that this site plays a crucial rule in controlling ACC1 activity in beta cells. This is contrary to some studies in the literature (Hardie et al) and in line with others (Wei, J. et al). The roles of ACC1S25 and ACC1S49 in controlling ACC1 activity is not known and have not been reported before in the literature. Therefore, more studies are needed to investigate the functional relevance of these sites and their role in beta cells function.

Moreover, we developed antibodies against these sites to validate the glucose response observed in these sites and to characterise these sites further. We also applied in silico methods to predict the kinases responsible for these sites. Our data shows that ACC1S1215 is phosphorylated by AMPK, which was confirmed using ACC1S1215 antibodies. While the predictions for other sites were inconclusive.

The vital regulatory role of ACC in fatty acid synthesis and oxidation pathways and the complex roles that fatty acids play as cellular components made it an attractive target for drug development against various metabolic diseases (i.e. obesity, insulin resistance, and T2D). Based on distinctive tissue distributions and cellular localisation of ACC1 and ACC2, it was hypothesised that combined ACC1 and ACC2 inhibition would result in a reduction of DNL in lipogenic tissues

while at the same time enhancing fatty acid oxidation in oxidative tissues [70]. Several *in vivo* studies strongly supported this hypothesis and showed that ACC inhibition could be beneficial and have therapeutic potential for the treatment of metabolic diseases[71]. The phosphosites identified in this project could be viable targets for ACC1 inhibition.

We also identified two novel phosphosites for PC. We observed that none of these sites showed a significant glucose response in response to 30 minutes of glucose stimulation.

Chapter 7.4 Future Perspectives

The studies of ACC1 phosphoproteomics presented in this thesis have clarified and challenged some aspects of the ACC1 literature, as well as raising new insights into ACC1 regulation in pancreatic beta cells. Given my results and the striking glucose response in ACC1S1215 and ACC1S25; further work is needed to understand how these sites control ACC1 activity and the role of these site in beta cell function and whole-body glucose homeostasis.

There are many more potential lines of investigation that have been suggested throughout this thesis. To summarise: Firstly, these sites could be investigated further using the validated antibodies described in this thesis. Investigating the glucose response of these sites in human islets, investigating the dynamics of these sites in response to hormones and nutrients, and investigating the kinases responsible for the phosphorylation events at these sites, using activators and inhibitors, would be informative. Secondly, a mouse model with knock-in mutation, to alanine (phospho-null) or aspartate (phosphomimic), for these sites could be developed. These mouse models would be informative in exploring the role of these sites not only in pancreatic beta cells function but also in other tissues like liver, muscles and adipose tissues. Thirdly, the developed phosphoproteomics workflow in this thesis could be applied to study different types of post-translational modifications

(including phosphorylation, glycosylation and hydroxylation) affecting the liver ACC1 in response to glucose.

In conclusion, our data provide a rationale for future hypothesis-driven research to filling the gap in the knowledge about the functional relevance of these sites. Thereby, contributing to our understanding of ACC1 regulation in beta cells and other tissues and to expand our understanding of how ACC1 is integrated into signalling pathways and networks. Studies of this kind will thereby contribute to our understanding of beta cells function and provide a broader view of biological systems.

References:

1 Cantley, J. *et al.* Disruption of beta cell acetyl-CoA carboxylase-1 in mice impairs insulin secretion and beta cell mass. *Diabetologia* **62**, 99-111, doi:10.1007/s00125-018-4743-7 (2019).

2 Fullerton, M. D. *et al.* Single phosphorylation sites in Acc1 and Acc2 regulate lipid homeostasis and the insulin-sensitizing effects of metformin. *Nature medicine* **19**, 1649-1654, doi:10.1038/nm.3372 (2013).

3 Perlmuter, L. C., Flanagan, B. P., Shah, P. H. & Singh, S. P. Glycemic control and hypoglycemia: is the loser the winner? *Diabetes Care* **31**, 2072-2076, doi:10.2337/dc08-1441 (2008).

4 Röder, P. V., Wu, B., Liu, Y. & Han, W. Pancreatic regulation of glucose homeostasis. *Exp Mol Med* **48**, e219-e219, doi:10.1038/emm.2016.6 (2016).

5 Goke, B. Islet cell function: alpha and beta cells--partners towards normoglycaemia. *International journal of clinical practice. Supplement*, 2-7, doi:10.1111/j.1742-1241.2007.01686.x (2008).

6 Aronoff, S. L., Berkowitz, K., Shreiner, B. & Want, L. Glucose Metabolism and Regulation: Beyond Insulin and Glucagon. *Diabetes Spectrum* **17**, 183, doi:10.2337/diaspect.17.3.183 (2004).

7 Youngren, J. F. Regulation of insulin receptor function. *Cellular and Molecular Life Sciences* **64**, 873, doi:10.1007/s00018-007-6359-9 (2007).

8 Dimitriadis, G., Mitrou, P., Lambadiari, V., Maratou, E. & Raptis, S. A. Insulin effects in muscle and adipose tissue. *Diabetes research and clinical practice* **93 Suppl 1**, S52-59, doi:10.1016/s0168-8227(11)70014-6 (2011).

9 Girard, J. Insulin's effect on the liver: "direct or indirect?" continues to be the question. *The Journal of clinical investigation* **116**, 302-304, doi:10.1172/JCI27743 (2006).

10 Edgerton, D. S. *et al.* Effects of insulin on the metabolic control of hepatic gluconeogenesis in vivo. *Diabetes* **58**, 2766-2775, doi:10.2337/db09-0328 (2009).

11 Pessin, J. E. & Saltiel, A. R. Signaling pathways in insulin action: molecular targets of insulin resistance. *The Journal of clinical investigation* **106**, 165-169, doi:10.1172/JCI10582 (2000).

12 Ramnanan, C. J., Edgerton, D. S., Kraft, G. & Cherrington, A. D. Physiologic action of glucagon on liver glucose metabolism. *Diabetes Obes Metab* **13 Suppl 1**, 118-125, doi:10.1111/j.1463-1326.2011.01454.x (2011).

13 Wilcox, G. Insulin and insulin resistance. *Clin Biochem Rev* **26**, 19-39 (2005).

14 American Diabetes, A. Diagnosis and classification of diabetes mellitus. *Diabetes Care* **32 Suppl 1**, S62-S67, doi:10.2337/dc09-S062 (2009).

15 Skyler, J. S. Diabetes Mellitus: Pathogenesis and Treatment Strategies. *Journal of Medicinal Chemistry* **47**, 4113-4117, doi:10.1021/jm0306273 (2004).

16 Papatheodorou, K., Banach, M., Bekiari, E., Rizzo, M. & Edmonds, M. Complications of Diabetes 2017. *J Diabetes Res* **2018**, 3086167, doi:10.1155/2018/3086167 (2018).

17 WH, O. Global report on diabtes: World Health Orgaization. (2016).

18 Ali, O. Genetics of type 2 diabetes. *World J Diabetes* **4**, 114-123, doi:10.4239/wjd.v4.i4.114 (2013).

19 Jura, M. & Kozak, L. P. Obesity and related consequences to ageing. *Age (Dordr)* **38**, 23-23, doi:10.1007/s11357-016-9884-3 (2016).

20 Abel, E. D., O'Shea, K. M. & Ramasamy, R. Insulin resistance: metabolic mechanisms and consequences in the heart. *Arterioscler Thromb Vasc Biol* **32**, 2068-2076, doi:10.1161/ATVBAHA.111.241984 (2012).
21 Kahn, S. E., Hull, R. L. & Utzschneider, K. M. Mechanisms linking obesity to insulin resistance and type 2 diabetes. *Nature* **444**, 840-846, doi:10.1038/nature05482 (2006).
22 Ahlqvist, E. *et al.* Novel subgroups of adult-onset diabetes and their association with outcomes: a data-driven cluster analysis of six variables. *The lancet. Diabetes & endocrinology* **6**, 361-369, doi:10.1016/s2213-8587(18)30051-2 (2018).
23 Cantley, J. & Ashcroft, F. M. Q&A: insulin secretion and type 2 diabetes: why do beta-cells fail? *BMC biology* **13**, 33, doi:10.1186/s12915-015-0140-6 (2015).
24 Nolan, C. J., Damm, P. & Prentki, M. Type 2 diabetes across generations: from pathophysiology to prevention and management. *The Lancet* **378**, 169-181, doi:https://doi.org/10.1016/S0140-6736(11)60614-4 (2011).
25 Marín-Peñalver, J. J., Martín-Timón, I., Sevillano-Collantes, C. & Del Cañizo-Gómez, F. J. Update on the treatment of type 2 diabetes mellitus. *World J Diabetes* **7**, 354-395, doi:10.4239/wjd.v7.i17.354 (2016).
26 Olokoba, A. B., Obateru, O. A. & Olokoba, L. B. Type 2 diabetes mellitus: a review of current trends. *Oman Med J* **27**, 269-273, doi:10.5001/omj.2012.68 (2012).
27 Atkinson, M. A., Eisenbarth, G. S. & Michels, A. W. Type 1 diabetes. *Lancet* **383**, 69-82, doi:10.1016/S0140-6736(13)60591-7 (2014).
28 Matschinsky, F. *et al.* Glucokinase as pancreatic beta cell glucose sensor and diabetes gene. *The Journal of clinical investigation* **92**, 2092-2098, doi:10.1172/JCI116809 (1993).
29 Matschinsky, F. M. Glucokinase, glucose homeostasis, and diabetes mellitus. *Current diabetes reports* **5**, 171-176, doi:10.1007/s11892-005-0005-4 (2005).
30 Iynedjian, P. B. Mammalian glucokinase and its gene. *The Biochemical journal* **293 (Pt 1)**, 1-13, doi:10.1042/bj2930001 (1993).
31 Thorens, B. GLUT2, glucose sensing and glucose homeostasis. *Diabetologia* **58**, 221-232, doi:10.1007/s00125-014-3451-1 (2015).
32 Matschinsky, F. M. Regulation of Pancreatic β-Cell Glucokinase. *Diabetes* **51**, S394, doi:10.2337/diabetes.51.2007.S394 (2002).
33 Sugden, M. C. & Holness, M. J. The pyruvate carboxylase-pyruvate dehydrogenase axis in islet pyruvate metabolism: Going round in circles? *Islets* **3**, 302-319, doi:10.4161/isl.3.6.17806 (2011).
34 Ashcroft, F. M. K(ATP) channels and insulin secretion: a key role in health and disease. *Biochemical Society transactions* **34**, 243-246, doi:10.1042/bst20060243 (2006).
35 Newgard, C. B. & McGarry, J. D. Metabolic coupling factors in pancreatic beta-cell signal transduction. *Annual review of biochemistry* **64**, 689-719, doi:10.1146/annurev.bi.64.070195.003353 (1995).
36 Henquin, J. C. Triggering and amplifying pathways of regulation of insulin secretion by glucose. *Diabetes* **49**, 1751-1760, doi:10.2337/diabetes.49.11.1751 (2000).
37 Jitrapakdee, S. *et al.* Structure, mechanism and regulation of pyruvate carboxylase. *The Biochemical journal* **413**, 369-387, doi:10.1042/BJ20080709 (2008).
38 Prentki, M. New insights into pancreatic beta-cell metabolic signaling in insulin secretion. *European journal of endocrinology* **134**, 272-286, doi:10.1530/eje.0.1340272 (1996).

39 McGarry, J. D. & Foster, D. W. Regulation of hepatic fatty acid oxidation and ketone body production. *Annual review of biochemistry* **49**, 395-420, doi:10.1146/annurev.bi.49.070180.002143 (1980).
40 Brun, T. *et al.* Evidence for an Anaplerotic/Malonyl-CoA Pathway in Pancreatic β-Cell Nutrient Signaling. *Diabetes* **45**, 190, doi:10.2337/diab.45.2.190 (1996).
41 Prentki, M., Corkey, B. E. & Madiraju, S. R. M. Lipid-associated metabolic signalling networks in pancreatic beta cell function. *Diabetologia*, doi:10.1007/s00125-019-04976-w (2019).
42 Khan, A., Ling, Z. C. & Landau, B. R. Quantifying the carboxylation of pyruvate in pancreatic islets. *The Journal of biological chemistry* **271**, 2539-2542, doi:10.1074/jbc.271.5.2539 (1996).
43 Han, J. & Liu, Y. Q. Reduction of islet pyruvate carboxylase activity might be related to the development of type 2 diabetes mellitus in Agouti-K mice. *J Endocrinol* **204**, 143-152, doi:10.1677/JOE-09-0391 (2010).
44 MacDonald, M. J., Dobrzyn, A., Ntambi, J. & Stoker, S. W. The role of rapid lipogenesis in insulin secretion: Insulin secretagogues acutely alter lipid composition of INS-1 832/13 cells. *Archives of biochemistry and biophysics* **470**, 153-162, doi:10.1016/j.abb.2007.11.017 (2008).
45 Brun, T. *et al.* Evidence for an anaplerotic/malonyl-CoA pathway in pancreatic beta-cell nutrient signaling. *Diabetes* **45**, 190-198, doi:10.2337/diab.45.2.190 (1996).
46 Roche, E. *et al.* Long-term exposure of beta-INS cells to high glucose concentrations increases anaplerosis, lipogenesis, and lipogenic gene expression. *Diabetes* **47**, 1086-1094, doi:10.2337/diabetes.47.7.1086 (1998).
47 Zhang, S. & Kim, K. H. Essential role of acetyl-CoA carboxylase in the glucose-induced insulin secretion in a pancreatic beta-cell line. *Cellular signalling* **10**, 35-42, doi:10.1016/s0898-6568(97)00070-3 (1998).
48 Guay, C., Madiraju, S. R., Aumais, A., Joly, E. & Prentki, M. A role for ATP-citrate lyase, malic enzyme, and pyruvate/citrate cycling in glucose-induced insulin secretion. *The Journal of biological chemistry* **282**, 35657-35665, doi:10.1074/jbc.M707294200 (2007).
49 MacDonald, M. J. *et al.* Decreased levels of metabolic enzymes in pancreatic islets of patients with type 2 diabetes. *Diabetologia* **52**, 1087-1091, doi:10.1007/s00125-009-1319-6 (2009).
50 Chen, S. *et al.* More direct evidence for a malonyl-CoA-carnitine palmitoyltransferase I interaction as a key event in pancreatic beta-cell signaling. *Diabetes* **43**, 878-883, doi:10.2337/diab.43.7.878 (1994).
51 Wakil, S. J. <A MALONIC ACID DERIVATIVE AS AN INTERMEDIATE IN FATTY ACID SYNTHESIS.pdf>. *Proceedings of the National Academy of Sciences of the United States of America* (1958).
52 Wakil, S. J. & Waite, M. On the mechanism of action of enzyme-bound biotin. *Biochemical and biophysical research communications* **9**, 18-24, doi:10.1016/0006-291x(62)90080-3 (1962).
53 Brownsey, R. W., Boone, A. N., Elliott, J. E., Kulpa, J. E. & Lee, W. M. Regulation of acetyl-CoA carboxylase. *Biochemical Society transactions* **34**, 223-227, doi:10.1042/bst20060223 (2006).
54 Wakil, S. J. & Abu-Elheiga, L. A. Fatty acid metabolism: target for metabolic syndrome. *Journal of lipid research* **50 Suppl**, S138-S143, doi:10.1194/jlr.R800079-JLR200 (2009).

55 Hunkeler, M. *et al.* Structural basis for regulation of human acetyl-CoA carboxylase. *Nature* **558**, 470-474, doi:10.1038/s41586-018-0201-4 (2018).
56 Lee, C. K. *et al.* Biotinoyl domain of human acetyl-CoA carboxylase: Structural insights into the carboxyl transfer mechanism. *Proteins* **72**, 613-624, doi:10.1002/prot.21952 (2008).
57 Abu-Elheiga, L., Jayakumar, A., Baldini, A., Chirala, S. S. & Wakil, S. J. Human acetyl-CoA carboxylase: characterization, molecular cloning, and evidence for two isoforms. *Proceedings of the National Academy of Sciences of the United States of America* **92**, 4011-4015, doi:10.1073/pnas.92.9.4011 (1995).
58 Thampy, K. G. Formation of malonyl coenzyme A in rat heart. Identification and purification of an isozyme of A carboxylase from rat heart. *The Journal of biological chemistry* **264**, 17631-17634 (1989).
59 Kreuz, S. *et al.* Acetyl-CoA carboxylases 1 and 2 show distinct expression patterns in rats and humans and alterations in obesity and diabetes. *Diabetes/metabolism research and reviews* **25**, 577-586, doi:10.1002/dmrr.997 (2009).
60 Abu-Elheiga, L. *et al.* Mutant mice lacking acetyl-CoA carboxylase 1 are embryonically lethal. *Proceedings of the National Academy of Sciences of the United States of America* **102**, 12011-12016, doi:10.1073/pnas.0505714102 (2005).
61 Abu-Elheiga, L., Almarza-Ortega, D. B., Baldini, A. & Wakil, S. J. Human acetyl-CoA carboxylase 2. Molecular cloning, characterization, chromosomal mapping, and evidence for two isoforms. *The Journal of biological chemistry* **272**, 10669-10677, doi:10.1074/jbc.272.16.10669 (1997).
62 Tong, L. & Harwood, H. J., Jr. Acetyl-coenzyme A carboxylases: versatile targets for drug discovery. *Journal of cellular biochemistry* **99**, 1476-1488, doi:10.1002/jcb.21077 (2006).
63 Abu-Elheiga, L. *et al.* The subcellular localization of acetyl-CoA carboxylase 2. *Proceedings of the National Academy of Sciences of the United States of America* **97**, 1444-1449, doi:10.1073/pnas.97.4.1444 (2000).
64 Wakil, S. J. & Abu-Elheiga, L. A. Fatty acid metabolism: target for metabolic syndrome. *Journal of lipid research* **50 Suppl**, S138-143, doi:10.1194/jlr.R800079-JLR200 (2009).
65 Dutta-Roy, A. K. Cellular uptake of long-chain fatty acids: role of membrane-associated fatty-acid-binding/transport proteins. *Cellular and molecular life sciences : CMLS* **57**, 1360-1372, doi:10.1007/pl00000621 (2000).
66 Kim, K. H. Regulation of mammalian acetyl-coenzyme A carboxylase. *Annual review of nutrition* **17**, 77-99, doi:10.1146/annurev.nutr.17.1.77 (1997).
67 FÆRgeman, N. J. & Knudsen, J. Role of long-chain fatty acyl-CoA esters in the regulation of metabolism and in cell signalling. *Biochemical Journal* **323**, 1-12, doi:10.1042/bj3230001 (1997).
68 Chamberlain, L. H. & Shipston, M. J. The physiology of protein S-acylation. *Physiol Rev* **95**, 341-376, doi:10.1152/physrev.00032.2014 (2015).
69 Falomir-Lockhart, L. J., Cavazzutti, G. F., Giménez, E. & Toscani, A. M. Fatty Acid Signaling Mechanisms in Neural Cells: Fatty Acid Receptors. *Front Cell Neurosci* **13**, 162-162, doi:10.3389/fncel.2019.00162 (2019).
70 Kim, C. W. *et al.* Acetyl CoA Carboxylase Inhibition Reduces Hepatic Steatosis but Elevates Plasma Triglycerides in Mice and Humans: A Bedside to Bench Investigation. *Cell metabolism* **26**, 394-406.e396, doi:10.1016/j.cmet.2017.07.009 (2017).

71 Harwood, H. J., Jr. Treating the metabolic syndrome: acetyl-CoA carboxylase inhibition. *Expert opinion on therapeutic targets* **9**, 267-281, doi:10.1517/14728222.9.2.267 (2005).
72 Abu-Elheiga, L., Oh, W., Kordari, P. & Wakil, S. J. Acetyl-CoA carboxylase 2 mutant mice are protected against obesity and diabetes induced by high-fat/high-carbohydrate diets. *Proceedings of the National Academy of Sciences of the United States of America* **100**, 10207-10212, doi:10.1073/pnas.1733877100 (2003).
73 Olson, D. P., Pulinilkunnil, T., Cline, G. W., Shulman, G. I. & Lowell, B. B. Gene knockout of Acc2 has little effect on body weight, fat mass, or food intake. *Proceedings of the National Academy of Sciences* **107**, 7598, doi:10.1073/pnas.0913492107 (2010).
74 Hoehn, K. L. *et al.* Acute or chronic upregulation of mitochondrial fatty acid oxidation has no net effect on whole-body energy expenditure or adiposity. *Cell metabolism* **11**, 70-76, doi:10.1016/j.cmet.2009.11.008 (2010).
75 Mao, J. *et al.* Liver-specific deletion of acetyl-CoA carboxylase 1 reduces hepatic triglyceride accumulation without affecting glucose homeostasis. *Proceedings of the National Academy of Sciences of the United States of America* **103**, 8552-8557, doi:10.1073/pnas.0603115103 (2006).
76 Harada, N. *et al.* Hepatic De Novo Lipogenesis Is Present in Liver-Specific ACC1-Deficient Mice. *Molecular and Cellular Biology* **27**, 1881, doi:10.1128/MCB.01122-06 (2007).
77 Mao, J., Chirala, S. S. & Wakil, S. J. Human acetyl-CoA carboxylase 1 gene: presence of three promoters and heterogeneity at the 5'-untranslated mRNA region. *Proceedings of the National Academy of Sciences of the United States of America* **100**, 7515-7520, doi:10.1073/pnas.1332670100 (2003).
78 Zhao, L. F. *et al.* Hormonal regulation of acetyl-CoA carboxylase isoenzyme gene transcription. *Endocrine journal* **57**, 317-324, doi:10.1507/endocrj.k09e-298 (2010).
79 Mao, J., Chirala, S. S. & Wakil, S. J. Human acetyl-CoA carboxylase 1 gene: presence of three promoters and heterogeneity at the 5'-untranslated mRNA region. *Proceedings of the National Academy of Sciences of the United States of America* **100**, 7515-7520, doi:10.1073/pnas.1332670100 (2003).
80 Zhang, Y., Yin, L. & Hillgartner, F. B. SREBP-1 integrates the actions of thyroid hormone, insulin, cAMP, and medium-chain fatty acids on ACCalpha transcription in hepatocytes. *Journal of lipid research* **44**, 356-368, doi:10.1194/jlr.M200283-JLR200 (2003).
81 Oh, S. Y. *et al.* Acetyl-CoA carboxylase beta gene is regulated by sterol regulatory element-binding protein-1 in liver. *The Journal of biological chemistry* **278**, 28410-28417, doi:10.1074/jbc.M300553200 (2003).
82 Shimano, H. *et al.* Sterol regulatory element-binding protein-1c and pancreatic beta-cell dysfunction. *Diabetes Obes Metab* **9 Suppl 2**, 133-139, doi:10.1111/j.1463-1326.2007.00779.x (2007).
83 Poungvarin, N. *et al.* Carbohydrate response element-binding protein (ChREBP) plays a pivotal role in beta cell glucotoxicity. *Diabetologia* **55**, 1783-1796, doi:10.1007/s00125-012-2506-4 (2012).
84 Kim, C.-W. *et al.* Induced polymerization of mammalian acetyl-CoA carboxylase by MIG12 provides a tertiary level of regulation of fatty acid synthesis. *Proceedings of the National Academy of Sciences* **107**, 9626, doi:10.1073/pnas.1001292107 (2010).
85 Martin, D. B. & Vagelos, P. R. The mechanism of tricarboxylic acid cycle regulation of fatty acid synthesis. *The Journal of biological chemistry* **237**, 1787-1792 (1962).

86 Beaty, N. B. & Lane, M. D. The polymerization of acetyl-CoA carboxylase. *The Journal of biological chemistry* **258**, 13051-13055 (1983).
87 Faergeman, N. J. & Knudsen, J. Role of long-chain fatty acyl-CoA esters in the regulation of metabolism and in cell signalling. *The Biochemical journal* **323 (Pt 1)**, 1-12, doi:10.1042/bj3230001 (1997).
88 Hardie, D. G. Regulation of fatty acid synthesis via phosphorylation of acetyl-CoA carboxylase. *Progress in lipid research* **28**, 117-146, doi:10.1016/0163-7827(89)90010-6 (1989).
89 Jang, S. *et al.* Activity and structure of human acetyl-CoA carboxylase targeted by a specific inhibitor. *FEBS letters* **592**, 2048-2058, doi:10.1002/1873-3468.13097 (2018).
90 da Silva Xavier, G. *et al.* Role for AMP-activated protein kinase in glucose-stimulated insulin secretion and preproinsulin gene expression. *The Biochemical journal* **371**, 761-774, doi:10.1042/bj20021812 (2003).
91 Jeon, S.-M. Regulation and function of AMPK in physiology and diseases. *Exp Mol Med* **48**, e245-e245, doi:10.1038/emm.2016.81 (2016).
92 Hardie, D. G., Carling, D. & Carlson, M. The AMP-activated/SNF1 protein kinase subfamily: metabolic sensors of the eukaryotic cell? *Annual review of biochemistry* **67**, 821-855, doi:10.1146/annurev.biochem.67.1.821 (1998).
93 Ha, J., Daniel, S., Broyles, S. S. & Kim, K. H. Critical phosphorylation sites for acetyl-CoA carboxylase activity. *The Journal of biological chemistry* **269**, 22162-22168 (1994).
94 Davies, S. P., Sim, A. T. & Hardie, D. G. Location and function of three sites phosphorylated on rat acetyl-CoA carboxylase by the AMP-activated protein kinase. *European journal of biochemistry* **187**, 183-190, doi:10.1111/j.1432-1033.1990.tb15293.x (1990).
95 Leclerc, I. & Rutter, G. A. AMP-activated protein kinase: a new beta-cell glucose sensor?: Regulation by amino acids and calcium ions. *Diabetes* **53 Suppl 3**, S67-74, doi:10.2337/diabetes.53.suppl_3.s67 (2004).
96 Ronnebaum, S. M. *et al.* Chronic suppression of acetyl-CoA carboxylase 1 in beta-cells impairs insulin secretion via inhibition of glucose rather than lipid metabolism. *The Journal of biological chemistry* **283**, 14248-14256, doi:10.1074/jbc.M800119200 (2008).
97 Zhang, S. & Kim, K. H. Glucose activation of acetyl-CoA carboxylase in association with insulin secretion in a pancreatic beta-cell line. *The Journal of endocrinology* **147**, 33-41 (1995).
98 Munday, M. R., Campbell, D. G., Carling, D. & Hardie, D. G. Identification by amino acid sequencing of three major regulatory phosphorylation sites on rat acetyl-CoA carboxylase. *European journal of biochemistry* **175**, 331-338, doi:10.1111/j.1432-1033.1988.tb14201.x (1988).
99 Beall, C. *et al.* Loss of AMP-activated protein kinase alpha2 subunit in mouse beta-cells impairs glucose-stimulated insulin secretion and inhibits their sensitivity to hypoglycaemia. *The Biochemical journal* **429**, 323-333, doi:10.1042/bj20100231 (2010).
100 Gelin, L., Li, J., Corbin, K. L., Jahan, I. & Nunemaker, C. S. Metformin Inhibits Mouse Islet Insulin Secretion and Alters Intracellular Calcium in a Concentration-Dependent and Duration-Dependent Manner near the Circulating Range. *J Diabetes Res* **2018**, 9163052, doi:10.1155/2018/9163052 (2018).

101 Lamontagne, J. *et al.* Identification of the signals for glucose-induced insulin secretion in INS1 (832/13) beta-cells using metformin-induced metabolic deceleration as a model. *The Journal of biological chemistry* **292**, 19458-19468, doi:10.1074/jbc.M117.808105 (2017).
102 Dufer, M., Noack, K., Krippeit-Drews, P. & Drews, G. Activation of the AMP-activated protein kinase enhances glucose-stimulated insulin secretion in mouse beta-cells. *Islets* **2**, 156-163, doi:10.4161/isl.2.3.11412 (2010).
103 Lupi, R. *et al.* Effects of glibenclamide and metformin (alone or in combination) on insulin release from isolated human pancreatic islets. *Acta diabetologica* **34**, 46-48 (1997).
104 Leclerc, I. *et al.* AMP-activated protein kinase regulates glucagon secretion from mouse pancreatic alpha cells. *Diabetologia* **54**, 125-134, doi:10.1007/s00125-010-1929-z (2011).
105 Steinberg, G. R. & Carling, D. AMP-activated protein kinase: the current landscape for drug development. *Nat Rev Drug Discov* **18**, 527-551, doi:10.1038/s41573-019-0019-2 (2019).
106 Tramunt, B. *et al.* Sex differences in metabolic regulation and diabetes susceptibility. *Diabetologia*, doi:10.1007/s00125-019-05040-3 (2019).
107 Mauvais-Jarvis, F. Sex differences in metabolic homeostasis, diabetes, and obesity. *Biology of sex differences* **6**, 14, doi:10.1186/s13293-015-0033-y (2015).
108 Macek, B., Mann, M. & Olsen, J. V. Global and site-specific quantitative phosphoproteomics: principles and applications. *Annual review of pharmacology and toxicology* **49**, 199-221, doi:10.1146/annurev.pharmtox.011008.145606 (2009).
109 Phosphonet http://www.phosphonet.ca/default.aspx#InfoBox.
110 Chan, C. Y., Gritsenko, M. A., Smith, R. D. & Qian, W. J. The current state of the art of quantitative phosphoproteomics and its applications to diabetes research. *Expert review of proteomics* **13**, 421-433, doi:10.1586/14789450.2016.1164604 (2016).
111 Steen, H. & Mann, M. The ABC's (and XYZ's) of peptide sequencing. *Nat Rev Mol Cell Biol* **5**, 699-711, doi:10.1038/nrm1468 (2004).
112 Shevchenko, A., Tomas, H., Havlis, J., Olsen, J. V. & Mann, M. In-gel digestion for mass spectrometric characterization of proteins and proteomes. *Nat Protoc* **1**, 2856-2860, doi:10.1038/nprot.2006.468 (2006).
113 Cox, J. *et al.* Andromeda: a peptide search engine integrated into the MaxQuant environment. *Journal of proteome research* **10**, 1794-1805, doi:10.1021/pr101065j (2011).
114 Tyanova, S., Temu, T. & Cox, J. The MaxQuant computational platform for mass spectrometry-based shotgun proteomics. *Nat Protoc* **11**, 2301-2319, doi:10.1038/nprot.2016.136 (2016).
115 Cox, J. & Mann, M. MaxQuant enables high peptide identification rates, individualized p.p.b.-range mass accuracies and proteome-wide protein quantification. *Nature biotechnology* **26**, 1367-1372, doi:10.1038/nbt.1511 (2008).
116 Tsiatsiani, L. & Heck, A. J. Proteomics beyond trypsin. *FEBS J* **282**, 2612-2626, doi:10.1111/febs.13287 (2015).
117 Giansanti, P., Tsiatsiani, L., Low, T. Y. & Heck, A. J. Six alternative proteases for mass spectrometry-based proteomics beyond trypsin. *Nat Protoc* **11**, 993-1006, doi:10.1038/nprot.2016.057 (2016).
118 http://www.matrixscience.com. <http://www.matrixscience.com> (2019).
119 *Mascot databse search. Matrix Science, 2016.2017.*

120 Xu, J., Han, J., Long, Y. S., Epstein, P. N. & Liu, Y. Q. The role of pyruvate carboxylase in insulin secretion and proliferation in rat pancreatic beta cells. *Diabetologia* **51**, 2022-2030, doi:10.1007/s00125-008-1130-9 (2008).
121 Wallace, J. C., Jitrapakdee, S. & Chapman-Smith, A. Pyruvate carboxylase. *The international journal of biochemistry & cell biology* **30**, 1-5 (1998).
122 Mann, M. & Jensen, O. N. Proteomic analysis of post-translational modifications. *Nature biotechnology* **21**, 255-261, doi:10.1038/nbt0303-255 (2003).
123 Zhu, W., Smith, J. W. & Huang, C. M. Mass spectrometry-based label-free quantitative proteomics. *J Biomed Biotechnol* **2010**, 840518, doi:10.1155/2010/840518 (2010).
124 Sharma, K. *et al.* Ultradeep human phosphoproteome reveals a distinct regulatory nature of Tyr and Ser/Thr-based signaling. *Cell reports* **8**, 1583-1594, doi:10.1016/j.celrep.2014.07.036 (2014).
125 Olsen, J. V. *et al.* Global, in vivo, and site-specific phosphorylation dynamics in signaling networks. *Cell* **127**, 635-648, doi:10.1016/j.cell.2006.09.026 (2006).
126 Wei, J. *et al.* A unified molecular mechanism for the regulation of acetyl-CoA carboxylase by phosphorylation. *Cell Discov* **2**, 16044, doi:10.1038/celldisc.2016.44 (2016).
127 Shi, S., Chen, Y., Siewers, V. & Nielsen, J. Improving production of malonyl coenzyme A-derived metabolites by abolishing Snf1-dependent regulation of Acc1. *MBio* **5**, e01130-01114, doi:10.1128/mBio.01130-14 (2014).
128 Choi, J. W. & Da Silva, N. A. Improving polyketide and fatty acid synthesis by engineering of the yeast acetyl-CoA carboxylase. *J Biotechnol* **187**, 56-59, doi:10.1016/j.jbiotec.2014.07.430 (2014).
129 Chen, X., Yang, X., Shen, Y., Hou, J. & Bao, X. Screening Phosphorylation Site Mutations in Yeast Acetyl-CoA Carboxylase Using Malonyl-CoA Sensor to Improve Malonyl-CoA-Derived Product. *Front Microbiol* **9**, 47, doi:10.3389/fmicb.2018.00047 (2018).
130 Lee, D. C., Jones, A. R. & Hubbard, S. J. Computational phosphoproteomics: from identification to localization. *Proteomics* **15**, 950-963, doi:10.1002/pmic.201400372 (2015).
131 Hogrebe, A. *et al.* Benchmarking common quantification strategies for large-scale phosphoproteomics. *Nature Communications* **9**, 1045, doi:10.1038/s41467-018-03309-6 (2018).
132 Chalkley, R. J. & Clauser, K. R. Modification site localization scoring: strategies and performance. *Molecular & cellular proteomics : MCP* **11**, 3-14, doi:10.1074/mcp.R111.015305 (2012).
133 Solari, F. A., Dell'Aica, M., Sickmann, A. & Zahedi, R. P. Why phosphoproteomics is still a challenge. *Mol Biosyst* **11**, 1487-1493, doi:10.1039/c5mb00024f (2015).
134 Arur, S. & Schedl, T. Generation and purification of highly specific antibodies for detecting post-translationally modified proteins in vivo. *Nat Protoc* **9**, 375-395, doi:10.1038/nprot.2014.017 (2014).
135 Huttlin, E. L. *et al.* A tissue-specific atlas of mouse protein phosphorylation and expression. *Cell* **143**, 1174-1189, doi:10.1016/j.cell.2010.12.001 (2010).
136 Meng, Y. Y. *et al.* Protection against Doxorubicin-Induced Cytotoxicity by Geniposide Involves AMPKalpha Signaling Pathway. *Oxidative medicine and cellular longevity* **2019**, 7901735, doi:10.1155/2019/7901735 (2019).

137 Powers, A. C. *et al.* Proglucagon processing similar to normal islets in pancreatic alpha-like cell line derived from transgenic mouse tumor. *Diabetes* **39**, 406-414, doi:10.2337/diab.39.4.406 (1990).
138 Obenauer, J. C., Cantley, L. C. & Yaffe, M. B. Scansite 2.0: Proteome-wide prediction of cell signaling interactions using short sequence motifs. *Nucleic Acids Res* **31**, 3635-3641, doi:10.1093/nar/gkg584 (2003).
139 Blom, N., Gammeltoft, S. & Brunak, S. Sequence and structure-based prediction of eukaryotic protein phosphorylation sites. *Journal of molecular biology* **294**, 1351-1362, doi:10.1006/jmbi.1999.3310 (1999).
140 Diella, F. *et al.* Phospho.ELM: a database of experimentally verified phosphorylation sites in eukaryotic proteins. *BMC bioinformatics* **5**, 79, doi:10.1186/1471-2105-5-79 (2004).
141 Puntervoll, P. *et al.* ELM server: A new resource for investigating short functional sites in modular eukaryotic proteins. *Nucleic Acids Res* **31**, 3625-3630, doi:10.1093/nar/gkg545 (2003).
142 Chang, E. J., Begum, R., Chait, B. T. & Gaasterland, T. Prediction of Cyclin-Dependent Kinase Phosphorylation Substrates. *PLOS ONE* **2**, e656, doi:10.1371/journal.pone.0000656 (2007).
143 Mok, J. *et al.* Deciphering protein kinase specificity through large-scale analysis of yeast phosphorylation site motifs. *Sci Signal* **3**, ra12-ra12, doi:10.1126/scisignal.2000482 (2010).
144 Obenauer, J. C., Cantley, L. C. & Yaffe, M. B. Scansite 2.0: proteome-wide prediction of cell signaling interactions using short sequence motifs. *Nucleic Acids Res* **31**, 3635-3641, doi:10.1093/nar/gkg584 (2003).
145 Juncker, A. S. *et al.* Sequence-based feature prediction and annotation of proteins. *Genome Biology* **10**, 206, doi:10.1186/gb-2009-10-2-206 (2009).
146 Distler, J. H. *et al.* Nucleofection: a new, highly efficient transfection method for primary human keratinocytes*. *Experimental dermatology* **14**, 315-320, doi:10.1111/j.0906-6705.2005.00276.x (2005).
147 https://www.thermofisher.com/uk/en/home/references/gibco-cell-culture-basics/transfection-basics/gene-delivery-technologies/cationic-lipid-mediated-delivery.html.
148 Dr Alejandra Solache, R. B., Trinette Chuang, Dr Robin Clark, Rey Dimagiba, Dr April Fisher, Dr Wayne Speckmann and Dr Chun Yang Evolving strategies for application-specific validation of research use antibodies.pdf>. (2013).
149 Marcon, E. *et al.* Assessment of a method to characterize antibody selectivity and specificity for use in immunoprecipitation. *Nature Methods* **12**, 725, doi:10.1038/nmeth.3472
https://www.nature.com/articles/nmeth.3472#supplementary-information (2015).
150 Michel, M. C., Wieland, T. & Tsujimoto, G. How reliable are G-protein-coupled receptor antibodies? *Naunyn-Schmiedeberg's Archives of Pharmacology* **379**, 385-388, doi:10.1007/s00210-009-0395-y (2009).
151 Tarrant, M. K. & Cole, P. A. The chemical biology of protein phosphorylation. *Annual review of biochemistry* **78**, 797-825, doi:10.1146/annurev.biochem.78.070907.103047 (2009).
152 Brumbaugh K. et al. (2011) Overview of the Generation, V., and Application of Phosphosite-Specific Antibodies. In: Kalyuzhny A. (eds) Signal Transduction

Immunohistochemistry. Methods in Molecular Biology (Methods and Protocols), vol 717. Humana Press.
153 Mnatsakanyan, R. *et al.* Detecting post-translational modification signatures as potential biomarkers in clinical mass spectrometry. *Expert review of proteomics* **15**, 515-535, doi:10.1080/14789450.2018.1483340 (2018).
154 Lundby, A. *et al.* Quantitative maps of protein phosphorylation sites across 14 different rat organs and tissues. *Nature Communications* **3**, 876, doi:10.1038/ncomms1871 (2012).
155 Ehrenberger, T., Cantley, L. C. & Yaffe, M. B. Computational prediction of protein-protein interactions. *Methods Mol Biol* **1278**, 57-75, doi:10.1007/978-1-4939-2425-7_4 (2015).
156 Zhang, S. & Kim, K. H. Protein kinase CK2 down-regulates glucose-activated expression of the acetyl-CoA carboxylase gene. *Archives of biochemistry and biophysics* **338**, 227-232, doi:10.1006/abbi.1996.9809 (1997).
157 Ampofo, E., Nalbach, L., Menger, M. D., Montenarh, M. & Götz, C. Protein Kinase CK2-A Putative Target for the Therapy of Diabetes Mellitus? *Int J Mol Sci* **20**, 4398, doi:10.3390/ijms20184398 (2019).
158 Santo-Domingo, J. *et al.* Glucose-dependent phosphorylation signaling pathways and crosstalk to mitochondrial respiration in insulin secreting cells. *Cell Communication and Signaling* **17**, 14, doi:10.1186/s12964-019-0326-6 (2019).
159 Ashcroft, S. J. Protein phosphorylation and beta-cell function. *Diabetologia* **37 Suppl 2**, S21-29, doi:10.1007/bf00400822 (1994).
160 Meng, R., Gotz, C. & Montenarh, M. The role of protein kinase CK2 in the regulation of the insulin production of pancreatic islets. *Biochemical and biophysical research communications* **401**, 203-206, doi:10.1016/j.bbrc.2010.09.028 (2010).
161 Sacco, F. *et al.* Glucose-regulated and drug-perturbed phosphoproteome reveals molecular mechanisms controlling insulin secretion. *Nature Communications* **7**, 13250, doi:10.1038/ncomms13250 (2016).
162 Nasri, M. *et al.* Fluorescent labeling of CRISPR/Cas9 RNP for gene knockout in HSPCs and iPSCs reveals an essential role for GADD45b in stress response. *Blood Adv* **3**, 63-71, doi:10.1182/bloodadvances.2017015511 (2019).
163 Song, J. *et al.* PhosphoPredict: A bioinformatics tool for prediction of human kinase-specific phosphorylation substrates and sites by integrating heterogeneous feature selection. *Scientific reports* **7**, 6862, doi:10.1038/s41598-017-07199-4 (2017).